# LUND UNIVERSITY

**NMR Diffusion Studies of Association in Surfactant Systems Inclusion Complexes, Micellar Solutions and Microemulsions**

Nilsson, Markus

2008

[Link to publication](#)

Total number of authors:
1

# NMR Diffusion Studies of Association in Surfactant Systems

*Inclusion Complexes, Micellar Solutions and Microemulsions*

# NMR Diffusion Studies of Association in Surfactant Systems

## *Inclusion Complexes, Micellar Solutions and Microemulsions*

# Markus Nilsson

Title and subtitle  **NMR Diffusion Studies of Association in Surfactant Systems.**
Inclusion Complexes, Micellar Solutions and Microemulsions.

Abstract

The aim of this thesis was to investigate the self-diffusion behavior of host-guest complexes, microemulsions and polymer solutions. Pulsed Field Gradient NMR (PFG-NMR) provided detailed molecular information about the systems studied. The general strategy was to measure the diffusivities of the species and from there get molecular insight into the aggregation and the dynamics of the system.

Guest-host interactions were studied between β-cyclodextrin (β-CD) and different cationic surfactants. The equilibrium constant (K11) increases as a function of the number of CH2 groups in the surfactant chain. It could be concluded that the cavity of β-CD could incorporate 10-12 CH2 groups and that it is the hydrophobic interaction that mainly is responsible for the inclusion complex formed. The interaction between the gemini surfactant and β-CD formed a 2:1 (CD:gemini) complex in a two step mechanism with the first association constant higher than the second one (K21), but both relatively small in comparison with analogue singled tailed surfactant. The values of the K11 and K21 increased with gemini spacer length which indicates that the available space on the gemini molecule is important. The second association constant shows no cooperativity and its magnitude are discussed in terms of steric constraints. Bolaform surfactant complexation was investigated with both β-CD and α-CD with Isothermal Titration Calorimetry (ITC). The K11, enthalpy and entropy of formation were obtained. From ITC a molecular interpretation is made explaining the enthalpy and entropy difference between α- and β-CD.

In a second study diblock copolymers of the type methoxy poly(ethylene oxide)-poly(alkylene oxide)s were incorporated into nonionic bicontinuous microemulsions at 298 K. An enhancement of the microemulsion in solubilising water and oil were observed with a boosting factor of 9. The self-diffusion coefficients of the components in the system were measured and provided molecular information on how the microstructure of the bicontinuous microemulsion changed upon addition of the polymers.

The diffusion study concerning the aqueous solution of the synthetic polymers, PEO-PPO-PEO, is focused towards analyzing the PFG-NMR decay correctly. The polydispersity has consequences on the polymer self-assembly, which were highlighted, modeled and discussed based on PFG-NMR data. The main conclusion is that the curved NMR echo decay as obtained for self-assembly can be explained with a multi-component ideal solution model.

Key words:  host-guest complexation, cyclodextrin, gemini surfactant, bolaform surfactant, self-diffusion NMR, polydispersity, Pluronic, bicontinuous microemulsion, boosting effect

Classification system and/or index termes (if any):

DOKUMENTDATABLAD enl SIS 61 41 21

# Contents

# List of Papers

**I.** **Interaction between n-octyl-β-D-glucosides and α- and β-cyclodextrin as seen by self-diffusion NMR.** Valente A.J.M.; Nilsson M.; Söderman O; *Journal of Colloid and Interface Science, 281, 218-224, 2005.*

**II.** **Self-Diffusion NMR studies of the host-guest interaction between β-cyclodextrin and alkyltrimethylammonium bromide surfactants.** Cabaleiro-Lago C.; Nilsson M; Söderman O. *Langmuir, 21(25) 11637-11644, 2005.*

**III.** **NMR diffusometry and conductometry study of the host-guest association between β-cyclodextrin and dodecane 1,12-bis(trimethylammonium bromide).** Cabaleiro-Lago, C., Nilsson M.; Valente A. J. M.; Bonini M.; Söderman O. *Journal of Colloid and Interface Science, 300, 782-787, 2006.*

**IV.** **Interaction between gemini surfactants, 12-*s*-12, and β-cyclodextrin as investigated by NMR diffusometry and electrical conductometry.** Nilsson M., Cabaleiro-Lago C.; Valente, A. J. M.; Söderman O. *Langmuir, 22 (21): 8663-8669, 2006.*

**V.** **Thermodynamic and kinetic charcterization of host-guest association between bolaform surfactants α- and β-cyclodextrins.** Nilsson M.; Valente A. J. M.; Olofsson G.; Söderman O. *Manuscript in preparation.*

**VI.** **The effect of polymer on the phase behavior of balanced microemulsions: block copolymer and comb polymers.** Nilsson M.; Söderman O.; Johansson I. *Colloid and Polymer Science, 284 (11): 1229-1241, 2006.*

**VII.** **Influence of polydispersity on the micellication of triblock copolymers investigated by pulsed field gradient nuclear magnetic resonance.** Nilsson, M; Håkansson, B.; Söderman O.; Topgaard, D. *Macromolecules, 40, 8250-8258, 2007.*

In the text the papers are referred to by their roman numerals.

## Papers not included in this thesis

**A small angle X-ray scattering, light scattering and NMR study of peo-ppo-peo triblock copolymer/cationic surfactant complexes in aqueous solution.** Jansson J.; Schillén K.; Nilsson M.; Söderman O.; Fritz G.; Bergmann A; Glatter O.; *Journal of Physical Chemistry B, 109 (15) 7073-7083, 2005.*

**Physico-chemical characterisation of PEG-12-acyloxy-stearate micelles and liquid crystalline phases.** McNamee C. E.; Nilsson M.; Corswant C.; Söderman; O. *Langmuir, 21, 8146-8154, 2005.*

**The octyl-β-D-glucoside/n-octane/1-octanol/water system. Phase diagrams and phase properties.** Reimer J.; Nilsson M.; Álvares M.; Söderman O.; *Journal of Colloid and Interface Science, 287, 326-332, 2005.*

# Preface

This thesis is the result of research that I have carried out at Physical Chemistry 1 in Lund, Sweden, between the years 2003 and 2008. The focus has mainly been on the use of Nuclear Magnetic Resonance Spectroscopy (NMR) as a tool to investigate the static and dynamic behavior of different colloidal systems. The main topic of this thesis is molecular self-diffusion, from which I have extracted molecular information and characterized various systems. This thesis deals with three different research areas, "host-guest complexation", "microemulsion based on amphiphilic polymer and surfactant" and "polymers in aqueous solution". In the host-guest complexation research field the self-diffusion coefficients of the guest and host molecule are measured and compared. A diffusion model is then used to obtain the equilibrium constant. In the case of microemulsions, the aim was to increase the efficiency of water and oil uptake of microemulsions by replacing some amount of surfactant with amphiphilic diblock copolymers. The effect the diblock copolymer had on the microemulsion extension (the swelling) was investigated by phase studies. The change in the microstructure of the microemulsions as a function of diblock copolymer addition was studied by probing the components self-diffusion coefficients of the microemulsion. Finally, the last project involves NMR self-diffusion measurements of the amphihilic synthetic polymer Pluronic F127. The aim was to analyze and model the influence of polydispersity on the self-diffusion signal (echo decay) when the conditions were set by concentration, temperature or salt to trigger self-assembly. The group Pluronic polymers is important for the industrial applications, so it is crucial to understand and control its self-assembly behavior.

An NMR self-diffusion experiment is relatively easy to set up and perform and the result is easy to evaluate. The technique has been very useful in the field of colloid and surface chemistry. The NMR self-diffusion technique can be applied to many different fields, for example to characterize cell size and the leakage of cell fluids. One could also study porous material for example wood and paper. Moreover, NMR self-diffusion can be used within food technology for example to characterize emulsions. In this thesis I want to emphasize the usefulness of self-diffusion NMR.

The thesis is divided into two parts. The first part is a summary of NMR theory/experiments, the experimental systems used in this thesis and the results from these experiments. The aim of this part is to introduce the scientific material at a level so that a natural science undergraduate student can grasp the content. The second part consists of publications.

Chapter 1 serves as a general introduction to the area of colloid and interfacial science, where the importance of non-covalent intermolecular interactions will be discussed briefly. Chapter 2 contains the general aspects of

the experimental systems, the structure and its molecular properties. Chapters 3 and 4 serve as a general introduction to the methodologies where "the toolboxes" and typical physical properties and parameters of the experiments will be discussed. Our experimental results will be highlighted and discussed in chapters 5 ("Cyclodextrin surfactant interaction"), chapter 6 ("Polymer microemulsion interactions") and chapter 7 ("Diffusion studies of triblock copolymers").

In papers I-IV, self-diffusion NMR was used to investigate host-guest systems consisting of cyclodextrin and a range of different surfactants. The important information from these systems can be derived directly without any approximations or advanced modeling. In paper V Isothermal Titration Calorimetry (ITC) was used to study the cyclodextrin surfactant interactions.

In paper VI we studied the effect of diblock copolymer addition on the phase behavior of alkylglucoside bicontinuous microemulsions. Self-diffusion NMR was used to characterize the microstructure of the complex microemulsions.

Finally in paper VII we use self-diffusion NMR to characterize aqueous solutions of synthetic polymers. In polymer systems, however, the situation is more complex mainly due to the polydispersity of the molecular weight. In this paper we recommend a procedure for how self-diffusion data from synthetic polymer should be treated and modeled.

# 1. Introduction

In this thesis the scientific work carried out falls under the category of colloid science. Colloid science describes solutions of large molecules, particles and aggregates of molecules and/or particles. One way to approach and understand colloidal systems is to consider the intermolecular interactions of the system, i.e. the forces that govern aggregation and self-assembly of molecules.

One of the first scientists to consider intermolecular interactions was Emil Fischer. In the 1890s Fischer postulated "lock and key" the specificity of enzymes (proteins) with respect to the substrate. Emil Fischer's picture was rather crude with the key that needs to fits physically in the lock. The general understanding nowadays is instead that the protein (lock) changes conformation during complexation with the substrate, which again tells us we need to understand the intermolecular interactions.

An important mechanism of interaction between molecules studied in this thesis is the hydrophobic interaction. The hydrophobic interaction is not an actual interaction; it is a solvent averaged induced interaction, a result from the fact that water molecules favor each other to non-polar species.[1] It is the possibility of water to rearrange the hydrogen bond network that allows for other molecules to be soluble. The positive free energy of hydrophobic interaction upon adding oil to water is primarily dominated by entropy at room temperature, whereas at higher temperature it is the enthalpy that gives the main positive contribution to the free energy.

The field of colloid science has important aspect; it is useful to employ colloidal systems (surfactants, polymers) as model systems, which often are simple and easy to investigate systematically. One model system that can be used to understand the nature of the hydrophobic effect is cyclodextrin-surfactants. Both the cyclodextrin and surfactant structures can be varied systematically. In this thesis (paper I-V) such interactions have been studied in aqueous solution, and the structures of the surfactant have been varied.

In paper VI, bicontinuous microemulsions were investigated, the interactions between the surfactants co-surfactants and polymers in the momolayer film is hydrophobic. In paper VII, the self-association of nonionic triblock copolymers was investigated, again the main driving force for the aggregation is the hydrophobic interaction.

Finally, the name "nanoscience" could also be used to describe the content in this thesis; the "nano" refers to the size of the aggregate which typically are in the range from a few nanometers to a few micrometers.

# 2. Components of the investigated systems

This chapter gives a background to the molecules used in this thesis.

## 2.1 Surfactants

Surfactants or surface-active agents (they assemble on interface to reduce the surface energy) are amphiphilic[i] molecules consisting of a hydrophilic (polar) part and a hydrophobic (nonpolar) part. The hydrophilic part is often referred to as the "head group" of the surfactant. The surfactant can be divided into four classes, depending on the nature of the head group: The four classes of surfactants are: nonionic, cationic, anionic and zwitterionic. The hydrophobic part is often referred to as the "tail" and normally consists of one or more chains of methylene groups.

The schizophrenic nature of the surfactant results in self-assembly. The self-assembly is a spontaneous co-operative process and the result is aggregation. The aggregates can form structures with different shapes (Figure 2.1), depending on the nature of the surfactant and the physical conditions. The self-assembly can be tuned by various physical parameters such as: concentration, temperature and salinity. The Critical Micelle Concentration (CMC) is the concentration at which the surfactants self-assemble and form micelles[ii]. Similarly, the Critical Micelle Temperature (CMT) is the temperature where surfactants start to self-assemble. At low surfactant concentrations but above CMC, spherical micelles are often formed. At higher surfactant concentrations the aggregates can grow in one or two dimensions. Rod-like micelles, disc-like micelles, and vesicles are examples of structures that can form. At even higher surfactant concentrations lamellar phases, cubic phases and hexagonal phases can form, which all show long-range order. The structures at higher concentrations can be characterized with small angle x-ray scattering due to the long range order. The characteristic length of a surfactant aggregate is typically between 20-1000 Å.

The driving force for self-assembly arises when water (polar media) avoids contact with the hydrophobic part of the molecule i.e. hydrophobic interaction" (see chapter 1). In a self-assembly the unfavorable interaction between water and the tail of the surfactant is minimized and there is a gain in entropy from the release of structurally bound water around the surfactant

---

[i] *Definition* amphiphile: The amphis is from the Greek word meaning both, and refers to the fact that a surfactant consists of at least two parts and philia meas love. The word amphiphile is a term describing a chemical compound possessing both hydrophilic and hydrophobic properties.
[ii] The word micelle comes from the Latin and means small piece.

monomers. The force that opposes self-assembly is head group repulsion. There are basically two main types of head group repulsions which depend on the nature of the surfactant. For surfactants with ionic head groups the repulsion is of electrostatic nature. In general the head group repulsion can be decreased by adding electrolyte since it screens the electrostatic repulsion. For surfactants with nonionic head groups, the repulsion comes mainly from steric hindrance.

The surfactants used in this thesis are summarized in Table 2.1-2.4. For further reading about self-assembly in colloidal system (surfactant and amphiphilic polymers) I recommend refs.[2, 3]
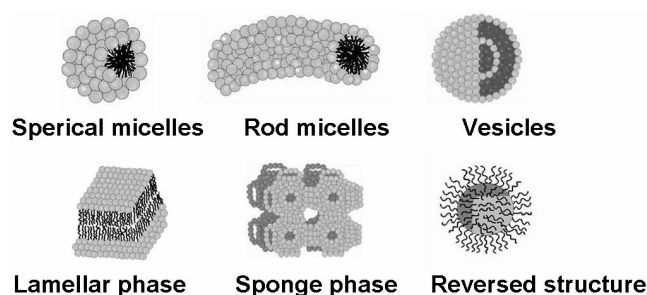


**Figure 2.1** Schematic illustrations of different self-assembled structures.

## 2.2 Cationic surfactants

The cationic surfactants used in this thesis all have a head group that consists of quaternary ammonium ion. The chemical structure of the surfactants along with the CMC values can be seen in Table 2.1.

### 2.2.1 The thermodynamics of cationic micellization

The cationic surfactants behave as electrolytes and are completely dissociated under the CMC. At CMC, and higher concentrations, approximately 70 % of the counterions are bound to the micelle surface.[4] The standard free Gibbs energy of transfer, $\Delta G^{\theta}(transfer)$, represents the standard free energy difference of transferring a monomer from the dispersed bulk phase into the micelle state.
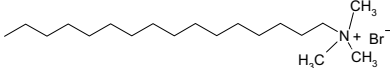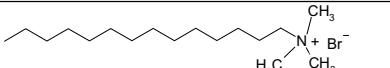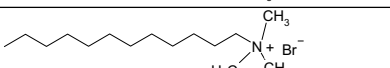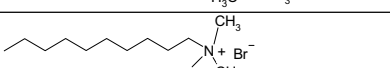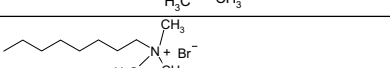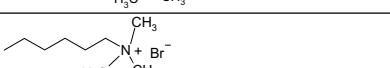
$$\Delta G^{\theta}(transfer) = RT(2 - \beta)\ln CMC \qquad (2.1)$$

Where $\beta$ is the degree of dissociation between the surfactant (in the micelle) and the counterion. If $\beta = 1$ there is no counterion binding, and if $\beta = 0$ all the counterions are bound to the surfactant. From a plot of the Gibbs free energy of transfer versus the number of methylene groups in the surfactant tail one gains physical insight into the association process of micelles. The parameter obtained is the free energy difference of transferring a $CH_2$-group from bulk solution into the micelle, which basically gives a measure of the hydrophobic interaction.

The free energy of transferring a $CH_2$ group into a micelle consisting of single tailed cationic surfactant is approximately -2.86 kJ/mol at 298 K [4].

**Table 2.1** Cationic surfactants used in this thesis. Structure, abbreviation and values of the CMC in $H_2O$ at 298 K.

| Cationic surfactant single tailed | Abbre-viation | Structure | CMC/mM Ref. |
|---|---|---|---|
| Hexadecyl trimethyl ammonium bromide | $C_{16}TAB$ | | 0.9 [5] |
| Tetradecyl trimethyl ammonium bromide | $C_{14}TAB$ | | 3.8 [6] |
| Dodecyl trimethyl ammonium bromide | $C_{12}TAB$ | | 16 [5] |
| Decyl trimethyl ammonium bromide | $C_{10}TAB$ | | 65 [5] |
| Octyl trimethyl ammonium bromide | $C_8TAB$ | | 220 [5] |
| Hexyl trimethyl ammonium bromide | $C_6TAB$ | | 580 [5] |

## 2.2.1 Gemini surfactants

The gemini surfactant may be viewed as a surfactant dimer where the two parts are connected by a spacer at the level of the head group (see Table 2.2).[7, 8] A gemini surfactant can be described as a sequence of a hydrocarbon tail, an ionic head group, a spacer, a second ionic head group and a second hydrocarbon tail. This sequence is usually described by the numbers *m-s-m*, where *m* is the numbers of carbons in the tails and *s* is the number of carbons in the spacer. A series of papers from Zana et al. report on the physical chemical properties of gemini 12-*s*-12.[9-13] The most interesting physical chemical properties of gemini surfactants are the low CMC values and the high surface activity. The CMC of gemini surfactants are at least one order of magnitude lower than the corresponding analogue with one tail (see Table 2.2). The length of the spacer (*s* = 2-10) has little influence on the CMC which is approximately 1±0.5 mM. In Figure 2.2 the CMC versus the spacer length has been plotted for *12-s-12*. In chapter 5 we will return to the effect of the spacer length on the complexation with β-cyclodextrin. The small variation of the CMC with spacer length is due to two effects:
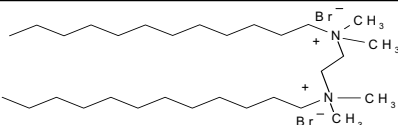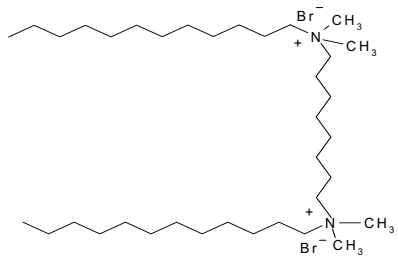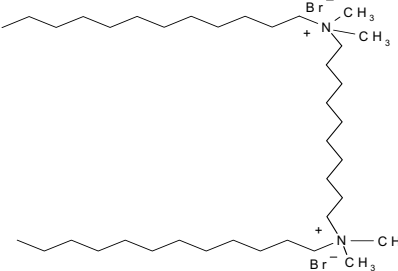
    i)      In the molecularly dispersed state there is a conformational change of the gemini surfactant as the spacer length is increased. The two tails of the gemini surfactant adopt a conformation that protects the hydrophobic part from water.

ii)     The spacer changes its conformation upon micellization. A progressive incorporation of the spacer into the micellar core occurs as *s* increases, due to the increased hydrophobic nature of the spacer and the gemini as whole.

The complexation between β-cyclodextrin and gemini surfactant has been studied in paper IV.

**Table 2**.2 Gemini surfactants used in this thesis. Structure, abbreviation and values for CMC in $H_2O$ at 298 K.

| Cationic surfactants doubled tailed "gemini" | Abbre-viation *m-s-m* | Structure | CMC/mM Ref. |
|---|---|---|---|
| Ethyl-α-ω-bis(dodecyldimethyl ammonium bromide) | *12-2-12* |  | 0,81±0.4 0.89±0.02 [13], [IV] |
| Octyl-α-ω-bis(dodecyldimethyl ammonium bromide) | *12-8-12* |  | 0.83±0.3 0.80±0.01 [13], [IV] |
| Decyl-α-ω-bis(dodecyldimethyl ammonium bromide) | *12-10-12* |  | 0.63±0.3 0.64±0.07 [13], [IV] |
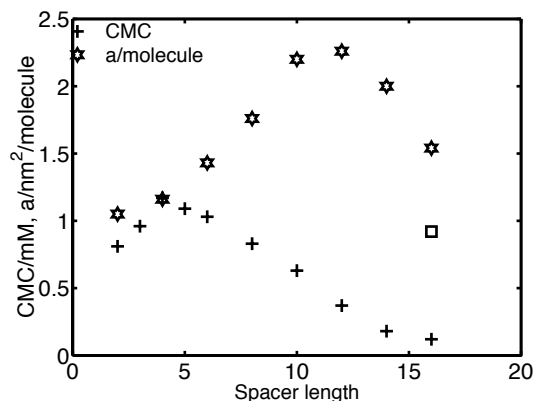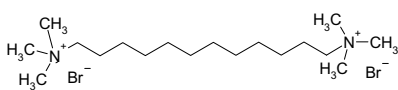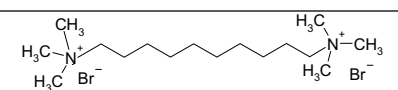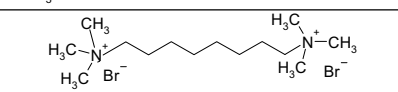
**Figure 2.2** CMC versus spacer length. Included in the graph is the surface area per surfactant, a, measured using surface tension versus spacer length. The graph contains data from references 13 and 9. The open square is the CMC of $C_{16}$TAB.

### 2.2.3 Bolaform surfactants

The bolaform surfactant (Table 2.3) has two head groups, separated by a hydrocarbon chain (spacer), *s,* and is denoted $B_s$ (where *B* stands for "*bolaform*" and *s* is the number of $CH_2$ groups in the spacer). In water solution they behave as a 2:1 electrolyte, like the gemini surfactants. At the air water interface the longer bolaform surfactant orients with the hydrophobic part towards the air and forming a loop where the charged head groups are at the water.[14] Comparing $C_{12}$TAB, *12-s-12* and $B_{12}$, the gemini and the traditional surfactant behave similar in aqueous solutions; both have well defined CMC and form micellar structures at low concentrations, whereas the $B_{12}$ surfactant only forms loose micelles with a low number of monomers.[14-16] Bolaform surfactants with a longer spacer are easier to characterize with respect to their surface chemistry properties, for example hexadecane-1,16-bis(trimethylammonium bromide) has a CMC of 45 mM[16] and docosane-1,22-bis(trimethylammonium bromide) has a CMC of 2.8 mM.[17] If one plots the CMC versus *s* of the bolaform surfactant $B_{16}$ and $B_{22}$ and extrapolate to *s = 12* one gets a CMC of 550 mM[17] (Cf. $C_6$TAB). No CMC or surface active properties are found for bolaform surfactant with spacer shorter than 10. The interactions between bolaform surfactant and α- and β-cyclodextrin have been studied in paper III and V.

**Table 2.3** Bolaform molecules used in this thesis. Structure, abbreviation and values for CMC in $H_2O$ at 298 K.

| Cationic surfactants doubled head "bolaform" | Abbre-viation $B_s$ | Structure | CMC/mM Ref. |
|---|---|---|---|
| Dodecane 1,12-bis(trimethyl ammonium bromide) | $B_{12}$ | | 20-50[15] 2-4[14] different values in literature. |
| Decyl 1,10-bis(trimethyl ammonium bromide) | $B_{10}$ | | no CMC |
| Octyl 1,8-bis(trimethyl ammonium bromide) | $B_8$ | | no CMC |

The nonionic surfactant of type n-$\beta$-D-alkylglucoside, has been used in paper I and VI, see Table 2.4.

**Table 2.4** Nonionic surfactants n-$\beta$-D-alkylglucoside used in this thesis. The structure, abbreviation and values for CMC in $H_2O$ at 298 K.

| Nonionic surfactants | Abbre-viation | Structure | CMC/mM |
|---|---|---|---|
| n-octyl-$\beta$-D-glucoside | $C_8G_1$ | | 25 [3] |
| n-nonyl-$\beta$-D-glucoside | $C_9G_1$ | | 6.5 [18] |

## 2.3 Polymers: structure and composition

Polymers[iii] are macromolecules, and are formed by polymerizing many small molecules called "monomers". Polymers can be classified as biological (DNA, protein, etc.) and non-biological macromolecules (adhesives, plastics, etc). Furthermore, the non-biological polymers can be characterised depending on the structure (architecture) and/or the chemical composition of the polymer. Linear, grafted or crosslinked polymers are example of polymers classified by their structure (see Figure 2.3a). Examples of polymers classified by their chemical composition are homopolymers, diblock copolymers, triblock copolymers, random block copolymers and grafted copolymers (see Figure 2.3b). Homopolymers consist of one type of monomers while the copolymer

---

[iii] The word polymer is a modern form of the Greek word "polymeros", where "poly" refers to many and "méros" to parts ( i.e. the polymers are made of monomers). The term polymer was probably first coined by the Swedish scientist Jöns Jacob Berzelius.

consists of different monomers (monomer A, B,...). The block of a polymer is a small homopolymer consisting of m monomers ($A_m$) sequentially attached. The block copolymer consists of blocks where each block has been attached to form the polymer. The abbreviations for a diblock copolymer and triblock copolymer are: $A_mB_n$ and $A_mB_nA_m$, where m and n are the numbers of monomers of A and B, respectively.
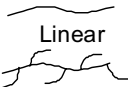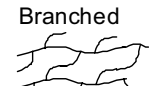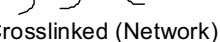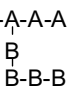
| (a) With respect to structure | (b) With respect to chemical composition | |
| --- | --- | --- |
| Linear | (i)   A-A-A-A-A-A-A-A-A-A-A | Homopolymer |
| Branched | (ii)  A-A-A-A-A-B-B-B-B-B-B | Diblock copolymer |
| | (iii) A-A-A-A-B-B-B-B-A-A-A-A | Triblock copolymer |
| Crosslinked (Network) | (iv) A-B-B-A-B-A-B-A-A-B-B-B | Random copolymer |
| | (v)  A-A-A-A-A-A-A-A-A-A-A-A | Grafted copolymer |
| | B | |
| | B-B-B | |

**Figure 2.3** Non-biological polymers are differentiated with respect to (a) structure and (b) chemical composition.

When a polymer is submerged into a solvent the monomer-monomer, (A-A, B-B and A-B) and the monomer-solvent interactions determine the configuration of the polymer, at dilute polymer concentrations. There are in general three extreme configurations the polymer can adopt: a random coil, a compact sphere and a stiff rod (e.g. the double helix of DNA).

In papers VI and VII of this thesis several different polymers have been investigated. In papers VI diblock copolymers of type poly(ethylene oxide)-poly(B), where B is a bulky hydrophobic monomer was investigated. In paper VII the triblock copolymer poly(ethylene oxide)-poly(propylene oxide)-poly(ethylene oxide) was investigated.

## 2.4. Nonionic triblock copolymers

Nonionic triblock copolymers of the type poly(ethylene oxide)-poly(propylene oxide)-poly(ethylene oxide), are commercial polymers and often referred to by their trade names "Pluronic", "Poloxamers" or "Synperonics". The abbreviation of the triblock copolymer is $EO_mPO_nEO_m$ where m and n are the numbers of ethylene oxide (EO) and propylene oxide (PO) monomers, respectively. This class of block copolymers is well known and has been studied for many years, and there are several reviews about its physical chemical properties in aqueous solution.[19-22] Triblock copolymers are a very useful group of polymers and therefore frequently used in the industry in a variety of

different areas such as in biomedical applications, cleaning applications, paints, etc.

The advantage of the Pluronics is that they can be tuned for specific purposes by changing the PPO/PEO ratio and PEO and PPO block lengths during the synthesis. Thus it is possible to find the optimum composition for a specific application. Physical chemical properties and trends that influences the self-assembly of Pluronics in water are:

1. Increasing the number of n at constant value of m in $EO_mPO_nEO_m$ at constant temperature gives lower CMC values.
2. Increasing the number of n for a constant value of m in $EO_mPO_nEO_m$ at constant concentration gives a lower CMT value.
3. Increasing the number of m at constant value of n in $EO_mPO_nEO_m$ gives the reverse situation to point 1 and 2 gives, i.e. an increase in CMC and CMT, the increase is, however, only moderate.
4. The CMC and CMT values for constant PPO/PEO ratio decrease with increasing molecular weight.

In conclusion, Pluronic self-assembly is mainly influenced by the hydrophobic size, the number of PO monomers (i.e. n).

Water is a poor solvent for the PPO and PEO; more so for PPO. Increasing the temperature means that both PEO and PPO segments will have poorer solubility in water and the polymer will cloud at some temperature and phase separate. The mechanism of the reversed solubility for PEO polymer and EO-containing surfactant with increasing temperature has been analyzed by Karlstöm et al.[23] At low temperature the PEO segment will have a higher probability for conformations that are more polar in comparison to the conformations at higher temperature. At higher temperature the PEO segment (and also the PPO segment) is less polar.

So far we have discussed ideal aspects of the Pluronic. In the real word it is more complicated, due to the fact that Pluronic is polidisperse both in molecular weight and in internal composition (PPO/PEO composition ratio). Whereas the CMC for surfactants is well defined, Pluronics display a broad unimer-to-micelle transition. The unimer-to-micelle transition occurs over a broad concentration range, possibly as much as 10 wt% at constant temperature. Similarly, at constant concentration the transition temperature (CMT) going from unimer-to-micelles is not well defined for Pluronics. The transition often spans a temperature interval of approximately 20 K. The micellization process of Pluronics in water is endothermic and driven by a decrease in the polarity of the PEO and PPO segment during self-assembly.[19, 20, 22] Thus the process is driven by entropy. Finally, it is fruitful to compare Pluronics with traditional nonionic ethoxylated surfactants ($C_xE_y$). The Gibbs free energy of transfer of one PO unit from water to the micelle core is (-0.62±0.12) kJ/mol[22], while the corresponding quantity for a methylene group of $C_xE_y$ is -3.1 kJ/mol.[2]

In paper VII we studied the association process of Pluronic F127 and F68 (see Table 2.5) as a function of concentration, temperature and addition of different inorganic salts with the aid of self-diffusion NMR. Some of the result will be discussed in chapter 7. The aim was to explain and model the effect of polydipersity on the NMR PGSE (see chapter 4) intensities.

**Table 2.5** The triblock copolymers used in this thesis

| Block copolymer | Averaged composition | Nominal molar mass/(g/mol) |
|---|---|---|
| F127[1] | $EO_{97}PO_{68}EO_{97}$ | 12600 |
| F68 | $EO_{76}PO_{29}EO_{76}$ | 8350 |

[1] Definition of the letter number code: The alphabetic letter refers to the physical form of the product; "F" stands for solid forms (flake). The first two digits in the three digit number multiplied by 300 indicate the approximate molecular weight of the hydrophobe. The last digit, when multiplied by 10, indicate the approximate ethylene oxide content in the molecule.

## 2.5 Diblock copolymers, synthesis and basic physical properties

In paper VI we studied the effect of adding diblock copolymers of type A-B, A being poly(ethylenoxide) and B a hydrophobic block (see Table 2.6), to a nonionic bicontinuous microemulsion. The aim was to modify the microemulsion in order to alter its efficiency in the uptake of water and oil. Below is a brief account of the diblock copolymer.

### 2.5.1 Synthesis of diblock copolymer

The polymers were synthesized at Akzo Nobel Surfactants Stenungsund through an anionic polymerization (see reaction scheme 2.1) using a one step mechanism without any solvent, and with KOH as catalyst (for further experimental details see reference 24). Similar products have been synthesized by Allgaier et al.[25] using another approach involving solvent and several reaction steps, and with a lower amount of byproducts. The method developed at Akzonobel Surfactants Stenungsund is however cheaper and does not involve any organic solvent.
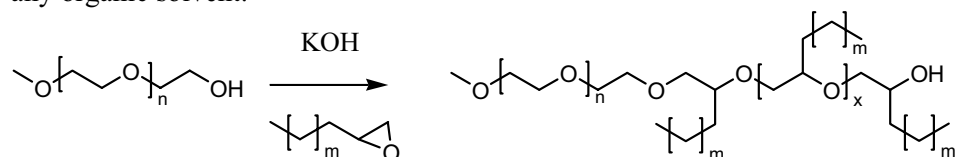


**Reaction scheme 2.1** The synthesis of the diblock copolymers through anionic polymerization, the epoxide is attached to the growing macroion.

The diblock copolymers synthesized are listed in Table 2.6. The polymers contain a polyethylene oxide block, PEO, which is the hydrophilic block. The hydrophobic block is an ethyleneoxide where one of the protons at the carbon close to the oxygen has been replaced by a straight hydrocarbon chain ($CH_2CH(CH_2)_{m+4}O$). The starting material for the hydrophobic part is an epoxide with a hydrophobic tail of m methylene groups. The polydispersity and molecular weight of the polymers was measured by Size Exclusion Chromatography (SEC). For calibration of the SEC in order to determinate the molecular weights of the polymers, polystyrene standards (pts) were used. The polydispersity index ($M_w/M_n$) was found to be between 1.03-1.04 which indicates that the polymers have a rather monodisperse molecular weight distribution. On the other hand there are still significant byproducts from the reaction. The byproducts are primarily homopolymer, i.e. the hydrophobic monomers have self-reacted.

**Table 2.6** The name and molecular weight of the synthesized diblock copolymer used in this thesis.

| Polymer name | Abbreviation | Number of CH$_2$ (m) | M$_w$ [1] (g/mol) | polymer/ homopolymer[3] |
|---|---|---|---|---|
| Methoxy-PEO | M-PEO | ≈113 EO groups | 5128[2] | --- |
| Methoxy-PEO-poly (OctaDecylene Oxide) | PEO-PODO | 14 | 9279 | 54/31+15 |
| Methoxy-PEO-poly (HexaDecylene Oxide) | PEO-PHDO | 12 | 9615 | 64/36 |
| Methoxy-PEO-poly (TetraDecylene Oxide) | PEO-PTDO | 10 | 9974 | 80/20 |
| Methoxy-PEO-poly (DoDecylene Oxide) | PEO-PDDO | 8 | 10085 | 69/31 |
| Methoxy-PEO-poly (Decylene Oxide) | PEO-PDO | 6 | 9008 | 77/23 |
| Methoxy-PEO-poly (Octylene Oxide) | PEO-POO | 4 | 9813 | 68/32 |
| Methoxy-PEO-poly (Hexylene Oxide) | PEO-PHO | 2 | 9417 | 93/7 |
| Methoxy-PEO-poly (Butylene Oxide)[4] | PEO-PBO | 0 | 10000 | --- |

[1] Molecular weight based on a pst standard. [2]Molecular weight based on a PEO standard. [3]It should be noted that it is uncertain if the diblock copolymers and the homopolymers give the same response in the refractive index detector used in GPC. [4]Paper VI.

At room temperature the polymers are in a waxy/solid like state, whereas at higher temperature the polymers melt.

One of the goals for synthesizing these polymers was to create amphiphilic polymers with different physical properties. The solubility was

tested in different solvents (see Table 2.7) at a concentration of 1.5-3 wt% at a temperature of 298 K (and for some samples at 333 K). The polymers are not soluble in water, whereas the solubility in an apolar solvent is significantly higher. The hydrophobic blocks are very bulky and it is probably difficult for them to arrange in closely packed aggregates or micelles, which results in low water solubility. The higher solubility in an apolar media stems from the possibility to form reversed micelles, since the PEO part can pack easier into aggregates. It is also difficult to test the solubility properly due to the fact that there are homopolymers (byproduct) that influences the result. The homopolymers are probably completely insoluble in water. The general outcome from the solubility test is that the polymers have low solubility, except in THF, chloroform and toluene. The polymer was used in a system containing water and n-octane (chapter 6).

**Table 2.7** The solubility of the polymer synthesized at 298 K.

| Polymer | Water | Acetone | Ethyl acetate | Iso-propanol | Chloro form | Toluene | *n*-octane | Acetic acid | THF | Ethanol | *n*-hexane |
|---|---|---|---|---|---|---|---|---|---|---|---|
| PEO-PODO | ±° | - | +° | +° | + | + | ± | +° | + | - | - |
| PEO-PHDO | - | - | +° | +° | + | + | +° | ± | + | ±° | ±° |
| PEO-PTDO | - | - | +° | +° | + | + | +° | + | + | ±° | ±° |
| PEO-PDDO | - | +° | +° | +° | + | + | +° | + | + | ±° | ±° |
| PEO-PDO | ±° | + | +° | +° | + | + | - | + | + | ±° | ±° |
| PEO-POO | - | + | + | +° | + | + | +° | + | + | + | ±° |
| PEO-PHO | +° | + | + | +° | + | + | ±° | + | + | + | ±° |

The solubility tests were performed in glass tubes. The concentrations of polymers were 1.5-3 wt%. Before visual inspection the samples were mixed and equilibrated. + stands for soluble, - for insoluble, ± for turbid solution or dispersion and ° for higher temperatures (i.e. 333 K). The solubility was estimated by visual inspection.

## 2.6 Cyclodextrin

In papers I-V, cyclodextrin (CD) has been extensively used. This paragraph will introduce CD. Cyclodextrin, sometimes called cycloamylose, constitutes a family of cyclic oligosaccharides. The smallest cyclodextrin is composed of 6 α-D-glucopyranoside units linked by 1-4 glucosidic bonds (see Figure 2.4 for molecular structure and a schematic structure). In this section cyclodextrins consisting of 6 (α-CD), 7 (β-CD) and 8 (γ-CD) α-D-glucopyranoside units will be discussed. The general structure of cyclodextrin can be described as a truncated hollow cone (see Table 2.8 for dimensions). The hollow cone of the CD possesses a hydrophobic cavity (or to be correct, a less polar site than the bulk water). The hydrophobic character of the interior cavity of CD gives it the

possibility to encapsulate hydrophobic molecules, which fact has lead to many industrial applications.[26] From the industrial point of view CDs are beneficial in comparison to others molecules of similar capacity. CD is for example easy to synthesize and has rather monodisperse end-products, the raw material is cheap and the degree of possible modifications of the structure is large which makes it possible to tune and optimize the structure to specific applications. Finally, many CDs have been approved by FDA to be used in living organisms.

### 2.6.2 Production of cyclodextrin

Cyclodextrin is made from enzymatic degradation of starch, often a linear $\alpha$-amylase. The enzyme commonly used for production of cyclodextrins is glycosyltransferase (CGTase). The starch is first liquefied and than the CGTase is added. The enzymatic degradation of starch with CGTase produces all CDs ($\alpha$, $\beta$ and $\gamma$), and the ratio of the conversion yield for the different CDs are highly dependent upon the type of CGTase used. To separate the $\beta$-CD one uses the fact that $\beta$-CD is much less soluble than $\alpha$- and $\gamma$-CD so it crystallizes easier. The separation of $\alpha$- from $\gamma$-CD is achieved by a chromatographic separation technique. The CDs crystallize from water as hydrates of varying composition, see Table 2.8.

### 2.6.3 Physicochemical properties of cyclodextrin

The solubility of CD in water is unusual as it shows an irregular trend from $\alpha$-, $\beta$- and $\gamma$-CD. $\beta$-CD is at least ten times less soluble than $\alpha$- and $\gamma$-CD. To understand the anomalous trend in solubility one has to analyze the crystal structure of CD but also the intramolecular bonds in the CD, specially the intramolecular hydrogen bonds between the $\alpha$-D-glucopyranoside units.[27] The enthalpy of solution of the three CDs is similar (see table 2.8), but the entropy of solution for $\beta$-CD is lower in comparison to $\alpha$- and $\gamma$-CD. Therefore, the lower solubility of $\beta$-CD is due to the less favorable entropy gain. Szejtli[27] explained the less favorable entropy for $\beta$-CD as due to complete hydrogen bond network in $\beta$-CD, which are incomplete in $\alpha$- and $\gamma$-CD. There are two "belts" of hydrogen bonds between the $\alpha$-D-glucose units in CD (see Figure 2.4b). The n (n = number of glucose units) primary hydroxyl groups are lined up at the narrow side of the cavity. The secondary hydroxyl groups are lined up at the wide side of the rim. Moreover in $\alpha$- and $\gamma$-CD one of the glucosidepyranoside units is distorted in the secondary hydrogen belt. The consequence of the imperfect hydrogen bonding belt is a more flexible molecule and thereof higher solubility for $\alpha$- and $\gamma$-CD in comparison to $\beta$-CD according to Szejtli.[27] Intramolecular bonds of the type CH··O also exist. The protons C3-H, C5-H and one of the C6-H interact with C1-O-C4.[28]

13
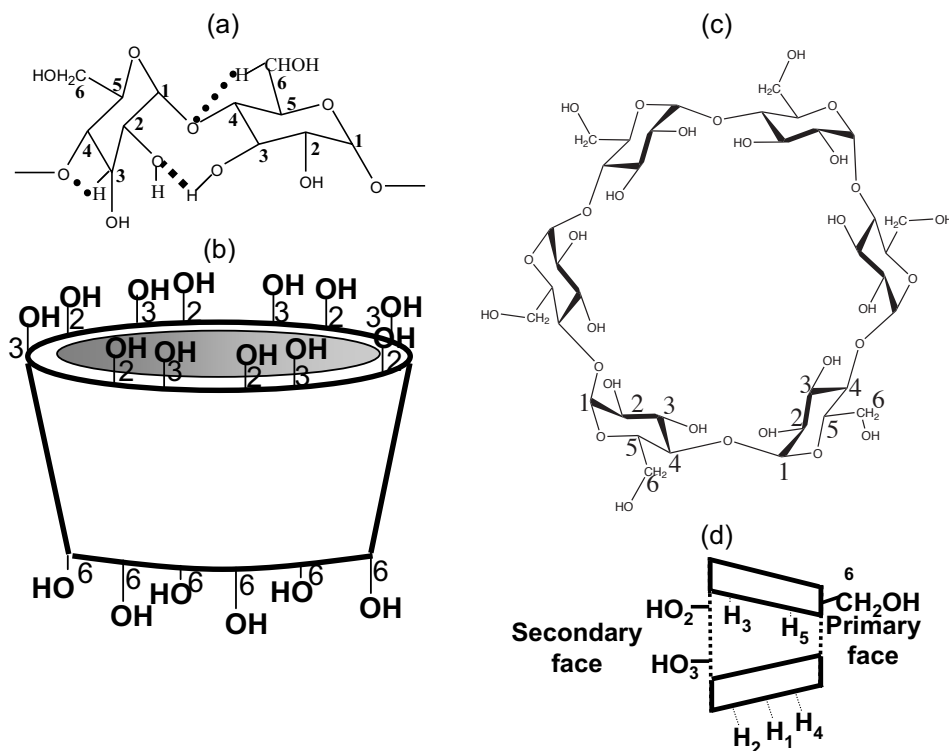
**Figure 2.4** (a) The glycoside units are connected by glycosidic $\alpha$-1,4 bonds. The squared and dotted lines are the hydrogen bonds. (b) Schematic structure of CD showing the position of OH-groups. (c) Chemical structures of $\alpha$-cyclodextrin and (d) schematic illustration of the cyclodextrin, illustrating how the protons are located.

The 1-4 glucosidic bond (C1-O-C4, see Figure 2.4 a and c) hold the $\alpha$-D-glucopyranoside unit together and forms a covalent "belt". The ether bonds plus the two rows of the CH groups arising from the C3 and C5 form the inside of the cavity (see Figure 2.4d). Therefore, the cavity is apolar in comparison to the outer surface of the CD. In the literature it is argued that the cavity environment is comparable or like that of an alcohol solvent or ethylene glycol.[29] The value of the dielectric constant is between 35-55 (there is a great spread of different dielectric constant values in the literature).

The thermodynamic properties of solubilizing the cyclodextrin from a given hydrated state to infinitely dilution are given in Table 2.8. Analyzing the thermodynamic properties, the interesting result is that the entropy of solution of $\beta$-CD is lower than for $\alpha$- and $\gamma$-CD. Therefore a reasonably conclusion would be that the lower solubility in water is driven by the less favorable entropy. The entropy of solubilization has been calculated from the enthalpy of solution and the Gibbs free energy of solution.[30, 31]

**Table 2.8** Physical hemical properties of CD at 298 K if not stated otherwise. Table 2.8 based on references. [27, 29-31]

| Property | α | β | γ |
|---|---|---|---|
| Formula [1] | $C_{36}H_{60}O_{30}$ | $C_{42}H_{70}O_{35}$ | $C_{48}H_{80}O_{40}$ |
| No. of glucose unit, n | 6 | 7 | 8 |
| $M_w$ /(g/mol) [1] | 972 | 1135 | 1297 |
| Solubility in $H_2O$/(g/l solvent) | 145 | 18.5 | 232 |
| Solubility in $H_2O$/(mol/l) | 0.1211 | 0.0163 | 0.168 |
| Outer diameter cavity of wide side/(Å) | 13.7 | 15.3 | 16.9 |
| Inner diameter cavity of wide side/(Å) | 5.7 | 7.8 | 9.5 |
| Volume of cavity/(Å$^3$) | 174 | 262 | 427 |
| Volume of cavity/(mol/ml) | 104 | 157 | 256 |
| Volume of cavity/(gram/ml) | 0.10 | 0.14 | 0.20 |
| Cavity length/(Å) | 7.9±0.1 | 7.9±0.1 | 7.9±0.1 |
| Water molecules in cavity | 2 | 6 | 8.8 |
| Water of crystallization (total)[2] | 6 | 11-12 | 7-18 |
| $\Delta_{sol}H_m^\infty$ /(kJ·mol$^{-1}$)[3] | 27.52 ± 0.43 | 29.48 ± 0.38 | 32.15 ± 0.50 |
| $\Delta_{sol}G_m^\infty$ /(kJ·mol$^{-1}$)[3] | 14.98 | 20.12 | 13.97 |
| $\Delta_{sol}S_m^\infty$ /(kJ·mol$^{-1}$)[3] | 42.5 | 31.4 | 61.0 |
| D/($10^{-10}$ m$^2$s$^{-1}$) at 313.2 K | 3.443 | 3.224 | 3.000 |
| Densities/(g/cm$^3$)[4] | 1.037 | 1.004 | 1.069 |

[1] Refers to anhydrous state. [2] Water of crystallization = water molecules in cavity + water molecules distributed on the outside of the cavity. [3] Refers to the process CD(s, equilibrium with its saturated aqueous solution) → CD(infinitely dilute aqueous solution). [4] The density of glucose is 1.580 g/cm$^3$.

Bonini et al.[32] (see also other references in[32]) measured DLS, Static Light Scattering and Transmission Electron Microscopy at Cryogen temperature (Cryo-TEM) and found that β-CD self-assembled at concentrations as low as 3 mM. The aggregate formed had a hydrodynamic radius of at least 90 nm. The shape of the aggregate formed was dependent on the concentration and both disks and sheets were observed. From NMR experiments by our group and others (Winner et al.[33]), we concluded that if aggregation occurred it was only in trace amounts below the detection limit for our equipment. No alterations in chemical shifts or broadening of the line-width of the peaks were observed. Moreover, the self-assembly of CD is clearly less stable than the aggregate formed by normal surfactants. In paper I-V where we study the host guest interaction of CD with surfactants the possible self-assembly of CD has been neglected.

The diffusion behavior for the different CDs at 298 K was measured with self-diffusion NMR, see Figure 2.5. The self-diffusion is, to good approximation, constant for β-CD in the small concentration interval possible for study. The α-CD and γ-CD self-diffusion decreases at higher concentrations. The diffusion at high concentrations of α- and γ-CD is influenced by the fact

that the CD molecules obstruct each other. Linear fits to the diffusion data (self-diffusion coefficient versus volume fraction CD) were performed giving the following equations (see also ref [34]).

$$D_{\exp,i-CD} = D^0_{i-CD} (1 - k \cdot \phi_{i-CD}) \tag{2.2}$$
$$3.0 \cdot 10^{-10} (1 - 2.1 \cdot \phi_{\alpha-CD})$$
$$2.7 \cdot 10^{-10} (1 - 2.5 \cdot \phi_{\beta-CD})$$
$$2.5 \cdot 10^{-10} (1 - 2.7 \cdot \phi_{\gamma-CD})$$

where $k$ is the slope in a plot of self-diffusion coefficient versus volume fraction of $i$-CD ($\phi_{i\text{-CD}}$) divided by $D^0_{i-CD}$. For calculation of the CD volume, $V_{CD}$, the densities at 298 K have been used (see table 2.8). It should be noted that we assume that the cavity is fully occupied with water.
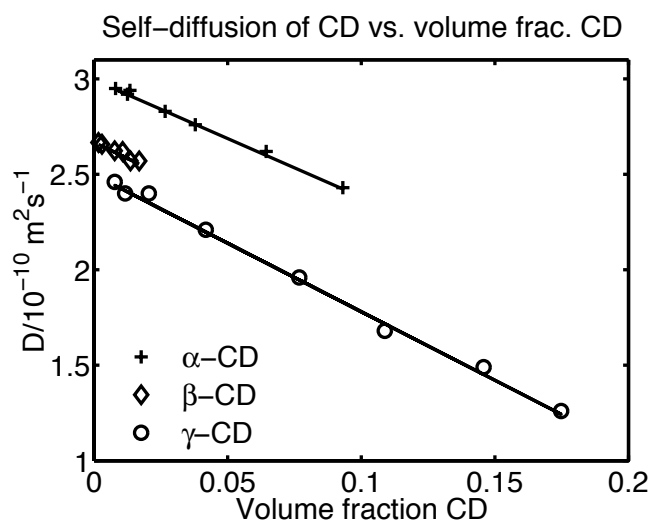


Figure 2.5 Self-diffusion coefficients versus volume fraction of cyclodextrin.

16

# 3. Nuclear Magnetic Resonance

The aim of this chapter is to introduce the NMR technique. To fully understand NMR one needs to treat it on the level of quantum mechanics. The approach used here will be on the semi-classical level, but for a more in-depth description I recommend the following books by Callaghan[35], Levitt[36] and Abragam.[37] The part written here about the basics of NMR is based on information from the books by Levitt[36], Harris[38], and Atkins.[39]

One definition of Nuclear Magnetic Resonance spectroscopy (NMR) is; *the interaction between radiofrequency electromagnetic radiation and atomic nuclei in a magnetic field*. Or to put it in other words: *NMR involves the energy of a nucleus when the nucleus is placed in a magnetic field, and the excitation i.e. the transitions between the different energy levels, occurs in the radio region.*

## 3.1 The spin of an atom

Magnetic nuclei posses an intrinsic angular momentum known as spin. The total spin angular momentum, **I**, is a vector and its magnitude and orientation in space are quantized in an external magnetic field. The magnitude of the spin angular momentum is given by

$$|\mathbf{I}| = [I(I+1)]^{1/2}\hbar, \qquad I = 0, \frac{1}{2}, 1, \frac{3}{2}, ... \qquad (3.1)$$

where $I$ is the spin quantum number and is either integral or a half-integral and is determined by the number of unpaired protons and neutrons. For example the isotope $^{12}C$ has an even numbers of protons and neutrons, giving a net spin angular momentum of zero. A nucleus with odd numbers of protons and neutrons e.g. $^{13}C$ posses a spin angular momentum, $I > 0$. The constant $\hbar$ is $h/2\pi$, where $h = 6.6262\cdot10^{-34}$ Js is known as Planck's constant. Since the spin angular momentum is a vector property a full description requires specification of the direction. Another quantum number $m_I$ is used to specify the direction of the angular momentum, **I**. The number of projections of the spin angular momentum onto an arbitrarily chosen axis is $2I+1$. The z component of **I** is called $I_Z$.

$$I_z = \hbar m_I, \qquad m_I = -I, -I+1, ..., I-1, I \qquad (3.2)$$

17

(a)

$m_I = +1$

$m_I = 0$

$m_I = -1$

(b)

$I_z = \hbar m_I$

$\theta$

$|\mathbf{I}|$

$m_I = +1,\ I = 1$
$I = \hbar 2^{\frac{1}{2}} = 1.5 \cdot 10^{34} Js$
$I_z = \hbar m_I = 1.1 \cdot 10^{34} Js$
$\cos \theta = m_I/[I\ (I{+}1)]^{\frac{1}{2}}$
$\theta = 40.5°$

$$|\mathbf{I}| = \hbar[I(I+1)]^{1/2}$$
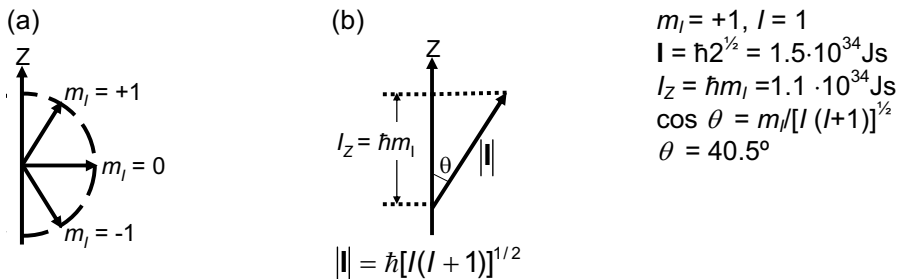
**Figure 3.1** (a) Angular momentum with spin quantum number of 1, in a magnetic field. Illustration of the possible space orientations on the z-axis. (b) An example showing the use of the quantum number $I$ ($I$=1) and $m_I$ ($m_I$ = +1).

## 3.2 The magnetic moment

Any motion of a charged body causes a magnetic field[iv]. Therefore nuclei with $I$ >0 have an associated magnetic moment, **μ**, which is a vector property. The magnitude and orientation are both quantized. The magnetic moment and the nuclear spin angular momentum are closely related by the proportionality constant, $\gamma$, called the gyromagnetic ratio (unit: $T^{-1}s^{-1}$) the value of which depends on the nuclei. The magnitude of **μ** is given by

$$|\mathbf{\mu}| = \gamma|\mathbf{I}|, \qquad\qquad \mu_z = \gamma I_z \qquad\qquad (3.3)$$

where $\mu_z$ is the z component of **μ** and $I_z$ is the z componet of **I**.

## 3.3 Nuclei in a magnetic field

In the absence of an external magnetic field the orientation of the isolated spin is random, and is independent of the spin quantum number $m_I$. The energy levels are degenerate in the absence of an external magnetic field. In a magnetic field, **B,** the energy levels of the spin split up. The quantization of the total spin angular momentum implies that only certain energy levels of the spin are allowed. The energy $E$ in a magnetic field is given by the magnetic moment

$$E = -\mathbf{\mu} \cdot \mathbf{B}_0, \qquad\qquad E = -\mu_z \cdot B_0 \qquad\qquad (3.4)$$

where $\mathbf{B}_0$ are the magnetic field parallel to z (a vector property) and $B_0$ is its magnetic strength, $\mu_z$ is the z component of **μ** (the projections of **μ** onto $\mathbf{B_0}$). Figure 3.2 illustrates the relationship between the magnetic field $\mathbf{B}_0$ (along z-direction) and the nuclear magnetic moment, **μ**.

---

[iv] The SI unit of magnetic field is Tesla, T. Sometimes the unit Gauss, G, is used, for magnetic field ($10000G = 1T$).

(a)                                        (b)



**Figure 3.2** (a) The interaction of the static magnetic field with the magnetic moment, and the projection of the magnetic moments z component onto **B**$_0$. (b) Coordinate system defined according to the time independent static magnetic field, **B**$_0$.

Combing equations 3.2, 3.3 and 3.4 gives the following equation:

$$E = -\gamma \hbar m_I B_0 \qquad\qquad (3.5)$$

There are $(2I+1)$ non-degenerate energy levels for the spins. The transitions between the levels can be induced by electromagnetic radiation of frequency, $v$, with a value obtained from $\hbar \gamma B_0 = vh$. Figure 3.3 illustrates the nuclear spin energy levels for one nuclei with spin $I = 3/2$ as a function of an external magnetic.
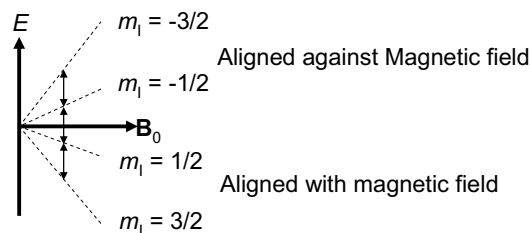


**Figure 3.3**. The nuclear spin energies for a spin nuclei with spin quantum number $I = 3/2$, plotted as a function of the magnetic field, **B**$_0$. There are four energy levels but only three transitions are allowed according to the selection rule of NMR, $\Delta m_I = \pm 1$ (transitions are only allowed between adjacent energy levels).

## 3.4 Spin precession

A compass needle aligns to the earth's magnetic field[v]. Spin polarization does not behave as a compass needle; it starts to move around the magnetic field and produces a torque which tends to align with the magnetic field.

$$d\mathbf{I} / dt = \boldsymbol{\mu} \times \mathbf{B} \qquad\qquad (3.6)$$

---

[v] The Earth magnetic field is between 0.3-0.6 Gauss depending where you are on earth. The earth magnetic field is weak in comparison to the NMR magnetic field which is typically of order $10^4$-$10^5$ G.

Combining equations 3.3 and 3.6 gives equation 3.7.

$$d\boldsymbol{\mu} / dt = \boldsymbol{\mu}\gamma \times \mathbf{B} \qquad (3.7)$$

Equation 3.7 gives is a new torque that is a change of an already existing angular momentum. Equation 3.7 holds for both a time dependent and a constant magnetic field. For a static constant magnetic field (for example $\mathbf{B}_0$), the net result of equation 3.7 is a constant rotation of the magnetic moment in a cone-like fashion around the magnetic field (see Figure 3.4). The traditional comparison is the spinning top in the earth's gravitational field. The rotation of the magnetic moment (the spins) is called precession and its angular frequency is known as the Larmor frequency, $\omega_0$ (unit: radians per second).

$$\omega_0 = B_0\gamma \qquad (3.8)$$
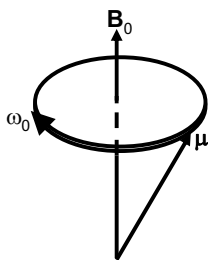


**Figure 3.4** Precession of a magnetic moment, $\mu$, in a static magnetic field, $\mathbf{B}_0$ with Larmor frequency $\omega_0$. The magnetic moment could be replaced by the macroscopic magnetic magnetization, $\mathbf{M}$. Here it is assumed that $\gamma$ is positive, as for protons.

## 3.5 Boltzmann distribution of the spins

NMR spectroscopy measures the average properties of macroscopic samples, containing n number of spins. A spin $I = \frac{1}{2}$ will have two orientations ($m_I = +\frac{1}{2}$ and $m_I = -\frac{1}{2}$) and, two energy states ($m_I = +\frac{1}{2}$, the $\alpha$-state and $m_I = -\frac{1}{2}$, the $\beta$-state). The state $\alpha$ has lower energy than the $\beta$ state. The ratio between the numbers of the spins in the different states is given by the Boltzmann distribution

$$n_\alpha / n_\beta = e^{-(\Delta E / k_B T)}$$

$$\qquad (3.9)$$

$$n_\alpha - n_\beta = \Delta n_0 \approx n\Delta E / 2k_B T = n\gamma\hbar B_0 / 2k_B T \qquad (\text{If } \Delta E \ll k_B T)$$

20

where the number of spins in the energy states $\alpha$ and $\beta$ is denoted $n_\alpha$ and $n_\beta$, respectively. The total number of nuclei (spins) is denoted $n$, and $\Delta n_0$ is the difference in number of spins at thermal equilibrium (the subscript zero in $\Delta n_0$ refers to the equilibrium situation). $T$ is the absolute temperature and $k_B$ is the Boltzmann constant, $k_B = 1.3807 \cdot 10^{23}$ JK$^{-1}$. 9.4 T is a typical magnetic field used in $^1$NMR. At 300 K such a field results in a value of $\Delta E/k_B T = 6.5 \cdot 10^{-5}$. Thus, the thermal energy dominates, and the population difference is very small. In this case $\Delta n_0 = n \cdot 3.1 \cdot 10^{-5}$ (one part in 32000). Nonetheless it still possible to use NMR since one has a very large number of particles (in the order of $10^{23}$).

The total magnetic moment, **M**, is a macroscopic magnetization vector of the sample, a result of the summation of all the $n$ individual magnetic moments. The thermal equilibrium magnetization, $M_0$, in a constant static magnetic field with magnetic field strength $B_0$ is given by

$$M_0 = \frac{n\gamma^2 \hbar^2 I(I+1)B_0}{3k_B T} \tag{3.10}$$

Equation 3.10 tells us four important things:

i) The magnetization increases with an increase in the static magnetic field, resulting in a stronger NMR signals.

ii) The magnetization decreases with temperature. Thus the NMR signal decreases as $T$ increases.

iii) The magnitude of the magnetization is directly proportional to the number of particles, i.e. NMR is quantitative.

iv) The magnetization increases with the gyromagnetic ratio.

## 3.6 Radiofrequency pulses

The separation between the energy states of the spins is very small, much smaller than the thermal energy (see section 3.5) i.e. the energy needed to excite the spin from the ground state to the excited state is very small. The frequency or the energy of a radio transmitter happens to be of the correct magnitude. For an NMR spectrometer the frequency is in the range of $\omega = 10^7\text{-}10^9$ Hz ($\lambda = 1\text{-}100$ m). Thus, the energy difference is in the order of $\Delta E = 4\text{-}4000$ mJ. An oscillating electromagnetic pulse of a certain duration time, $t$, is used to excite the spins. The magnetic part of the electromagnetic radiation pulse is called **B**$_1$ and in an experiment the pulse is often referred to as a radio frequency (rf) pulse. When the rf pulse frequency matches the energy difference between the spin states, resonance is achieved. The **B**$_1$ pulse is applied perpendicular to the static magnetic field, i.e. in the xy-plane. The **B**$_1$-field is small in comparison to the **B**$_0$-field. One can treat the effect of **B**$_1$-field on the magnetization with two different mathematical formalisms, in the "laboratory frame of reference" (solve

the time dependent equation) or in the "rotating frame of reference". In the rotating frame of reference a new coordinate system is introduced rotating with the frequency of the $\mathbf{B}_1$-field. In the rotating frame of reference the $\mathbf{B}_0$-field vanishes and $\mathbf{B}_1$ is stationary upon resonance. The mathematics gets simpler in the rotating frame of reference, and instead of having time dependent precession of the magnetization one gets a relative precession.

The evolution of $\mathbf{M}$ is given by equation 3.11 (cf. with equation 3.7), treated within the laboratory frame of reference.

$$d\mathbf{M}/dt = \left[\mathbf{B}_0 + \mathbf{B}_1(t)\right] \times \gamma \mathbf{M} \tag{3.11}$$

The position and magnitude in the xy-plane of the $\mathbf{B}_1(t)$ field are given by $B_1\cos(\omega t)\mathbf{i} + B_1\sin(\omega t)\mathbf{j}$, where $\mathbf{i}$ and $\mathbf{j}$ are unit vectors in the x- and y-direction, respectively.

Two important flip angles are the 90º and 180º-pulses. If an rf pulse is applied in the x-direction these flip angles rotates the magnetization from z to y and from z to -z, respectively. The pulse length is in the order of 1-100µs. The 90º pulse disrupts the system in such a way that the energy levels become equally populated. The 180º pulse inverts the spin population.

## 3.7 NMR relaxation

After the magnetization of a system has been pertubated by an external field, $\mathbf{B}_1$, it approaches Boltzmann equilibrium, through a relaxation mechanism with characteristic time constants. In NMR, one discriminates between two relaxation times: the longitudinal relaxation time (along the z-axis) denoted $T_1$, and the transverse relaxation time denoted $T_2$ (in the xy-plane). The total magnetic field acting on a sample is given by equation 3.12 (in the laboratory frame) is

$$\mathbf{B} = B_1 M_y \cos\omega t\, \mathbf{i} + B_1 M_x \sin\omega t\, \mathbf{j} + B_0 \mathbf{k} \tag{3.12}$$

where $\mathbf{i}$, $\mathbf{j}$ and $\mathbf{k}$ are the unit vectors in the x, y and z direction. Using equation 3.11 and 3.12 and taking the longitudinal and transverse relaxation into account one ends up with the Bloch equations.

$$dM_x/dt = \gamma(B_1 M_z \sin\omega t + B_0 M_y) - M_x/T_2$$
$$dM_y/dt = -\gamma(B_0 M_x + B_1 M_z \cos\omega t) - M_y/T_2 \tag{3.13}$$
$$dM_z/dt = -\gamma(B_1 M_y \cos\omega t + B_1 M_x \sin\omega t) - (M_z - M_0)/T_1$$

The solution to the coupled differential Bloch equations after a $90^\circ_x$ pulse is of special interest (turning the equilibrium magnetization to the y-direction) and gives the following magnetization.

$$M_x = M_0 \sin(\omega_0 t) \exp(-t/T_2)$$
$$M_y = M_0 \cos(\omega_0 t) \exp(-t/T_2) \qquad\qquad (3.14)$$
$$M_z = M_0[1 - \exp(-t/T_1)]$$

Transitions between the energy states are not spontaneous; they must be induced. Magnetic noise (or magnetic interactions) caused by molecules, is one source for triggering both $T_1$ and $T_2$ relaxation. Dipolar-dipolar interactions between molecules causes nuclear spins to experience time-dependent local magnetic fields which may contain a component of the right NMR frequency ($\omega_0$) to induce transition and bring the spins to equilibrium. Other sources are for example shielding anisotropy, scalar interactions, spin rotation and interaction with unpaired electrons.[38]

## 3.8 Chemical shift

The Larmor frequency of a given nucleus is proportional to the total magnetic field denoted $\mathbf{B}_{loc}$ at the nucleus. The assumption that the applied $\mathbf{B}_0$ is the magnetic field that every nuclei experience is not correct, because all molecules have charges, electrons and protons, which cause tiny local fluctuating magnetic fields. For example the electron motion tends to shield the nucleus ($\mathbf{B}_{loc} < \mathbf{B}_0$). It is convenient to define a dimensionless shielding constant, $\sigma$, which can be both positive and negative. The resulting frequency $\omega_{tot}$ is given by equation 3.15.

$$\omega_{tot} = \gamma B_0 (1 - \sigma) \qquad\qquad (3.15)$$

The strength of the resulting total magnetic field experienced by a nucleus is complex and depends on details of the electronic structure in the nearby environment. As a result nuclei in different chemical groups or different environments have different shielding constants.

## 3.9 Signal detection, time domain and frequency domain

In an NMR experiment the sample is placed in the static magnetic field inside the rf-coil. The $\mathbf{B}_1$-field is then turned on for a time $t$, which creates magnetization in the xy-plane. The $\mathbf{B}_1$-field is turned off, and the magnetization starts to relax back to Boltzmann equilibrium. The signal detected is caused by the signal from both $M_x$ and $M_y$ (see equation 3.14), i.e. the transverse magnetization. The same rf-coil is used for detection as was used for excitation.

The rotation of the magnetization around the $\mathbf{B}_0$-field will produce an electromotive force (emf). The signal in the time domain is called the Free Induction Decay (FID), see Figure 3.5a. Normally the system contains more than one spin, i.e. the observed signal is complex and consists of several oscillating exponentially decaying signals. The standard way to analyze the FID is to perform a numerical Fourier Transform (FT). The FT picks out the frequencies of the different oscillating signals. The result of a FT is a frequency spectrum, i.e. the conventional NMR spectrum (see Figure 3.5b). If the time domain signal exponentially decays with time, the corresponding FT gives a Lorentzian line shape in the frequency domain.
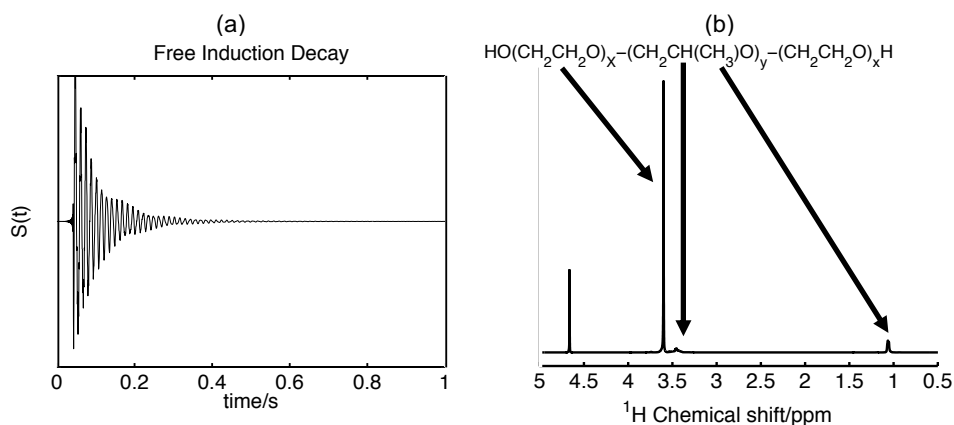


**Figure 3.5** (a) FID of a 1 wt% Pluronic F127 polymer at 298.2 K in $D_2O$ recorded at a NMR 500 MHz spectrometer and (b) Fourier Transform of the FID, the spectrum. The left peak is due the residual protons in $D_2O$.

## 3.10 The time scale of NMR: from fast to slow exchange times

Molecular systems change structures over a wide range of time scales. For example, a surfactant in a micelle (see chapter 2) is in dynamic equilibrium with the surfactant monomer in the bulk solution. Another example of a dynamic structure is the "host-guest" complex formed between cyclodextrin (CD) and surfactant molecules (see chapter 5) that under normal conditions form and break up quickly. The time scale of NMR refers to the rates of chemical (physical) processes that can be measured with NMR. The time scale is important in NMR and contains important information of the investigated system. The NMR time scale of events will be defined here, and is divided in three regions; fast, intermediate and slow exchange.

### 3.10.1 Slow exchange rate

We consider a 2-site exchange process in which A and B represent two sites (see Figure 3.6) each having a unique chemical shift value, $v_A$ and $v_B$,

respectively. The difference in chemical shift is $\Delta v_{AB}$. The time of exchange, $\tau_{ex}$, is then compared to the inverse of the frequency difference of interest. In the case of slow exchange, the exchange is slow in comparison to the inverse difference in chemical shift, $\tau_{ex} \gg (\Delta v_{AB})^{-1}$. The line widths of the peaks are narrow and the area of each peak A and B give the fraction of molecules in state A and B, respectively.

**What is the time scale of exchange?**



$$K = \frac{k_{on}}{k_{off}}$$

$k_{on}$ and $k_{off}$ are rate constants
$K$ is the equilibrium constant

**Guest**
(e.g. ligand
drug
surfactant)

**Host**
(e.g. protein
cyclodextrin
micelle)
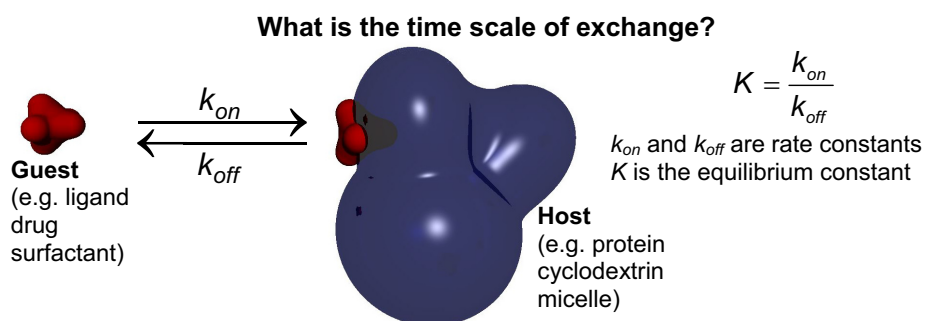
**Figure 3.6** Schematic illustration of a 2-site exchange process in which A and B represents two sites of the guest, free and bound.
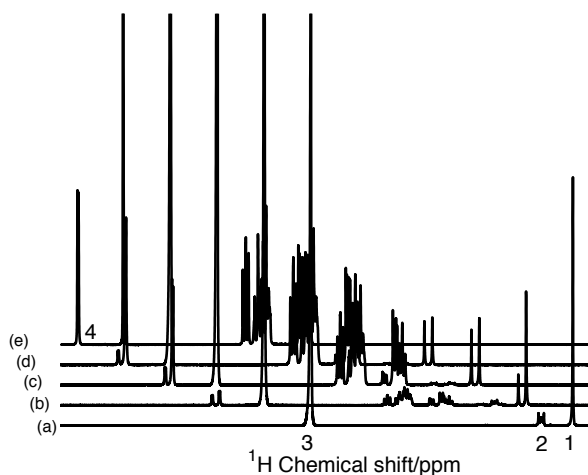


**Figure 3.7** Proton spectra from bottom to top: (a) pure $B_{10}$ at 1.0 mM, (b) $r = 1$, (c) $r = 5.5$, (d) $r = 9.8$ and (e) is pure $\alpha$-CD. $r$ is defined as $r \equiv [\alpha\text{-CD}]/[B_{10}]$. All samples prepared in $D_2O$ and measured at 298 K with a 500 MHz NMR spectrometer. The numbers in the figure denote the following peaks, 1 is $N(CH_3)_3$, 2 is $NCH_2$, 3 is the $H_2O$ peak and 4 is the $H_1$ peak of $\alpha$-CD (see Figure 2.4 d).

An example of slow exchange is the host-guest complex formed between $\alpha$-CD and the surfactant, $B_{10}$ (see Table 2.3). There are two distinctly separate resonances, one for the "free state" and one for the "bound state". Two different states are found for all the protons of the host and guest molecules (see Figure 3.7 for proton spectra), i.e. there are twice as many peaks in the spectrum of

both components compared to spectra where each component is treated separately.

A simple model for calculating the equilibrium constant, $K$, can be used when the exchange between the guest and host and its complex is slow

$$CD + S \rightleftharpoons CD - S \qquad K = [CD - S]/([CD][S]) \qquad (3.16)$$
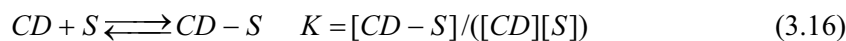
where $[S]$, $[CD]$ and $[CD\text{-}S]$ are the concentrations of surfactant, cyclodextrin and the complex, respectively. The proton NMR spectra in Figure 3.7 are considered in this discussion. The areas ($A$) under the peaks of the free ($A_f$) and bound ($A_b$) states are proportional to the concentration of free, $C_f$ and bound molecule $C_b$. The sum of the areas $A_{tot}$ of the free and bound states of the molecules are proportional to the total concentration, $C_{tot}$ ($[S]_{tot}$ and $[CD]_{tot}$ for surfactant and cyclodextrin, respectively). The resulting equations follow here

$$r = [CD]/[CD - S] = [A_f]/[A_b] \qquad (3.17)$$

$$[CD]_{tot} = [CD] + [CD - S] \qquad (3.18)$$

$$[S]_{tot} = [S] + [CD - S] \qquad (3.19)$$

$$[CD]_{tot} = r[CD - S] + [CD - S] = [CD - S](1 + r) \qquad (3.20)$$

$$[CD - S] = [CD]_{tot} /(1 + r) \qquad (3.21)$$

$$[CD]_{tot} = [CD] + [CD]_{tot} /(1 + r) = [CD](1 + 1/r) \qquad (3.22)$$

$$[CD] = [CD]_{tot} r /(1 + r) \qquad (3.23)$$

$$[S] = [S]_{tot} - [CD]_{tot} /(1 + r) \qquad (3.24)$$

Replacing the concentrations in equation 3.16 with the corresponding areas and total concentration gives

$$K = (1 + r) / \left( r([S]_{tot} (1 + r) - [CD]_{tot} ) \right) \qquad (3.25)$$

Thus the equilibrium constant can be calculated directly from the NMR spectrum by integrating the peaks of bound and free host molecule.

### 3.10.2 Intermediate exchange time

In the intermediate exchange time regime the NMR spectrum is more complex. The peaks of the intermediate exchanging species are significantly broadened which often leads to overlap.

### 3.10.3 Fast exchange time

In this case the exchange time is fast compared to the inverse chemical shift, $\tau_{ex}<<(\Delta\nu_{AB})^{-1}$. The observed chemical shift, $\delta_{obs}$, is one sharp signal at the weighted average of the individual resonances.

$$\delta_{obs} = P_A\delta_A + (1-P_A)\delta_B \qquad\qquad (3.26)$$

$P_A$, $P_B$, are the molar fraction of component $A$ and component $B$, and $\delta_{obs}$, $\delta_A$ and $\delta_B$ are the observed chemical shift, chemical shift of component $A$ and chemical shift of component $B$.

## 3.11 Determination of the $T_1$ relaxation times
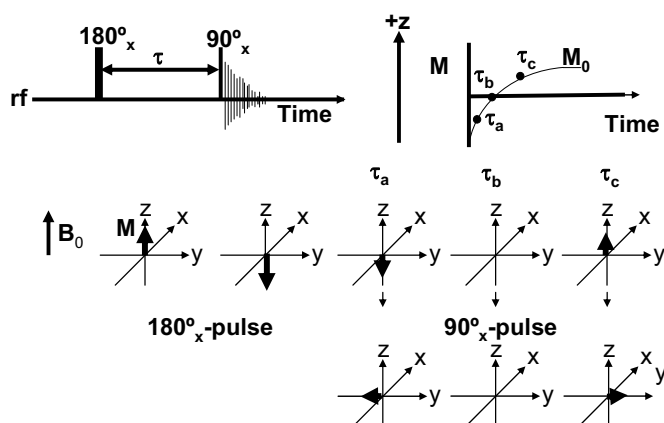


**Figure 3.8** Principles of an IR experiment.

The first report about $T_1$ measurements was made by Bloembergen et al.[40] $T_1$ relaxation times are normally measured with an Inversion Recovery (IR) experiment. The pulse sequence used is 180º-$\tau$-90º-fid (Figure 3.8). The 180º pulse inverts the equilibrium magnetization, $M_z$ from the positive z direction. As a result of longitudinal relaxation, the value of $M_z$ increases with time, $\tau$. This has been illustrated in Figure 3.8. After the time $\tau$ a 90º pulse is applied to detect the magnetization at time $\tau$. The IR experiment is performed as a function of $\tau$. The FID is Fourier transformed and the intensity, $I(\tau)$, of the different peaks are proportional to $M_z(\tau)$. Equation 3.27 is the solution to the Block equation after a 180º pulse.

$$M_z(\tau) = M_0[1 - 2\exp(-\tau/T_1)] \qquad (3.27)$$

## 3.12 Determination of the $T_2$ relaxation times

Magnetic moments interact with each other, (see section 3.7) causing a decrease in the transverse magnetization after the 90º pulse. Furthermore, magnetic inhomogeneities in the $\mathbf{B}_0$-field also cause the transverse magnetization to decrease. In order to increase the $\mathbf{B}_0$-field homogeneity in the sample volume, "shimming" is performed. Shimming is a standard technique used to minimize the magnetic inhomogeneities in the $\mathbf{B}_0$-field.[41] The $T_2^*$ relaxation is the total transverse relaxation, where inhomogeneities of the $\mathbf{B}_0$-field and genuine, $T_2$, relaxation are included.

$$\left(T_2^*\right)^{-1} = \left(T_2\right)^{-1} + (\text{effects due to the inhomogenity in } \mathbf{B}_0) \quad (3.28)$$

The line-widths of the peaks in an NMR spectrum are proportional to $1/T_2^*$. Thus spin-bearing molecules with short $T_2$ values give broad peaks in an NMR spectrum. In order to measure genuine $T_2$ an NMR pulse technique called spin echo (or sometimes Hahn echo) is used. This technique was invented by Hahn[42] and first modified by Purcell et al.[43] and later by Meiboom et al.[44] One of the simplest pulse sequences used for $T_2$ measurements is the $90º_x$-$\tau$-$180º_y$-FID (Figure 3.9). A $90º_x$ pulse is applied and a signal is formed which decays with $T_2^*$. After a delay time $\tau$ a $180º_y$ pulse is applied. The purpose of the $180º_y$ is to remove effects due to inhomogeneities in the $\mathbf{B}_0$-field. After an additional time $\tau$, the spins have refocused and a signal echo appears. The $T_2$ experiment is performed as a function of $\tau$ and the magnetization ($M_{xy}$) at the top of the echo ($2\tau$) is recorded and Fourier transformed.

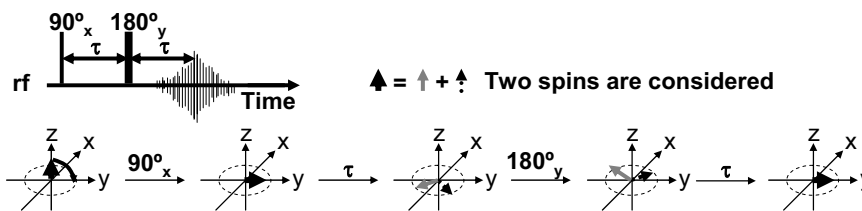$$M_{xy}(\tau) = M_0\exp(-2\tau/T_2) \qquad (3.29)$$



**Figure 3.9** Principles of the spin echo experiment. Two spins are introduced in the figure. Two spins with different Larmor frequencies relative to the rotating frame of reference are shown.

28

# 4. Diffusion experiments and models

In this section the focus will be on the details of the self-diffusion NMR experiments. The basic theory of diffusion, dynamics of colloidal aggregates and the diffusion model developed for the host-guest interaction are included in this chapter.

## 4.1 Diffusion
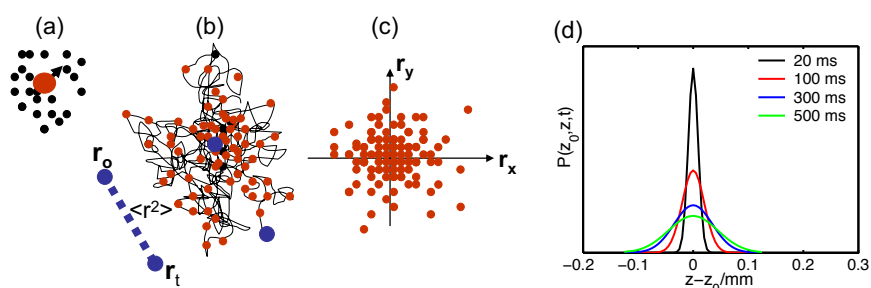


**Figure 4.1** (a) Micro-event in an isotropic solution. Particles collide due to internal kinetic energy and cause particles to diffuse randomly. The black colored particles collide with the red colored ones and push them in a random direction. (b) The trajectory of a random moving particle (red colored), the blue colored dots indicate $r_0$ (the position at $t = 0$) and $r_t$ (the position at time = $t$). The effective distance moved in two dimensions is given by $<r^2> = 4Dt$, $D$ is the self-diffusion of the particle and $t$ is the diffusion time. (c) The position of random moving particles in two dimensions after a time $t$, with start position at the origin. (d) The probability distribution $P(z_0, z, t)$ that a particle moves a distance $\Delta z$ during time $t$ (see equation 4.2).

Diffusion is a fundamental process occurring in chemical and biological systems and often governs the rate of a chemical reaction. The term diffusion is derived from the Latin verb "diffundere" which means to "spread out". The mechanism of diffusion is Brownian motion[vi]. In a liquid at constant temperature, particles move in a random fashion (Figure 4.1). It is the inter-particle collisions driven by internal kinetic energy that give rise to these random motions. The average distance a molecule travel between collisions is characterized by the mean free paths, $\lambda$. In a liquid the typical value of $\lambda$ is approximately the diameter of the particles; for example for water $\lambda$ is approximately 300 pm and the collision time between the particles, is of the order of ps. The Einstein-Smoluchowski equation 4.1[39] is the link

---

[vi] Brownian motion: The botanist Robert Brown reported in 1828 that pollen grains ($\mu$m) suspended in a water solution observed under microscopy moved in a very irregular, zigzag fashion (random). *Definition* Brownian motion: "the random movement of microscopic particles suspended in a fluid"

between the macroscopic and the microscopic world, which relates the diffusion coefficient to the step length, $l_{step}$ and the time it takes to jump one step length, $\tau$

$$D = l_{step}^2 / 2\tau \tag{4.1}$$

where $D$ is the diffusion coefficient. For water at 298 K with $D = 2.0 \cdot 10^{-9}$ m$^2$s$^{-1}$, and $l_{step} = 300$ pm, the time step is calculated to $\tau = 20$ ps. Because $\tau$ is the time it takes to jump one step length, water can make $5 \cdot 10^{10}$ jumps per second.

## 4.2 The propagator

The propagator describes the probability for a particle to translate from one position $z_0$ to another position $z$ in a given time, $t$ (see Figure 4.1). The propagator for an isotropic homogeneous solution in one dimension is given by equation 4.2. It is Gaussian since it is a sum of many randomly moving particles (due to the central limit theorem[vii]).[45]

$$P(z_0, z, t) = (4\pi Dt)^{-1/2} \exp(-(z - z_0)^2 / 4Dt) \tag{4.2}$$

In an isotropic homogeneous solution the propagator is independent of the history. If there is no external force (e.g. thermal, concentration, or pressure gradients) acting on the particles the displacement is zero, since movements in all directions are equally probable. The mean square displacement in one dimension, $<z^2>$, on the other hand is non-zero and is given by the classical Einstein relation.

$$\left\langle z^2 \right\rangle = 2Dt \tag{4.3}$$

The Fourier transform of the one-dimensional average propagator $<P(z_0,z,t)>$ (i.e. $P(z_0,z,t)$ average over all start positions) can be measured in an NMR diffusion experiment.

The diffusion coefficient (at infinite dilutions, $D_0$) is related to the friction coefficient, $f$, (basically a measurement of the forces that retard a particles motion) through the relation

$$f = k_B T / D_0 \tag{4.4}$$

---

[vii] Central limit theorem (CLT) states that if the sum of independent identically distributed random variables has a finite variance, then it will be approximately normally distributed, i.e. following a Gaussian distribution.

Equation 4.4 can be combined with Stokes law assuming spherical symmetry ($f = 6\pi\eta R_H$, where $R_H$ is the hydrodynamic radius of the spherical aggregate and $\eta$ is the viscosity of the solvent) which results in the so called Stokes-Einstein equation.[39]

$$D_0 = k_B T / 6\pi\eta R_H \qquad (4.5)$$

Assuming that the water molecule is spherical, the size of a water molecule can be estimated from the value of $D_0$ at 298 K to $R_H$ = 1.1 Å ($\eta_{H2O}$ = 0.891·10$^{-3}$ kgm$^{-1}$s$^{-1}$ [39]). This can be compared to the $R_H$ of the known $R_H$ of a water molecule i.e. 1.9 Å.

## 4.3 Diffusion and reactions

Many chemical reactions are diffusion controlled. The rate of a diffusion controlled reaction is calculated by considering the rate at which the particles (a and b) approach each other. The rate constant for a diffusion controlled reaction is given by

$$k_d = 4\pi R^* D^* N_A \qquad (4.6)$$

where $R^*$ is the distance at which the molecules react with each other ($R^* = R_{Ha} + R_{Hb}$). $D^*$ is the sum of the diffusion coefficients, $D^* = D_a + D_b$. We approximate that the hydrodynamic radii, $R_{Ha}$ and $R_{Hb}$ are equal, and that equation 4.5 is valid. Equation 4.6 can then be rewritten as

$$k_d = 8RT / 3\eta \qquad (4.7)$$

where $R$ = 8.3412 JK$^{-1}$mol$^{-1}$, not to be confused with the particle radius. In this simple approach, the identity of the particle has no meaning, only the viscosity of the solvent and temperature matters. An example of a diffusion controlled reaction will be exemplified with the equilibrium between surfactant monomers and a surfactant aggregate. We note that there may exist a reaction barrier (activation energy) between the micelle and surfactant which stems from the head group repulsion; such barriers are neglected in this simple approach. The equilibrium between aggregate $A_{n-1}$ and monomer $A$ at steady state is given by

$$A + A_{n-1} \xrightleftharpoons[k_{off}]{k_{on}} A_n, \qquad k_{on}[A][A_{n-1}] = k_{off}[A_n] \qquad (4.8)$$
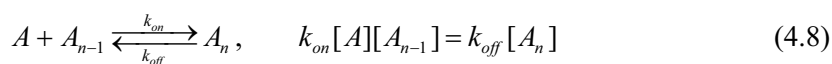
$$K = k_{on} / k_{off} \qquad (4.9)$$

where $n$ is the number of monomers in the aggregate and $k_{on}$ and $k_{off}$ are the rate constants (see Figure 3.6). Furthermore we assume that two particular aggregation numbers dominate the distribution of micelle aggregation numbers and that $[A_n] \cong [A_{n-1}]$. The monomer concentration $[A]$ is approximately equal to the CMC. By using these approximations equation 4.8 can be written as

$$k_{on}\text{CMC} = k_{off} \qquad (4.10)$$

We define a time constant $\tau_{off}$ as $1/k_{off} \equiv \tau_{off}$

$$\tau_{off}^{-1} = k_{on}\text{CMC} \qquad (4.11)$$

Given the statement above for a diffusion controlled reaction, $k_{on} = k_d$, equation 4.11 can be rewritten as

$$\tau_{off}^{-1} = k_{on}\text{CMC} = k_d\text{CMC} = 4\pi R^* D^* N_A \text{CMC} \qquad (4.12)$$

Equation 4.12 gives a rough estimate of the exchange time, which is in the order of μs typical for surfactants in micelles. In NMR self-diffusion experiments we are limited to use diffusion times in the order of 10-1000ms.

## 4.4 External magnetic gradient as spatial labels



$$\omega = \gamma(\mathbf{B}_0 + gz)$$

$$\omega = \gamma\mathbf{B}_0$$

$$\omega = \gamma(\mathbf{B}_0 - gz)$$
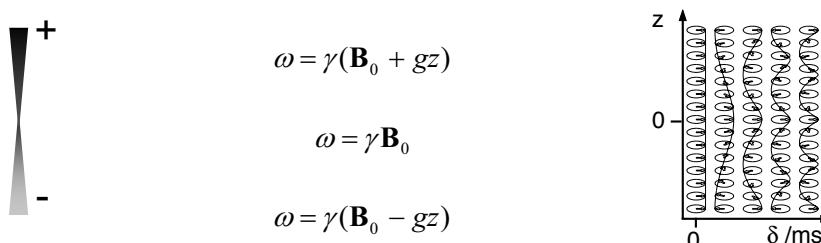
**Figure 4.2** The effect of the externally applied gradient on the spin phases at different positions in the sample. The variation of the spins throughout the sample volume in z-direction can be described by a helix with pitch $q^{-1}$ where $q$ is defined as $q \equiv \gamma g\delta/2\pi$. Figure due to Daniel Topgaard.

Having introduced the diffusion, we turn the focus to the NMR diffusion experiment. The local strength of the Larmor frequency, $\omega_{\text{eff}}$, in the presence of a gradient (see Figure 4.2) is given by:

$$\omega_{eff}(z) = B_0\gamma + \gamma gz \qquad \text{with} \qquad g = \frac{\partial B}{\partial z} \qquad (4.13)$$

where $z$ is the nuclear spin coordinate in the z-direction and $g$ is the gradient strength. The purpose of the varying magnetic field is that it creates spatially varying Larmor frequencies. (cf. chapter 3, were the spin frequencies were completely independent of position). In other words, particles in a particular position along the z-axis become "spin" labeled with a particular frequency. The gradient is applied during a certain time, $\delta$, with a gradient strength (unit: T/m or Gauss cm$^{-1}$, 1 Gauss cm$^{-1}$=10 mTm$^{-1}$).

## 4.5 Measuring self-diffusion with magnetic field gradients

The general description of the self-diffusion measurement can be found in references.[35, 46-48] Before going into the derivation of the self-diffusion equation, I stress that it is the self-diffusion that can be measured with NMR, not the collective diffusion, which can be measured in a Dynamic Light Scattering (DLS) experiment.

The self-diffusion equation for a self-diffusion NMR experiment will be derived under the Short Gradient Pulse (SGP) limit approximation.[49] In the SGP limit approximation one assumes that the spins do not diffuse during the gradient pulse. Moreover, in this simplified derivation we also assume that $T_1$ and $T_2$ relaxations are infinitely long and that the sample only contains one spin (on resonance).
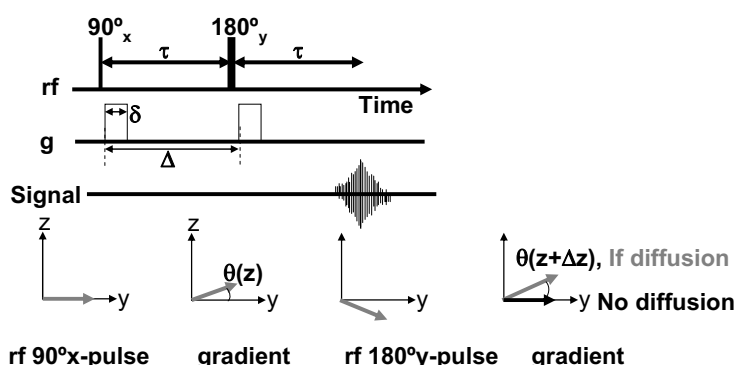


**Figure 4.3**. The basic Stejskal-Tanner PGSE pulse sequence, for self-diffusion measurements.

In Figure 4.3 the spin echo pulse sequence is depicted with gradient pulses included, as developed by Stejskal and Tanner.[50] The Stejskal and Tanner experiment is often called the Pulse Gradient Spin Echo (PGSE) experiment. The PGSE experiment is performed as follows: a rf $90^{\circ}_x$-pulse is applied which rotates the magnetization into the xy-plane. A gradient pulse of amplitude $g$ and duration $\delta$ is applied to dephase the spins. The dephasing is given by

$$\theta(z) = \gamma \delta g z \tag{4.14}$$

where $\theta(z)$ is the phase at spin coordinate $z$. After a time $\tau$ a $180^{\circ}_y$-pulse is applied to reverse all the spin phases. A second gradient is then used to refocus the magnetization after a time $\Delta$. The two gradient pulses are separated by a time $\Delta$. The phase of the magnetization after the second gradient at time $\tau + \delta$ is given by

$$\theta(z + \Delta z) = \gamma \delta g(z + \Delta z) \qquad (4.15)$$

where $z + \Delta z$ is the new spin coordinate due to diffusion of the particles. After the rf $180^{\circ}_y$-pulse the magnetization starts to loose phase coherence due to diffusion. If the particles were stationary there would be no loss of phase coherence. On the other hand if the particles have diffused during the diffusion time ($\Delta$), the refocusing of the phase coherence will "mismatch". The mismatching of the phase angle at time $2\tau$ is given by

$$\Delta \theta = \theta(z + \Delta z) - \theta(z) = \gamma \delta g \Delta z \qquad (4.16)$$

The measured intensity of the echo at $2\tau$, $I(2\tau)$ is given by

$$I(2\tau) = I(2\tau)_{g=0} \int_{-\infty}^{\infty} P(\Delta\theta, 2\tau) \cos(\Delta\theta) d\theta \qquad (4.17)$$

where $P(\Delta\theta)$ is the relative phase distribution function and $I(2\tau)_{g=0}$ is the intensity in absence of field gradients. In a PGSE experiment it is the probability distribution displacement $P(z_0, z, t)$ in the direction of the gradient that is measured (equation. 4.2). There is a direct correspondence between the displacement $\Delta z$ and the phase difference $\Delta\theta$. For an unrestricted (Gaussian) diffusion process in the same direction as the linear gradient, a probability distribution in phase space can be obtained by combining equations. 4.2 and 4.16.

$$P(\theta) = \frac{1}{2\sqrt{\pi D \Delta}} \exp(-\Delta\theta^2 / ((\gamma g)^2 4D\Delta)) \qquad (4.18)$$

The diffusion equation for the PGSE experiment is given by equation 4.19 (equation 4.17 combined with equation 4.18, and then integrated).

$$I(2\tau) = I(2\tau)_{g=0} \exp((-\gamma \delta g)^2 \Delta D) \qquad (4.19)$$

Taking the transverse relaxation, $T_2$ explicitly into account and correcting for the diffusion during the gradient pulse, $\delta$.

$$I(2\tau) = I_0 \exp(-2\tau / T_2) \exp((-\gamma\delta g)^2 (\Delta - \delta / 3)D) \qquad (4.20)$$

where $I(2\tau)_{g=0} = I_0 \exp(-2\tau/T_2)$ with $I_0$ defined as the intensity following a single 90º pulse. A simplified version of equation 4.20 is often used because the relaxation term is constant and some of the parameters are combined into a machine constant, $k$.

$$I_n = \exp(-kD) \qquad (4.21)$$

Where $k \equiv (\gamma\delta g)^2 (\Delta-\delta/3)$ with the unit sm$^{-2}$ and $I_n$ is the normalized intensity.

## 4.6 The stimulated echo method

The PGSE experiments are feasible only if the $T_2$ relaxation time is long. If the $T_2$ relaxation time is short the signals disappear fast and the diffusion experiment becomes difficult to perform. This is often the case for large polymers. An alternative approach is to use the "three pulse" sequence, STimulated Echo (STE) and incorporate two field gradients [46, 51, 52], see Figure 4.4. The first field gradient is applied after the first 90º$_x$-pulse and the second after the last 90º-pulse. The pulse sequence is called Pulsed Gradient STimulated Echo (PGSTE).

In the STE pulse sequence the first 90º$_x$-pulse rotates the magnetization into the xy-plane. After a time delay $\tau_1$, a second 90º$_x$-pulse is applied which rotates the ±y magnetization into the ±z-axis, where the magnetization is stored during a time $\tau_2$. The x-component of the transverse magnetization remains unaltered by the second 90º$_x$-pulse and will not contribute to the "stimulated echo". The third 90º$_x$-pulse brings back the magnetization to the ±y-direction. After a time $\tau_1$ ($t_{total} = 2\tau_1 + \tau_2$) there will be an echo.

The field gradients in the PGSTE pulse sequence have the same purpose as in the PGSE pulse sequence, namely, to spatially label the spins and will not be discussed here (see section 4.5).

The intensity, $I$ obtained from a STE experiment is given by

$$I(2\tau_1 + \tau_2) = I_0 \frac{1}{2} \exp\left(-\frac{2\tau_1}{T_2} - \frac{\tau_2}{T_1}\right) = A \qquad (4.22)$$

The intensity, $I$, for the PGSTE experiment is given by

$$I(2\tau_1 + \tau_2) = A\exp((-\gamma\delta g)^2(\Delta - \delta/3)D) = A\exp(-kD) \qquad (4.23)$$

The factor 1/2 in equation 4.22 (cf. equation 4.20) arises because it is only the y magnetization of the transverse magnetization that is stored during $\tau_2$.
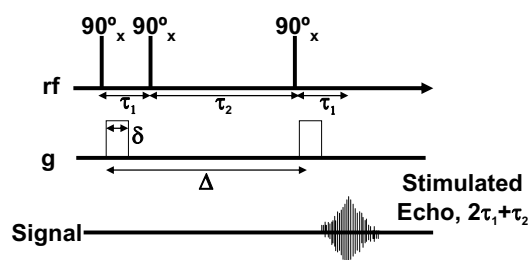


**Figure 4.4** The PGSTE pulse sequence. Only one of several echoes is shown.

## 4.7 Example of a diffusion experiment

In a diffusion experiment the intensity is measured as a function of $g$ or sometimes as a function of $\delta$ or $\Delta$. If the logarithm of the normalized intensity is plotted versus the machine constant, $k$, the self-diffusion coefficient is given by the slope. Figure 4.5a gives an example of the effect of the field gradient on the intensity in a PGSTE experiment. In Figure 4.5b the raw data extracted from Figure 4.5a is shown.
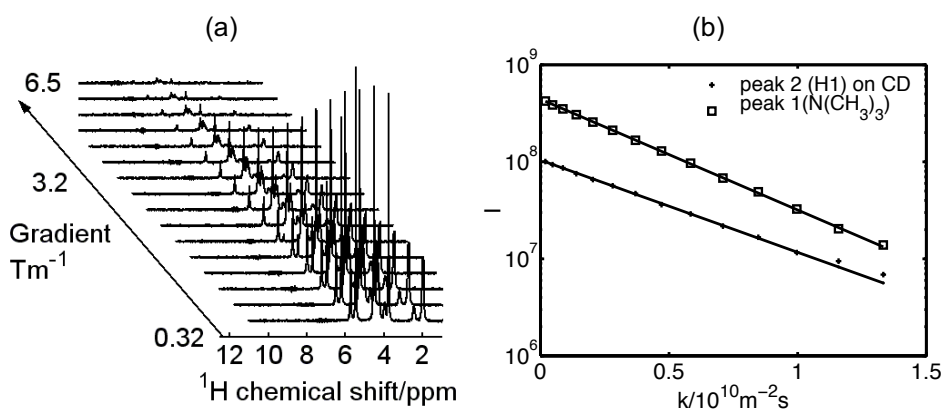


**Figure 4.5 (a)** Intensity as a function of gradient and chemical shift obtained from self-diffusion measurements of β-cyclodextrin (6.9 mM) and the surfactant, $B_{10}$ (6.3 mM) at 298 K with $\Delta$ = 20 ms $\delta$ = 0.5 ms, and $g_{max}$ = 6.5T/m, (b) Intensity versus $k$.

## 4.8 Diffusion model for host and guest interaction

Levay et al.[53] pointed out in the 1970s that the equilibrium constant of a 1:1 complex formation could be measured with the aid of self-diffusion NMR. One

of the first papers in this field is that of Stilbs et al.[54] who measured the host-guest interaction between cyclodextrins and alcohols. In 1998 there was a review article "NMR Studies of Cyclodextrins and Cyclodextrin Complexes[55] describing several different NMR techniques to measure host-guest interaction, self-diffusion was not included. There are a number of techniques for measuring host-guest complexation, which have their strengths and limitations. Some papers in this area that need to be mentioned are the ones by Winner at el. (2002) and Cameron et al. (2001)[56, 57] which both used NMR diffusiometry. Winner et al. [33] measured the host guest interaction between cyclodextrin and amino acids. They include in the paper model calculations of the diffusion behavior in order to evaluate the range of equilibrium constants suitable for use in self-diffusion NMR. Cameron et al.[56] developed the diffusion model further, by taking into account the diffusion behavior of all the species in the data treatment when determining the association constant. The diffusion models that have been used in paper I-IV will be introduced here.

## 4.8.1 Modeling the self-diffusion for the 1:1 complex

The model here will deal with the host (cyclodextrin) and the guest (surfactant) complexation. The possible counterion complexation with CD will not be included in the model.[29] The starting is the equilibrium between the cyclodextrin, the surfactant and the cyclodextrin-surfactant complex formed, given by equation 3.16. The host-guest complex is a dynamic complex which is assumed to form and break up on the time scale of $\mu s$ to sub ms, much faster than the diffusion time in a diffusion experiment. The standard way to treat concentration dependent self-diffusion data in which the particles rapidly exchange between $n$-sites (on the NMR time scale) is to use an $n$-site exchange model[58]

$$D_{obs} = \langle D \rangle = \sum_n P_n D_n \,, \qquad\qquad \sum_n P_n = 1 \qquad\qquad (4.24)$$

where $P_n$ represents the molar fraction of particles in the $n$th state and $\langle D \rangle$ is the average self-diffusion which is equal with the observed self-diffusion, $D_{obs}$. The first step involved when using this kind of diffusion model is to identify the number of different diffusion sites, $n$. If $n = 2$

$$D_{S,obs} = P_{S,f} D_{S,f} + (1 - P_{S,f}) D_{CD-S} \qquad\qquad (4.25)$$

$$P_{S,f} = ([S_T] - [CD-S])/[S_T] \qquad\qquad (4.26)$$

where $D_{S,obs}$, $D_{S,f}$ and $D_{CD-S}$ are the observed, free surfactant and complex self-diffusion coefficients, respectively, and $P_{S,f}$ is the fraction of free surfactant, $[CD-S]$ and $[S_T]$ are the concentration of the complex and total concentration of surfactant, respectively. Equation 4.25 is valid below the concentration where the surfactants self-aggregate in the presence of cyclodextrin (CD). The self-aggregation concentration in presence of cyclodextrin is called the CAC. At the CAC the surfactant can be at three different sites: in the bulk, in the complex and in a micelle. The observed self-diffusion for the surfactant in the presence of a micelle is given by

$$D_{S,obs} = D_{S,f} P'_{S,f} + D_{CD-S} P'_{CD-S} + D_M P'_M \tag{4.27}$$

$$P'_{S,f} = (\text{CAC} - [CD - S]_{\text{CAC}})/[S_T] \tag{4.28}$$

$$P'_{CD-S} = [CD - S]_{\text{CAC}}/[S_T] \tag{4.29}$$

$$P'_M = ([S_T] - \text{CAC})/[S_T] \tag{4.30}$$

where $P'_{S,f}$, $P'_{CD-S}$ and $P'_M$ are the fractions of the complexed surfactant, free surfactant, and surfactant in micelles respectively and $[CD-S]_{\text{CAC}}$ is the concentration of the complex at CAC. The fractions given by the symbol $P'$ indicate that we have surfactants in micelles. Please not that at CAC and at higher surfactant concentration we assume that $[CD-S]_{\text{CAC}}$ is constant.

Turning to a similar analysis for CD as above and again, starting by finding the number of sites CD can exchange between. For CD it is a two site exchange. The observed self-diffusion for the CD is then given by

$$D_{CD,obs} = D_{CD,f} P_{CD,f} + D_{CD-S} (1 - P_{CD,f}) \tag{4.31}$$

$$P_{CD,f} = ([CD_T] - [CD - S])/[CD_T] \tag{4.32}$$

where $D_{CD,f}$ is the self-diffusion of CD in the absence of surfactant, $P_{CD,f}$ is the fraction of free CD, and $[CD_T]$ is the total concentration of CD. Above the CAC, the observed CD self-diffusion is defined as follows

$$D_{CD,obs} = D_{CD} P'_{CD,f} + D_{CD-S} (1 - P'_{CD,f}) \tag{4.33}$$

$$P'_{CD,f} = ([CD_T] - [CD - S]_{\text{CAC}})/[CD_T] \tag{4.34}$$

Summarizing, there are three ways the self-diffusion experiment could be designed

1. Single point experiments with previous knowledge of $D_{S,f}$ and the assumption that $D_{CD\text{-}S} \approx D_{CD,f}$.[54] (*Method 1*)
2. Keeping the concentration of surfactant constant but varying the concentration of CD, paper II-IV. (*Method 2*)
3. Keeping the CD concentration constant and varying the concentration of surfactant (from low concentration up to concentration above CMC), paper I-II and IV. (*Method 3*). These methods will be discussed in detailed later in this thesis

I end this section with a note on the obstruction effect when micelles are present. A simple obstruction model can be used in order to correct for the reduction of CD self-diffusion due to the obstructing micelles.[59]

$$\frac{D}{D_0} = \left(1 + \frac{\phi}{2}\left(1 + \frac{r}{R}\right)^3\right)^{-1} \qquad (4.35)$$

where $\phi$ is the volume fraction of obstructing particles, $D_0$ is the self-diffusion in the absence of obstructing objects, and $D$ is the diffusion when obstructing particles are present. $R$ and $r$ correspond to the radii of the obstructing particles and the diffusing species, respectively.

$$D_{CD,obs} = (D_{CD,f}P'_{CD,f} + D_{CD\text{-}S}(1 - P'_{CD,f})) / \left(1 + \frac{\phi}{2}\left(1 + \frac{r}{R}\right)^3\right) \qquad (4.36)$$

Obstruction effects due to the presence of surfactant micelles, affect the self-diffusion of all the species in the micellar solution. The obstruction effect experienced by the surfactants has been neglected in the model since its contribution can not be separated from the decrease in the surfactant diffusion on account on the micellization process. We do take into account the obstruction effect on the CD (equation 4.36).

### 4.8.2 Modeling the self-diffusion for the 1:1 and 2:1 complex

Depending upon the size (i.e. the number of methylene groups and tails) and nature of the surfactant, the complexation stoichiometry can be of higher order than 1:1 (papers II and IV). If one assumes that higher order complexes, other than the 1:1 complex are formed and exist simultaneously, a second equilibrium is established i.e.

$$CD + S \rightleftharpoons CD - S \qquad K_{11} = [CD - S]/([CD][S]) \qquad (4.37)$$

$$CD + CD - S \overset{\longrightarrow}{\longleftarrow} CD_2 - S \quad K_{21} = [CD_2 - S]/([CD - S][CD]) \quad (4.38)$$
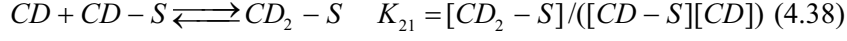
$K_{11}$ and $K_{21}$ are the binding constants for the 1:1 and 2:1 complexes, respectively. Following the same procedure as above, finding the number of the $n$ different diffusion sites for the surfactant and the cyclodextrin below the CAC (i.e. no micelles presents) one obtains

$$D_{S,obs} = D_{S,f} P_{S,f} + D_{CD-S} P^S_{CD-S} + D_{CD2-S} P^S_{CD2-S} \tag{4.39}$$

$$D_{CD,obs} = D_{CD,f} P_{CD,f} + D_{CD-S} P^{CD}_{CD2-S} + 2D_{CD2-S} P^{CD}_{CD2-S} \tag{4.40}$$

$D_{S,f}$, $D_{CD,f}$, $D_{CD-S}$ and $D_{CD2-S}$ are the diffusion coefficients for surfactant, cyclodextrin the 1:1 complex, and the 2:1 complex, respectively. The different molar fractions in equations 4.39 and 4.40 are related to the total concentration of surfactant and CD and are defined as follows:

$$P_{S,f} = [S]/[S_T] \tag{4.41}$$

$$P^S_{CD-S} = [CD - S]/[S_T] \tag{4.42}$$

$$P^S_{CD2-S} = [CD_2 - S]/[S_T] \tag{4.43}$$

where $P_{S,f}$, $P^S_{CD-S}$, $P^S_{CD2-S}$ are the molar fractions of free surfactant, of the 1:1 complex and the of the 2:1 complex, respectively and

$$P_{CD,f} = [CD]/[CD_T] \tag{4.44}$$

$$P^{CD}_{CD-S} = [CD - S]/[CD_T] \tag{4.45}$$

$$P^{CD}_{CD2-S} = [CD_2 - S]/[CD_T] \tag{4.46}$$

where $P_{CD,f}$, $P^{CD}_{CD-S}$ and $P^{CD}_{CD2-S}$ are the molar fractions of free CD, of the 1:1 complex and the of the 2:1 complex, respectively.

### 4.8.3 The strengths, weaknesses and limitations of using self-diffusion NMR to probe host-guest interaction

The approximations, strengths and weaknesses of using self-diffusion measurements for host-guest interaction studies will now be discussed. As pointed out in section 4.8.1 there are in principle three different ways of performing self-diffusion for measurements of host guest interaction. Method 1 is the simplest and quickest way, but there are clearly two drawbacks. The assumption that $D_{host} \approx D_{host\text{-}guest}$ is not always true, although it can be expected to hold well for small guests in comparison to the host. The second drawback is that the precision in the equilibrium constant is rather poor. It is better to perform a series of experiment as a function of *guest* or *host* concentrations and obtain the relevant parameters through a least square fit. As described under method 2, titrating with host, keeping the concentration of guest constant, is probably the best way to set up the experiment (less fitting parameters, no micelles present, do not need to involve obstruction effects on the self-diffusion coefficients). The numbers of independent fitting parameters are of importance; the fewer the better. Following the approach of method 2 (assuming 1:1 stoichiometry), the model have four independent fitting parameters, $D_{S,f}$, $D_{CD,f}$, $D_{CD\text{-}S}$ and $K_{11}$. The self-diffusion coefficients $D_{S,f}$ and $D_{CD,f}$ are obtained from independent measurements, so it is only necessary to use two fitting parameters. The approach described under method 3 is more complex due to the possible presence of a third exchangeable site, the micelles. The fitting needs to take into consideration the presence of micelles at higher surfactant concentrations and the obstruction effects affecting the CD diffusion (see equation 4.36). There are seven fitting parameters, $D_{S,f}$, $D_{CD,f}$, $D_{CD\text{-}S}$, $D_M$, CMC, $K_{11}$ and $c$ (a constant quantifying the obstruction effect, defined as $c \equiv (1 + r / R)^3 / 2$).

The NMR self-diffusion methods has some clear advantages: it is a direct technique, that measures the self-diffusion of all the particles involved and does not rely on any probe or specific physical properties of the guest or host, such as electrochemical, optical properties. The concentrations used for both the guest and host can be quite low. The changes of the guest or host self-diffusion coefficient are significant upon complexation. Compare this with, for example, chemical shift changes upon complexation that are often very small and insignificant, especially for higher order complexation.

The drawbacks of the self-diffusion method are that a titrator can not easily be connected to the NMR tube in the spectrometer, so samples need to be prepared manually. The method works best when there is a relative difference in size between the host and guest (i.e. a difference in magnitude between the self-diffusion coefficients). Upon complexation the cyclodextrin diffusion and the complex self-diffusion are similar so the relevant information relies mainly on the variation of the guest self-diffusion upon complex formation.

The limitations of the self-diffusion method are not unique for this technique, but are general problems. The interaction strength, reflected in the equilibrium constant, can be divided into three different regions: weak, intermediate and strong interactions. The weak and strong interactions are more difficult to study. In the weak case, the alterations of the physical parameters are too small and for the strong interaction case, the alterations in the physical parameter are too large and take place in a very small concentration window. One of the important criteria is that the measurements should cover a large portion of the saturation curve (defined down below) in order to assign experimental meaning to the slope and intercept (in a graph there the measured quantity is plotted versus the concentration) of the fitted data. Deranleau[60] suggests that measurements should cover roughly 75% of the saturation curve, however the criteria is only applicable for systems with low or intermediate values of association constants. The definition of the saturation criteria (*sat*) is given by equation 3.47

$$sat \equiv [CD\text{-}S]/[S_T]=K_{11}([CD])/(1+K_{11}([CD]) \qquad (3.47)$$

where *sat* can have values between $0 \leq sat \leq 1$. Given the definition, $S_T$ is the dilute species maintained at constant concentration. The saturation fraction can be obtained from self-diffusion measurements and is proportional to the concentration of the formed complex, and is given in equation 3.48

$$\frac{D_{S,obs} - D_S}{D_{CD-S} - D_S} = \frac{[CD - S]}{[S_T]} \qquad (3.48)$$

Using the approach as described under method 2, the saturation curve criteria according to Deranleau were not satisfied for all the guests studied (see chapter 5) due to the low solubility of CD in water (see Table 2.8).

Using the diffusion model for a 1:1 complexation (method 2) with a guest concentration of 1 mM, and simulating the data for different equilibrium constants while keeping all other parameters constant (see Figure 4.6), it is clear that the curves initial slope becomes more and more similar and the, $D/D_0$ curves overlap for $K_{11}$-values higher than 10000 M$^{-1}$ and it becomes difficult to differentiate the curves from each other.

Turning to higher order complexation, i.e. 2:1 (2CD:1S). As was pointed out above, the determination of the binding constant becomes inaccurate as the magnitude $K_{11}$ increases; the curve is insensitive towards changes in $K_{11}$. For a 2:1 complexation as for example for $C_xTAB$ (x>14) with β-CD the first binding constant is very high and the second association constant generally (much) weaker (paper II). The magnitude of the first association constant in this cases are generally associated with large error and often the error in $K_{11}$ are greater than the error in the second binding constant, $K_{21}$. The

second binding constant can not be calculated accurately as well because of covariance between the variables.
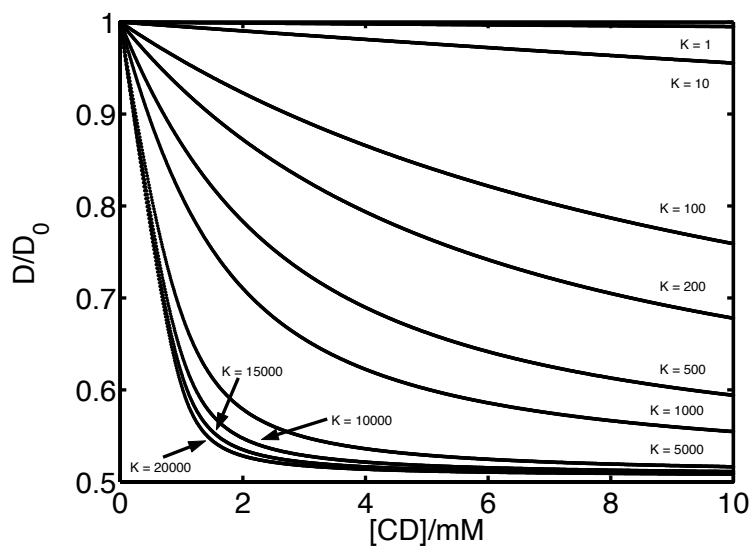


**Figure 4.6** Simulated normalized self-diffusion data versus [CD] for a 1:1 complexation. It can be seen that with increasing $K_{11}$ the curves initial slope become insensitive towards high values of $K_{11}$. The curves in the graph are calculated based on a concentration of guest molecules of 1 mM and the $D_{S,f} = 4.96 \cdot 10^{-10}$ m$^2$s$^{-1}$, $D_{CD,f} = 2.64 \cdot 10^{-10}$ m$^2$s$^{-1}$ and $D_{CD-S} = 2.51 \cdot 10^{-10}$ m$^2$s$^{-1}$ (i.e. realistic values).

# 5. Cyclodextrin surfactant interactions

This chapter is a summary of the research presented in papers I-V. The aim of these studies was two-fold. The first goal was to systematically study the host-guest interaction between cyclodextrin and surfactant. Cyclodextrin-surfactant mixtures offer the possibility of systematically studying the association process since the properties of the solution can be modulated by systematic variations of surfactant structure, such as tail length, number of tails, number of headgroups and the types of headgroup (see Table 2.1-2.4). The second goal was to develop a diffusion model that can describe the host-guest interaction under all normal circumstances (see Section 4.8.1) in conjunction with self-diffusion NMR. Earlier diffusion models [33, 54, 56, 57] for host-guest interaction only consider 1:1 complexation and do not include 2:1 (2CD:1S) complexation and the presence of micelles.

## 5.1 Interpretation of self-diffusion data

Two different sets of experiments will be considered here. In set (A) (corresponding to method 2 in section 4.8.1) the surfactant concentration is constant and the cyclodextrin concentration is changed. In set (B) (corresponding to method 3 in section 4.8.1), the concentration of CD is constant and the surfactant concentration is changed.

### 5.1.1 Set (A)

The complexation behavior of $C_{12}TAB$ and β-CD will be considered in detail (see also paper II). The measured self-diffusion data and the fits are presented in Figure 5.1. The experimental data can be split up in two different regions (indicated by the dotted line in Figure 5.1). As the concentration of β-CD increases, the self-diffusion coefficient of $C_{12}TAB$ decreases as a result of the inclusion complex formed with β-CD, until the maximum concentration of complex is formed (Figure 5.1, region I). After that (Figure 5.1, region II) the self-diffusion remains constant since no more complexes are formed. Turning to the self-diffusion of β-CD, it can be seen that the self-diffusion remains constant in the beginning and then increases slightly towards the value of free self-diffusion for β-cyclodextrin. The experimental data only show a minor difference between the surfactant diffusion (the diffusion of the complex) and cyclodextrin diffusion at high concentration. This is because the hydrodynamic radii of the aggregate and cyclodextrin species do not differ markedly; clearly indicating that most of the surfactant molecule is located inside the cavity of CD with only a small part sticking out (a few methylene groups and the head group).
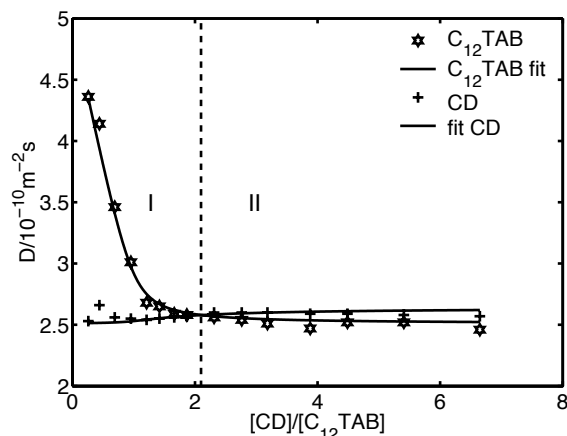
**Figure 5.1** Self-diffusion coefficients versus concentration of β-CD at 298.2 K. The $C_{12}TAB$ concentration was constant, $[C_{12}TAB]$ = 2 mM. The graph is divided into two regions, I and II (see the text).

### 5.1.2 Set (A), 2:1 model

For the $C_{16}TAB$ and the gemini surfactants the 1:1 model fails to fit the experimental data and higher order complexation need to be taken into account. In Figure 5.2a and b the self-diffusion data for $C_{16}TAB$ and gemini *12-2-12* are given, respectively, a long with a fit to the 1:1 model. In Figure 5.2a at high β-CD concentration the self-diffusion of surfactant shows a noticeable decrease. The 1:1 model fails to fit this experimental behavior. The model predicts a leveling off (saturation level) of the self-diffusion coefficients for this surfactant for high concentration of cyclodextrin. The formation of a second complex (2:1, 2CD:1S), which has a lower self-diffusion coefficient than the self-diffusion coefficient of the (1:1) complex explains the data. At low concentration of β-CD it is mainly the 1:1 complex that is formed, whereas as the concentration of β-CD increases more and more 2:1 complexes form and a monotonic decrease is seen in the self-diffusion coefficient for the surfactant. The cyclodextrin self-diffusion coefficient at high and intermediate concentrations of β-CD is approximately constant. Upon increasing the β-CD concentration, more and more β-CD is free in solution, which is why the β-CD self-diffusion does not decrease monotonically as for the surfactant self-diffusion. At low β-CD concentrations there is noise in the β-CD self-diffusion data, but the self-diffusion coefficients are lower here, whereas the 1:1 model predicts a smooth increase of β-CD self-diffusion in the whole concentration region.

Turning to the gemini surfactant in Figure 5.2b, there is a dip in self-diffusion coefficients at low β-CD concentrations for β-CD. The self-diffusion of the surfactant goes down upon the addition of cyclodextrin and reaches a

45

plateau at approximately a concentration of 3.5 mM, while the self-diffusion of the β-CD decreases until a concentration of 1.6 mM β-CD and, after that, increases in the rest of the β-CD concentration interval approaching the value of β-CD in $D_2O$. The 1:1 model cannot predict a dip in the self-diffusion coefficient at low β-CD concentrations. The addition of a small amount of β-CD reduces the self-diffusion of β-CD, first mainly by 1:1 complexation, then, upon further addition of β-CD, mainly by 2:1 complexation, which lowers the self-diffusion of β-CD even more. Further addition of β-CD causes a progressive increase in β-CD self-diffusion as the fraction of unassociated β-CD increases in comparison to the fraction being complexed.
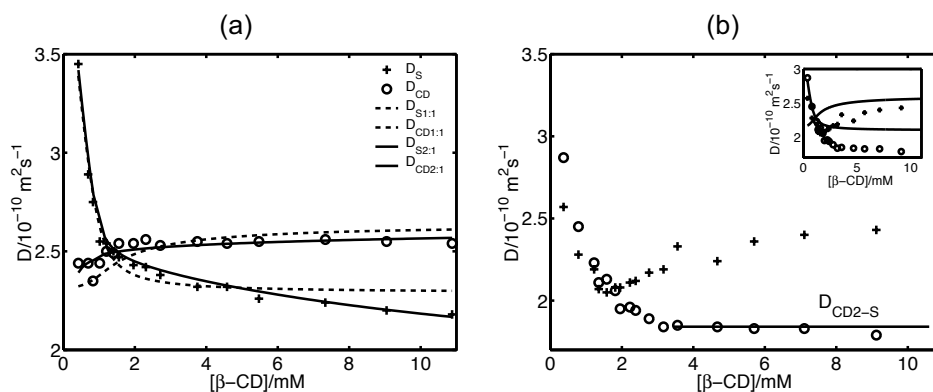


**Figure 5.2** (a) Self-diffusion coefficients of $C_{16}TAB$ (O) and β-CD (+) for varying β-CD concentrations at $[C_{16}TAB]$ = 2 mM. Lines show the best fit to the model with a 1:1 complex (--) and to the model with a 2:1 complex (-). (b) Self-diffusion coefficients of gemini *12-2-12* surfactant (O) and β-CD (+), as a function of β-CD for [*12-2-12*] = 0.83 mM. The line drawn indicates the diffusion of the 2:1 (2CD:1S) complex. The insert shows the same data and the prediction of a 1:1 model, where a binding constant of 12000 $M^{-1}$ has been used. All data is recorded at 298 K.

## 5.1.3 Set (B)

Figure 5.3 shows the self-diffusion data for α-CD and $C_8G_1$ (see Table 2.4) when the concentration of $C_8G_1$ is varied for a constant solution concentration of α-CD at 298 K (paper I). The experimental data can be split up into three different regions (the dotted lines in Figure 5.3). In region I, the surfactant self-diffusion is almost constant and the values of the self-diffusion coefficient of surfactant and cyclodextrin are almost the same in this region, strongly indicating that complexation occurs. In region II, a sharp increase of the self-diffusion coefficient of the surfactant is observed due to the presence of monomers in solution after the saturation point of the cyclodextrin is reached. Further addition of surfactant will start the critical aggregation process and consequently the self-diffusion of the surfactant decreases progressively as more and more aggregate forms in the solution, region III. The cyclodextrin

profile decreases slightly in regions I and II, until a plateau is reached in region II (maximum of complex is formed). In region III a constant value of the self-diffusion for cyclodextrin is expected but a decrease is observed which is due to the obstruction effect arising from the surfactant aggregates. Moreover, the affinity for cyclodextrin to micelles cannot be excluded and there is an ongoing debate concerning this issue.[61-63] We interpret the effect as caused by obstruction, see papers I and II.
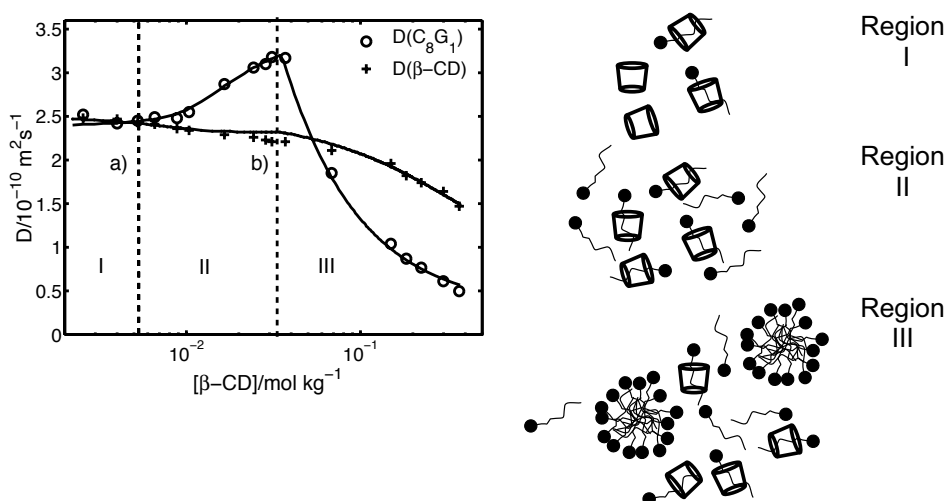


**Figure 5.3** Self-diffusion coefficients versus concentration of $C_8G_1$ for a constant concentration of [β-CD] = 0.0105 mol kg$^{-1}$ at 298 K. The graph is divided into three regions I, II and III (see text). A schematic representation of events taking place in the three different regions is shown. Region I, all surfactant is more a less complexed, [cyclodextrin]>[surfactant]. At position a) $[C_8G_1]/[β\text{-CD}] = 1$ and at position b) CAC = CMC + [β-CD].

## 5.2 Interpretation of the complexation results

### 5.2.1 Straight chain and bolaform surfactant complexation with β-CD

In Figure 5.4 (paper II and III) the self-diffusion for a range of different n-akyltrimethylammonium bromide and bolaform surfactants are plotted versus the ratio of [β-CD]/[S]. As the number of metylene groups in the tail or spacer of the surfactant increases, the decrease of the diffusion self-coefficient is faster and the plateau is reached for lower β-CD/surfactant ratios. This clearly indicates stronger binding constant for the complex with increasing number of methylene groups in the tail of the surfactant for the same type of surfactant group. Self-diffusion measurements of the tetramethyl ammonium bromide (denoted $C_1$TAB), as a function of β-CD concentration was measured as a control experiment, to ensure that it is only the tail or spacer of the surfactants that interacts with the cyclodextrin and not the headgroup (see Figure 5.4).

47

Surfactants which have a shorter tail than six methylene groups do not interact. The bolaform surfactant $B_{10}$ interacts very weakly and the $B_8$ do not interact at all at 298 K. The reason why the bolaform surfactants give a lower association constant with β-CD than the corresponding homologous single-head-group surfactant is because it is a more hydrophilic molecule. The CMC is an important parameter in predicting the magnitude of the association constant, this will be discussed next.

The standard Gibbs free energies of transfer of hydrophobic molecules from an aqueous solution into a hydrophobic environment (from solubility $K_{11}$ and CMC values) versus the number of carbons in the tail of the molecule, are given in Figure 5.5 for a range of different substances. Binding constant values increase linearly up to $C_{12}TAB$ and than levels off for $C_{14}TAB$. Similar patterns have been observed for alkylsulfonates.[64] Twelve methylene groups seem to be the maximum number of carbon that can be inserted inside the cavity. The volume of twelve methylene groups is 324 $\text{Å}^3$ (one $CH_2$ has a volume of 27 $\text{Å}^3$) to be compared with the volume of the cavity of β-CD, 262 $\text{Å}^3$ (see Table 2.8). The inclusion of one methylene group into a β-CD cavity contributes -2.3 kJ/mol to the standard Gibbs free energy of transfer. It is interesting to compare this with the Gibbs free energy of transfer a surfactant from bulk solution into the micelle, see Figure 5.5. The Gibbs free energy of transfer a $CH_2$ of an ionic surfactant ($C_xTAB$) into micelles is -2.85 kJ/mol and for a nonionic surfactant ($C_xE_y$ and $C_xG_1$) -3.1 kJ/mol.[2, 3, 65] The $\Delta G^o(\textit{transfer})$ for n-alcohols is -3.2 kJ/mol per $CH_2$-group.[54] And finally, the Gibbs free energy of transfer a hydrocarbon (methane, ethane, …etc) from water to its apolar environment is -3.7 kJ/mol per $CH_2$ group as estimated from the solubility in water.[66] In papers I, II and IV we have measured the association process varying the surfactant concentration with constant concentration of β-CD (α-CD). The complexation process shifts the CMC (CAC) values to higher concentrations, approximately CAC ≈ CMC +[β-CD] for 1:1 complexation and for 2:1 complexation CAC ≈ CMC + $^1/_2$·[β-CD]. The self-association of an ionic and nonionic surfactant is less energetically favorable in comparison to the association process with β-CD (and also α-CD). The reason why complexation is favored is because the head group interaction in a micelle is unfavorable, whereas in the host-guest complexation these head group repulsions do not exist. Moreover, the standard Gibbs free energy of transfer of a $CH_2$ group is lower for host-guest interaction. The explanation is that in the host-guest interaction some of the $CH_2$ groups might be partially surrounded by water whereas in a micelle the $CH_2$ groups are only surrounded by other $CH_2$ groups. Another reason is that the cyclodextrin cavity has a higher polarity than the interior of a micelle.

48
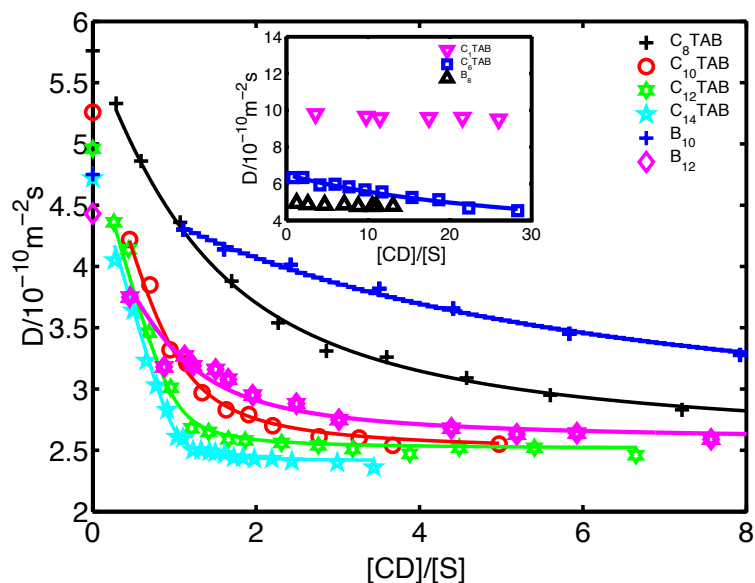
**Figure 5.4** Self-diffusion coefficients for n-akyltrimethylammonium bromide surfactants and bolaform surfactants plotted versus the ratio of [β-CD]/[S] at 298 K. The concentration of the surfactants are: $[C_1TAB]$ = 0.43 mM, $[C_6TAB]$ = 0.47 mM, $[C_8TAB]$ = 1.6 mM, $[C_{10}TAB]$ = 2.0 mM, $[C_{12}TAB]$ = 2.0 mM, $[C_{14}TAB]$ = 3.5 mM, $[B_8]$ = 1.1 mM, $[B_{10}]$ = 0.98 mM and $[B_{12}]$ = 1.0 mM.
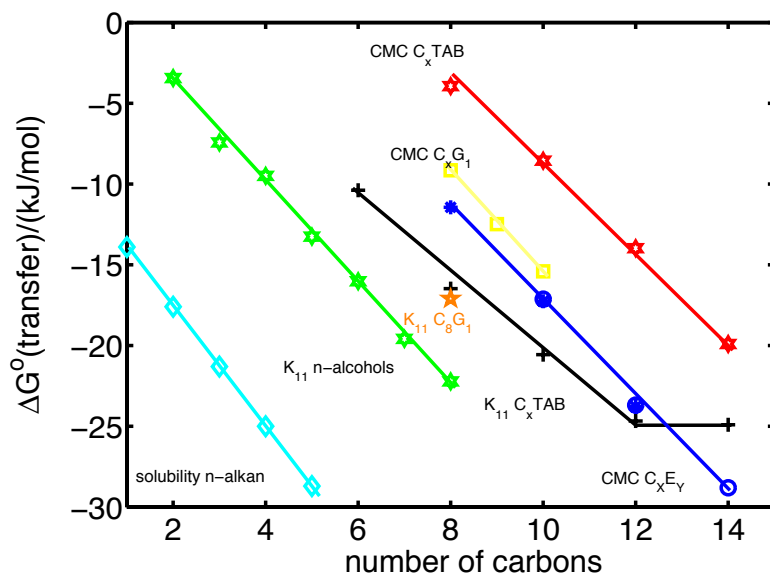


**Figure 5.5** Gibbs free energy of transfer calculated from $K_{11}$, CMC and solubility versus the number of carbons in the hydrophobic chain for different chemical compounds as indicated in the figure. The solid lines are guides for the eyes. The data in the graph are reproduced from references 2, 3, 54, 66 and papers I and III.

49

So far we have only focused on the interaction β-CD with surfactants. In paper I both α-CD and β-CD interactions were studied with the nonionic sugar surfactants, $C_8G_1$ and $C_9G_1$. By decreasing the radius, $r$, of the hydrophobic cavity, $r_{\beta\text{-CD}} \rightarrow r_{\alpha\text{-CD}}$ the equilibrium constant of the complex increases. Liveri et al. [67] studied $C_{12}TAB$ interaction with α-CD, β-CD and γ-CD and found that as the CD cavity size increases the equilibrium constant decreases.

**Table 5.1** Summary of results obtained from paper I-IV (298 K).

| Surf. + β-CD + $D_2O$ Set (A) | $D/$ $10^{-10}$ $m^2s^{-1}$ | $K_{11}/M^{-1} \cdot 10^3$ | $K_{21}/M^{-1}$ | $D_{CD\text{-}S}/$ $10^{-10}$ $m^2s^{-1}$ | $D_{CD2\text{-}S}/$ $10^{-10}$ $m^2s^{-1}$ |
|---|---|---|---|---|---|
| $C_{16}TAB$ | 4.16±0.06 | 45.5±10.5 | 76±40 | 2.47±0.01[(2)] | 1.75±0.27 |
| $C_{14}TAB$ | 4.72±0.02 | 23±5 | ---- | 2.41±0.04 | ---- |
| $C_{12}TAB$ | 4.96±0.01 | 21±3 | ---- | 2.50±0.06 | ---- |
| $C_{10}TAB$ | 5.26±0.04 | 4.0±0.3 | ---- | 2.48±0.02 | ---- |
| $C_8TAB$ | 5.76±0.06 | 0.77±0.03 | ---- | 2.49±0.03 | ---- |
| $C_6TAB$ | 6.51±0.01 | 0.066±0.002 | ---- | 2.5[(1)] | ---- |
| $C_1TAB$ | 9.83±0.01 | ---- | ---- | ---- | ---- |
| $B_8$ | 5.06±0.02 | ---- | ---- | ---- | ---- |
| $B_{10}$ | 4.75±0.03 | 2.3±0.5 | ---- | 2.5±0.1 | ---- |
| $B_{12}$ | 4.43±0.01 | 3.0±0.4 [2.5±0.1] | ---- | 2.53±0.03 | ---- |
| *12-2-12* | 3.28±0.01 | [1.97±0.15] | 600±240 | 2.10[(2)] | 1.80 |
| *12-8-12* | 3.00±0.01 | [3.15±0.53] | 1340±270 | 2.00[(2)] | 1.75 |
| *12-10-12* | 2.80±0.02 | [3.13±0.79] | 2120±430 | 1.90[(2)] | 1.65 |

The values in square brackets refer to complexation studies in $H_2O$ with electrical conductivity. The errors given in the table is from the fitting procedure. [(1)] An estimated value for CD-S is locked in the fit to determine $K_{11}$ more accurately. [(2)] The self-diffusion of the 2:1 complex is taken as the self-diffusion at the plateau in a plot with $D_{CD,obs}$ versus [β-CD], see for example Figure 5.2b. The self-diffusion of the 1:1 complex is calculated based on equation 4.5 and the relation $D_{21}/D_{11} = (V_{11}/V_{21})^{1/3}$, where $V_{11}$ and $V_{21}$ are the volume of the 2:1 and 1:1 complex, respectively.

## 5.2.2 Gemini surfactant complexation

The complexation of the gemini surfactants, *12-2-12*, *12-8-12* and *12-10-12*, was studied by self-diffusion NMR and electrical conductivity (EC); see paper IV. From the NMR self-diffusion measurements the stoichiometry was determined whereas from EC measurements the association constants were determined. The self-diffusion data for *12-2-12* and β-CD as a function of β-CD is shown in Figure 5.2b and is typical for the other gemini surfactant studied. The 1:1 model fails to fit the data, as mentioned earlier. Fitting the self-diffusion data with the 2:1 model gave inaccurate values due to the many fitting parameters involved ($D_{S,f}$, $D_{CD\text{-}S}$, $D_{CD2\text{-}S}$, $D_{CD,f}$, $K_{11}$ and $K_{21}$). Data from EC, which consist of many more data points, are used for determination of the equilibrium constant. As a control experiment, $C_{12}TAB$ was measured and

compared to the results obtained from self-diffusion measurements. The results were found to be consistent.

All the genminis studied have at least 30 carbons (in the case of *12-2-12*) and a maximum of 38 carbons (in the case of *12-10-12*). Compared to $C_xTAB$ the magnitude of the association constant should be high for both $K_{11}$ and $K_{21}$. For the three geminis studied, the association constant $K_{11}$ is higher than $K_{21}$, but $K_{21}$ approaches $K_{11}$ when the spacer length increases. Thus the binding of β-CD to the surfactant is anti-cooperative. The magnitude of $K_{11}$ is 5-10 times smaller than $C_{12}TAB$. The free energy gain to form a complex between the first gemini and the β-CD is less than for a single-chain surfactant of the same chain length. Since hydrophobic interactions drive the complexation, the free energy change, to a first approximation, is proportional to the hydrocarbon area exposed to water. The tails of the gemini surfactant self-interact in order to minimiz the contact with water so the gain in free energy is lower in comparison to the single tailed surfactant.

The anti-cooperativity is due to sterical hindrance. Once the first CD sits on one of the gemini tail, the available space for the second CD to associate with the free chain is limited. In figure 5.6, a space filling model of the molecules illustrates the rather crowded situation once one of the β-CD is complexed (remember that the CD is much larger than the surfactant).

(a)                                              (b)
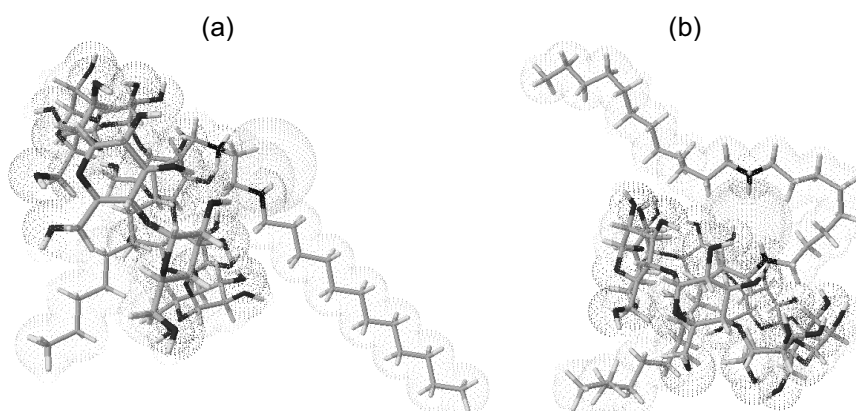


**Figure 5.6** Schematic representation of the structure of a 1:1 inclusion complex between CD and (a) *12-2-12* (b) *12-8-12*. The figures were generated using CambridgeSoft©-package (CS Chem3D Pro®).

Independently, another group[34] studied the complexation between β-CD and a gemini surfactant of type bis(dodecyl dimethylammonium)diethyl ether dibromide, *12-EO₁-12*. Interestingly, they found the opposite behavior to our findings, a cooperative process with large binding constants for both $K_{11}$ and $K_{21}$ mainly based on proton chemical shift data but also self-diffusion NMR. Another interesting study from the same group[68] is the complexation between

51

the gemini surfactant mentioned and $\gamma$-CD, were they reported that both of the tails of the gemini surfactant bound into one $\gamma$-CD.

## 5.2.3 Bolaform surfactant complexation with $\alpha$-CD and $\beta$-CD

In paper V we studied the interactions between surfactant $B_8$, $B_{10}$ and $B_{12}$ with $\alpha$-CD and $\beta$-CD with the aid of Isothermal Titration Calorimetry (ITC) (see Figure 5.7a for an example of an ITC experiment) and proton NMR (see Figure 3.7). The systems have been studied earlier by Lyon et al.[69] We extend the study to include thermodynamic and kinetic parameters at 308.2 K (and some at 298.2 K). The enthalpy of association ($\Delta H^o_{ass}$), Gibbs free energy of association ($\Delta G^o_{ass}$), entropy and association ($\Delta S^o_{ass}$) and $K_{11}$ were obtained for $\alpha$-CD and $\beta$-CD and are listed in Table 5.2. There is a paper by Rekharsky et al.[70] reviewing thermodynamic properties of host-guest formation between different guests with different cyclodextrins. The data we present in Table 5.2 are similar in magnitude (with sign) for related molecules.
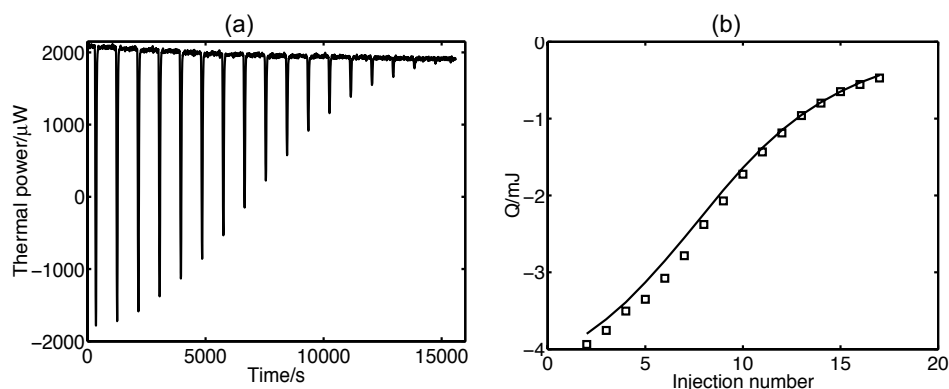


**Figure 5.7** (a) Thermal power as a function of time for sequential 4.16 µL injections of 0.1116 mol kg$^{-1}$ $B_{12}$ into 4.746 mmol kg$^{-1}$ $\beta$-CD aqueous solution at 308.20 K. (b) Heat (*Q)* per injection versus injection number at 308.20 K,($\square$) are experimental points and (——) fitted line.

The interpretation of thermodynamic data on a molecular level is difficult because all processes occurring in the system need to be analyzed in detail. The processes occurring upon complexation for a three component system (water, cyclodextrin and surfactant) are the following:

- Dehydration of surfactant (both head group and tail).
- Interaction between surfactant and CD.
- Water release from cavity to bulk.
- Conformation change of cavity upon complexation.
- Conformation change of the hydrocarbon chain upon complexation.
- Rearrangement of water around the CD-S complex.

As realized from the list above some of the contributions are mainly enthalpic in nature whereas others are entropic and some probably both. Starting with β-CD, the enthalpy is rather small and the entropy dominates the contribution to the free energy of formation, this is typical for a classical hydrophobic interaction (around room temperature). The entropy contribution stems from the dehydration of the water close to the surfactant, relaxing the more rigid water structures formed, upon complexation. The squeezing-out of water from the cavity is another source of the hydrophobic effect that contributes to the free energy. Turning to α-CD the situation is different with negative enthalpy and entropy. The enthalpy effect is larger for α-CD than for β-CD. The driving force for complexation for α-CD is enthalpic (308.2 K). The curvature (1/r, see Table 2.8) for the α-CD cavity is high and the water molecules inside the cavity might not be able to rearrange and adopt to the CD cavity while maintaining their hydrogen bonds. When the water molecules are released to the bulk phase they are able to reform the hydrogen bonds and there is an enthalpy gain, the penalty is a more ordered system i.e. a decrease in entropy. Another contribution to the enthalpy is the van der Waals interaction (vdW) which might be of more important for α-CD than for β-CD (the distance of separation of guest from the cavity wall is shorter for α-CD than for β-CD). The vdW interaction depends on electron density (i.e. size) and polarisability. The polarisability of water is lower than that of the organic molecules lining the CD cavity, so it is possible for the dispersion effect to have an effect.[29]

Another possible contribution to the entropy change is the conformational entropy of the hydrocarbon chain in the cavity. Since the two charges at the ends must reside outside the cavity this leads to a stretching of the hydrocarbon chain when it enters the cavity, which leads to a lowering of the conformational entropy. This effect is expected to be larger for the more narrow cavity of α-CD compared to β-CD.

**Table 5.2**. Values of thermodynamic parameters for the association of bolaform surfactant with α- and β-CD at 308.2 K. Errors quoted for $K$ and $\Delta H^o_{ass}$ are obtained from the fittings. Errors for $\Delta G^o_{ass}$ and $\Delta S^o_{ass}$ are propagated errors.

| CD | $B_i$ | $K$ / (kg mol$^{-1}$) | $\Delta H^o_{ass}$/ (kJ mol$^{-1}$) | $\Delta G^o_{ass}$$^{(1)}$/ (kJ mol$^{-1}$) | $\Delta S^o_{ass}$$^{(2)}$/ (J K$^{-1}$ mol$^{-1}$) |
|---|---|---|---|---|---|
| α– | n=8 | 35 ± 1.4 | -16.8 ± 0.05 | -9.1 ± 0.1 | -25.0 ± 0.4 |
| | n=10 | 764 ± 100 | -24.8 ± 1.0 | -17.0 ± 0.3 | -25.3 ± 3.4 |
| | n=12 | 3817 ± 340 | -30.7 ± 1.5 | -21.2 ± 0.2 | -31 ± 1.5 |
| β– | n=8 | - | - | - | - |
| | n=10 | 137 ± 10 | -4.7 ± 0.13 | -12.6 ± 0.7 | 25.6 ± 0.2 |
| | n=12 | 1953 ± 100 | -9.7 ± 0.1 | -19.4 ± 0.1 | 31.5 ± 0.5 |

$^{(1)}\Delta G^o_{ass} = -RT\ln(K)$. $^{(2)}$From $\Delta G^o_{ass} = \Delta H^o_{ass} - T\Delta S^o_{ass}$

# 6. Polymer-microemulsion interaction

This chapter serves two purposes; firstly to introduce microemulsions, and, secondly, to discuss some of the results obtained when diblock copolymer (see section 2.5) have been added to microemulsions. In paper VI we studied some diblock copolymers addition to bicontinuous microemulsion. Here we extend the study and present some new results.[24] The purpose of these studies was to modify the microemulsions by diblock copolymer addition in order to increase the water and oil uptake efficiency in the microoemulsions.

## 6.1 Basics of microemulsions

Microemulsions are thermodynamically stable, homogeneous liquids and consist of oil, water, surfactant, and often a fourth component such as salt (for ionic surfactants) or a cosurfactant (such as an alcohol in the case of nonionic glycoside surfactants). Microemulsions can be characterized on the basis of their microstructure into three main types of aggergate: oil-in-water droplets (o/w), water-in-oil drolets (w/o), and bicontinuous microemulsions. In the bicontinuous microemulsion (bi-$\mu$) both the oil and water domains are continuous and are separated by a monolayer film of surfactant.

A way to describe and understand microemulsions is to use the curvature concept developed by Helfrich[71], often referred to as "the flexible surface model". The basis for this description is that one sees the monolayer of surfactant (the interface between the head and tail of the surfactant) as a geometrical surface, and for each configuration one assigns a curvature free energy. The geometrical surface is given a mathematical/theoretical description characterized through five phenomological constants. The curvature at each point on the surface is characterized by two principal radii of curvature, $r_1$ and $r_2$ which are related to the two orthogonal principal curvatures, $c_1$ and $c_2$. It is also customary to define the mean curvature ($H = \frac{1}{2}(r_1^{-1} + r_2^{-1}) = \frac{1}{2}(c_1 + c_2)$) and the Gaussian curvature ($K = (r_1 r_2)^{-1} = c_1 c_2$) which basically describes the shape of the film. The curvature free energy of the film is given by

$$g_c = 2\kappa_0 (H - H_0)^2 + \overline{\kappa}_0 K \qquad (6.1)$$

where $\kappa_0$ is the bending rigidity modulus (describes the energy of bending a single surface), $\overline{\kappa}_0$ is the saddle splay modulus (is a measure of the energy cost to create a saddle-type deformation) and $H_0$ is the spontaneous curvature (a useful parameter in describing microemulsions). The reference state is a planer film. When $H_0 > 0$ the preferred curvature is towards oil and an o/w microemulsion is formed, but when $H_0 < 0$ a w/o microemulsion is formed. For

$H_0 \approx 0$ a bi-μ or lamellar, $L_\alpha$ structure is formed. $H$ is zero for $L_\alpha$, and for bi-μ, $K$ on the other hand is less than zero for bi-μ and zero for $L_\alpha$.

Of particular interest, both from the scientific and industrial point of view, is knowing which surfactant is most efficient in solubilizing of equal volumes of water and oil. Ternary phase diagrams are used to map out the different phases formed for water, oil and surfactant mixtures at a given temperature and pressure. To map out one entire phase diagram is very tedious and often a lengthy process, because often it takes time for the sample with high fraction of surfactant to reach equilibrium. Furthermore, the phase diagram's phase borders and phases change with temperature etc. To rationalize this and to cope with the effect of temperature or other variables such as alcohol and salinity, special versions of the phase diagram have been developed. The χ-cut, "Shinoda cut" (after the inventor) is a phase diagram where the surfactant concentration is fixed and one varies the volume fraction of oil ($\phi_o$) i.e.

$$\phi_o = V_o / (V_o + V_w) \tag{6.2}$$

where $V_o$ and $V_w$ are the volumes of oil and water, respectively. The temperature and $\phi_o$ are the two independent variables. Another type of phase diagram of interest is when the water to oil ratio (by volume) is fixed and the temperature and the amphiphilic amount are the independent variables. This kind of phase diagram is called a "fish diagram" which stems from the shape of the phase boundaries.

## 6.2 Fish phase diagram and Winsor states

A fish phase diagram is a planar cross section through the phase prism at a given ratio of water-to-oil, usually at 1:1 (called balanced microemulsion), see Figure 6.1. The fish phase diagram consists of six different areas. At low temperature an o/w microemulsion coexists with an excess oil phase (often denoted $\underline{2}$ or called a Winsor I). At higher temperature, a w/o microemulsion coexists with an excess water phase (often denoted $\overline{2}$ or Winsor II). At intermediate temperatures there is a three phase coexistence with an excess water phase, a microemulsion phase (often a bicontinuous type, called Winsor III), and an excess oil phase. At intermediate temperatures and relative high amounts of surfactant concentration a one phase area starts to grow, often a bi-μ. The concentration of surfactant for the starting point of this one phase area (the X-point in figure 6.1c), $\tilde{\gamma}$ (or $\tilde{\gamma}_1$ when the tuning parameter is co-surfactant), is important especially in balanced microemulsions because it give the minimum amount of surfactant that is needed to solubilize equal volumes of water and oil, and is thus a measure of how effective the surfactant is in solubilizing water and oil. The temperature at $\tilde{\gamma}$ is denoted $T_0$. At high
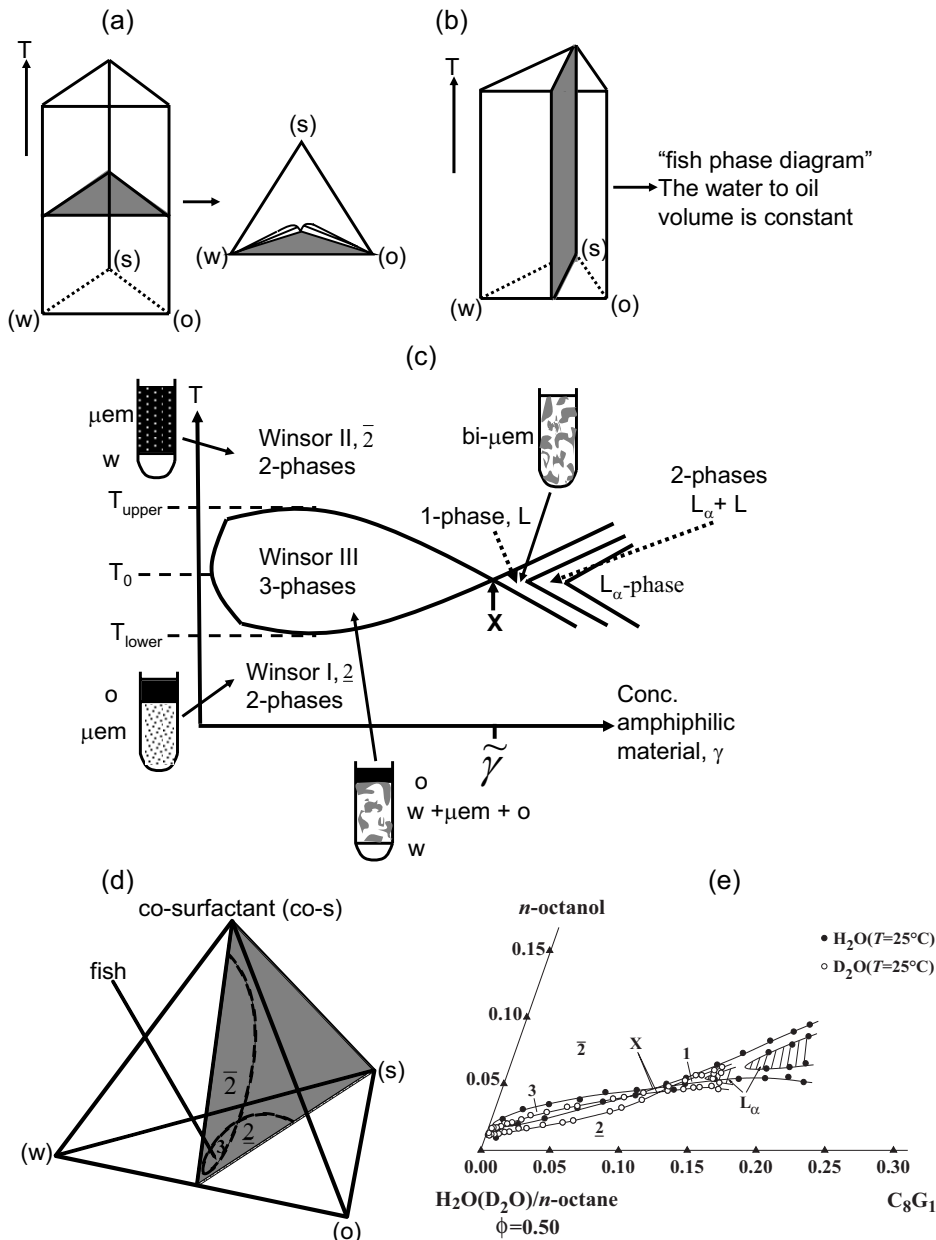
55

**Figure 6.1** (a) Phase prism of a ternary w/s/o system versus T (b) Schematic illustration of the section through the phase prism $\phi_0 = 0.5$. (c) Schematic fish phase diagram plotted as a function of T versus $\gamma$. (d) Schematic phase tetrahedron of a quaternary w/o/s/co-s system. The gray cut is through the phase tetrahedron at $\phi_0 = 0.5$. (e) Fish phase diagram (water or heavy water/n-octane/$C_8G_1$/n-octanol) mass n-octanol as a function of $\gamma_1$ from Sottmann et al. [72]

56

concentrations of surfactant a lamellar phase, $L_\alpha$, starts to form. The value of $\gamma$ is calculated using

$$\gamma = \frac{m_s}{m_s + m_o + m_w}, \qquad \gamma_1 = \frac{m_s}{m_s + m_o + m_w + m_{co-s}} \qquad (6.3)$$

where $m_s$, $m_o$, $m_w$ and $m_{co-s}$ are the masses of surfactant, oil, water and co-surfactant, respectively.

In Figure 6.1c the schematic fish phase diagram with temperature versus concentration of surfactant is shown. The parameter on the y-axis is called the tuning parameter because with this parameter the surfactant monolayer film is tuned, either bending bended towards the water, oil or in a planar configuration. The surfactant $C_8G_1$ (Table 2.4) that we have been working with is insensitive towards temperature changes in comparison to the nonionic ethoxylated surfactants ($C_yEO_x$). A typical binary phase diagram of $H_2O + C_yEO_x$ has horizontal phase boundaries whereas for the n-alkyl-β-D-glucoside the phase boundaries are vertical. The key quantity in describing the phase behavior is instead the composition of the internal film after addition of the co-surfactant, often an alcohol. The alcohol increases the hydrophobicity of the film and also acts as a co-solvent for the oil making the oil more polar. In Figure 6.1e the fish phase diagram of $H_2O$/n-octane/$C_8G_1$/n-octanol[72] is shown, which will be discussed later.

## 6.3 Polymer addition to bicontinuous microemulsion, background

This paragraph will review polymer addition to a balanced microemulsion. Adsorbing and non adsorbing polymers will be considered.

### 6.3.1 The effect of different types of polymers on the phase behavior of a balanced microemulsion.

The interaction between the monolayer film, separating the oil and water domains, and polymer is important. The response of water and oil uptake upon addition of polymer to a Winsor III state depends strongly on the type of polymer used (see Figure 2.3). One distinguishes between polymers that do not adsorb and polymer that do adsorb onto the surfactant film.

Many homopolymers that are water soluble (or oil soluble) will not interact (adsorb) with the surfactant film in a bi-μ. Homopolymers with a radius of gyration $R_g$, larger than the pore size of the water (or oil) domain will not penetrate into the bi-μ. If the $R_g$ of the homopolymer is smaller than the pore size they will be soluble in the domains of water (or oil). There will be a partition of the homopolymer between the bi-μ phase (middle phase) and the

excess phase (top or bottom phase). Kabalnov et al.[73] studied dextran, poly(ethylene glycol) and poly(isobutylene) interaction with a balanced microemulsion ($C_{12}E_5$/n-decane/$H_2O$). The generalized results are given in Figure 6.2a. For low molecular weight dextran the excess water phase increased slightly in volume, due to the higher amount of dextran in the excess water phase. For high molecular weight dextran the excess water phase increased in volume substantially (the polymer osmotic pressures squeezes out water from the middle phase). The same is true for the excess oil phase for a hydrophobic homopolymer.

Kabalnov et al.[74] also studied the effect of hydrophobically (HM) modified polymers (hydrophobically modified ethyl hydroxyethyl cellulose), in the same microemulsion system. The polymers adsorb to the film and modify the bicontinuous microemulsion by incorporating water from the excess phase (also a minor fraction of excess oil). The $R_g$ for these HM-polymers were greater than the size of the water domains, so the polymer is not trapped in the water domains, but anchored at the oil-water interface. The HM-part sits in the hydrophobic part of the film, while the much greater hydrophilic part of the polymer sits and sticks out from the other side of the film. Figure 6.2b shows the general behavior and Figure 6.3c shows schematic drawing of the film decoration.

The addition of symmetric diblock copolymers, e.g. poly(ethylenoxide)poly(butylmethacrylate), poly(ethyleneoxide)poly(styrene) poly(ethyleneoxide)poly(ethylene-co-propylene) (PEO-PEP) to various bicontinuous microemulsion systems at the balanced temperature and $\phi_o = 0.5$ has been studied by Jakobs et al.[75, 76] Kumar et al.[77] studied the addition of a silicone type polymer ($Si_xC_3EO_y$) to a bicontinuous microemulsion consisting of $C_{12}E_5$/$H_2O$/n-dodecane at the balanced temperature and $\phi_o = 0.5$. The diblock copolymer modifies the bicontinuous microemulsion phase dramatically, by swallowing water (lower phase) and oil (top phase) symmetrically at low amount of diblock copolymer addition. The mesh size of the water and oil domains grows upon diblock copolymer addition, and eventually the domain sizes (the structural length scale) are so big so that the domains start to scatter light. In other words, the efficiency-boosting is accompanied by an increase in the structural length scales of the bi-μ. One can imagine that the polymers decorate the interface with the hydrophobic part of the diblock copolymer sticking into the oil domain and the hydrophilic part of the diblock copolymer sticking out into the water domain. A schematic drawing (see figure 6.3) illustrates how the different types of polymers can decorate the film (on the microscopic scale).

The efficiency enhancement (equation 6.4), the increased capacity of uptake of water and oil by the bicontinuous microemulson (the shift of the X-

point in Figure 6.1c towards lower amphiphilic concentrations) can be calculated and is called the efficiency boosting factor

$$f_B \equiv (\tilde{\gamma} - \tilde{\gamma}_2 (1 - \delta_{film,T})) / (\tilde{\gamma} \delta_{film,T}) ,$$

$$(6.4)$$

$$\gamma_2 = \frac{m_s + m_p}{m_s + m_o + m_w + m_p} , \qquad \delta_{film,T} \equiv m_p / (m_p + m_s)$$

where $m_p$ is the mass of polymer, the index $T$ in $\delta_{film,T}$ is included because the tuning parameter for these microemulsion is temperature. Equation 6.4 relates how much surfactant is replaced $\tilde{\gamma} - \tilde{\gamma}_2 (1 - \delta_{film,T})$ by the diblock copolymer, $\tilde{\gamma}_2 \delta_{film}$. The boosting factor Jacobs et al.[75, 76] reported for PEO-PEP $12 < f_B < 22$ depended on the type of microemulsion system, in particular the value of $\tilde{\gamma}$. The less efficient the base microemulsion system is the higher is the boosting factor. The polymer weight of the diblock copolymer does not influence the boosting factor significantly (comparing equal polymer mass fractions).[75, 76]

Finally, turning to the effect the addition of amphiphilic block copolymer adsorption at the interface water/oil have on the curvature of a bi-μ. The anchored polymer modifies the curvature properties of the bi-μ monolayer film significantly according to phase diagrams and small angle neutron scattering results.[78-80] The equation 6.1 used for calculating the curvature free energy of the film will be modified upon block copolymer addition. The bending rigidity and saddle splay modulus will be expressed as an effective bending rigidity ($\kappa_{eff}$) and saddle splay modulus ($\bar{\kappa}_{eff}$) instead. The new important parameter that affect $\kappa_{eff}$ and $\bar{\kappa}_{eff}$ are the end-to-end distance of the diblock copolymers respective block and the grafting density ($\sigma$). Two different regimes can be defined depending upon the grafting density of the polymers. At low grafting density the regime is called the "mushroom" regime and at high grafting density it is called the "brush" regime. The equations describing the new effective curvature moduli, $\kappa_{eff}$ and $\bar{\kappa}_{eff}$, are only correct at the overlap concentrations (mushroom regime→brush regime).

$$\kappa_{eff}(\sigma) = \kappa_0 - \frac{k_B T}{12}\left(1 + \frac{\pi}{2}\right)\sigma(R_w^2 + R_o^2) \qquad (6.5)$$

$$\bar{\kappa}_{eff}(\sigma) = \bar{\kappa}_0 - \frac{k_B T}{6}\sigma(R_w^2 + R_o^2) \qquad (6.6)$$

where $R_w$ and $R_o$ are the end-to-end distance of the hydrophilic and hydrophobic polymer blocks. $\sigma$ is the polymer grafting density. Finally, Endo et al.[78, 79] explain the efficiency boosting effect of the tethered polymer in terms of the variation of the saddle-splay modulus by the tethered chains. Increasing the polymer size at constant $\delta_{film,T}$ the efficiency boosting effect does not increase due to the interplay of two opposite effects; $R_w$ and $R_o$ increase whereas the grafting density decreases, see equations 6.5 and 6.6. The curvature of the film is also modified, the effective spontaneous curvature, $H_{0,eff}$, is defined in equation 6.7. Please note when $R_w = R_o$ the curvature is zero.

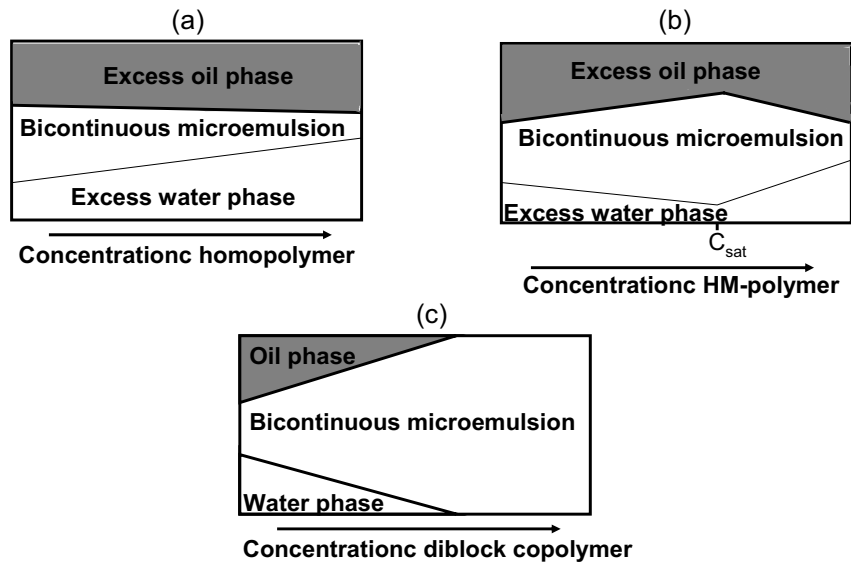$$H_{0,eff} = H_0(T) + \frac{1}{4}\sqrt{\frac{\pi}{6}}\frac{Tk_B}{k_{eff}}\sigma(R_w - R_o) \qquad (6.7)$$

(a)

**Excess oil phase**

**Bicontinuous microemulsion**

**Excess water phase**

**Concentrationc homopolymer**

(b)

**Excess oil phase**

**Bicontinuous microemulsion**

**Excess water phase**

$C_{sat}$

**Concentrationc HM-polymer**

(c)

**Oil phase**

**Bicontinuous microemulsion**

**Water phase**

**Concentrationc diblock copolymer**

**Figure 6.2** A bicontinuous balanced microemulsion (at $T_0$) with excess water and oil phase is considered. Typical variations of the relative volumes of the excess water, the bicontimuous microemulsion and the excess oil as a function of polymer concentration are shown. (a) Addition of a non adsorbing hydrophilic homopolymer, (b) water soluble HM-polymers, and (c) for a symmetric diblok copolymer consisting of one hydrophilic block and one hydrophobic block. In figure 6.2b the saturation concentration $C_{sat}$ is indicated, which is the concentration at which the bicontinuous microemulsion phase is saturated with polymer. After $C_{sat}$ the polymer goes into the excess water phase, where the osmotic pressure of the polymer drives out the water from the bicontinuous microemulsion.
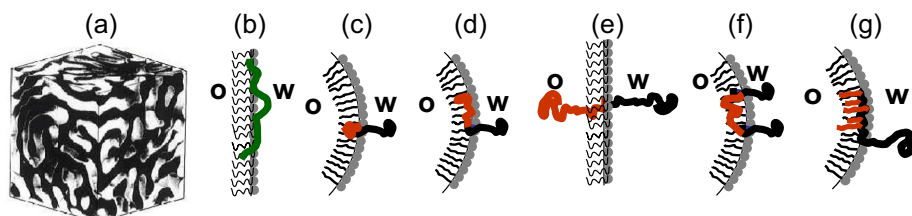
**Figure 6.3** Schematic pictures showing how the decoration of the different types of polymers influences the films curvature in a bi-μ. (a) A bi-μ. (b) A polymer that interacts with the bi-μ in a "pancake like manner". (c) HM-polymer (hydrophilic) bi-μ interaction. (d) A diblock copolymer interacting with the bi-μ . The hydrophobic block has high affinity for the interface whereas the hydrophilic block sticks out into the water. (e) Symmetric diblock copolymer bi-μ interaction affects the curvature of the film equally on both sides. (f) Hydrophilic triblock copolymer interaction with the bi-μ. (g) An diblock copolymer where the back bone of the hydrophobic block consists of grafted small hydrophobic tails like a "brush", see paper VI for more details and example of polymers giving this effect on the curvature

## 6.4 Diblock copolymer addition to microemulsions

The starting point of these studies is the fish diagram consisting of water/n-octane/$C_8G_1$/n-octanol at equal volumes of water and oil at 298 K. A sample in the Winsor III phase area of the following weight % composition was used: 4.31/2.87/38.99/53.83. The volumes of the bottom phase, the middle phase and the top phase are roughly equal, so it is a good model sample to observe the volume changes upon the diblock copolymer addition. Surfactants were replaced by diblock copolymer (see Table 2.6) keeping $\gamma_3$ constant at 0.043. $\gamma_3$ is given by

$$\gamma_3 = \frac{m_s + m_p}{m_s + m_o + m_w + m_{co-s} + m_p} = \frac{m_a}{m_a + m_o + m_w + m_{co-s}} \tag{6.8}$$

In figure 6.4 the results of the diblock copolymer addition are shown. Three observations immediately apparent:

*Firstly*: The effect of diblock copolymers (see table 2.6) decorating the microemulsion films are more efficient in the oil uptake from the excess oil phase, than the water uptake from the excess water phases. The swelling is unsymmetric.

*Secondly*: The values for $\delta_{film}$ (equation 6.9) were all water and oil is swallowed by the middle phase (only bi-μ phase), all are between 0.15-0.18, which is a relative small concentration interval for the polymer. The architecture, block size (molecular weight end-to-end distance) and bulkiness of the diblock copolymer seems to have little influence on the efficiency as also reported by Jakobs et al.[75] The boosting effect (equation 6.8) is approximately between

(8-9) for all systems (the uncertainty is ± 1 in the boosting factor). The value of $\tilde{\gamma}_1$ was taken to be 0.1609 from Sottmann et al.[72]

$$f_B \equiv (\tilde{\gamma}_1 - \tilde{\gamma}_3(1 - \delta_{film}))/(\tilde{\gamma}_1 \delta_{film}) \qquad \delta_{film} \equiv m_p /(m_p + m_s + m_{co-s}) \qquad (6.9)$$

*Thirdly*: A lamellar phase, $L_\alpha$-phase appears at high concentration of diblock copolymer.
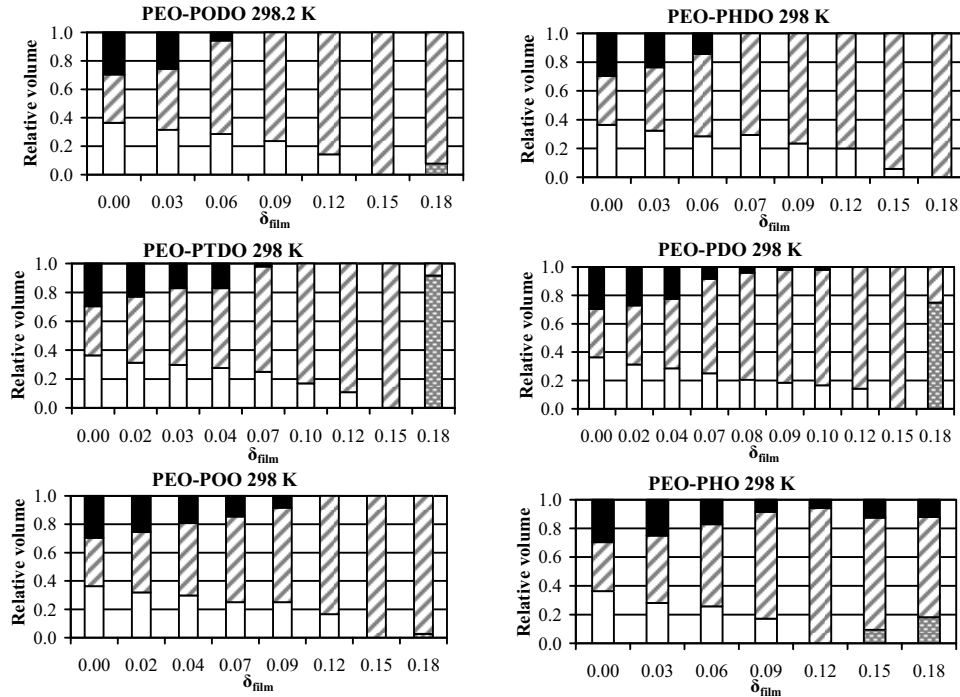


**Figure 6.4** Swelling behaviour of the different polymers in the Winsor III system containing $C_8G_1$/1-octanol/n-octane/$H_2O$ (composition by weight %: 4.32, 2.87, 38.99 and 53.83) as a function of $\delta_{film}$. The volumes are measured with a ruler and the error in the volumes is estimated to be ± 1%. The appearance of $L_\alpha$-phases was detected with a polarizer.

Jakobs et al.[75] report that addition of small amount of diblock copolymer suppressed the $L_\alpha$-phase Frank et al.[81] studied the factors that govern the appearances of $L_\alpha$ in more detail. They concluded that at low amount of diblock copolymer $\delta_{film,T} < 0.01$ the $L_\alpha$-phase was suppressed to higher values of $\gamma_2$. At higher amount of the $\delta_{film,T}$, the $L_\alpha$-phase were shifted to lower amounts of $\gamma_2$. Furthermore, they concluded that an increase in polymer size results in a suppression of the $L_\alpha$-phase more efficiently for the same $\delta_{film,T}$. Frank et al.[81]

have mapped the fish diagram, but care should be taken when interpreting the results. Firstly the phase diagram around the X-point is very complex and secondly, there have to exist several 2-phase areas in order to fulfill the Gibbs phase rule.

Turning the focus to the effect the addition of homopolymers has on the minimum amount of surfactant needed to solubilize water and oil at $\phi_o = 0.5$. This is of relevance because the polymers synthesized (see Table 2.6) contain significantly amounts of hydrophobic homopolymer as contamination so its effect is important to know. Byelov et al.[82] studied the simultaneous effect of the homopolymers PEO and PEP (both at approximately 5000 g/mol) on the fish phase diagram $H_2O$/n-decane/$C_{10}E_4$. Addition of small amounts of homopolymers increase the minimum amount of surfactant ($\tilde{\gamma}$) needed to solubilise equal volumes of oil and water. Diblock copolymers and homopolymers were added simultaneously to the above mentions system and the X-point were shifted to higher amphiphilic amount in order to reach the one phase area. Homopolymers exert an antiboosting effect in microemulsions. Higher amount of amphiphilic amount is required to achieve a one phase.

Due to the known antiboosting effects[82], we examine the effect of di(propyleneoxide)-poly(dodecyleneoxide) of molecular weight (2±0.5) kg/mol, a compound similar to the by-products obtained during the synthesis of the diblock copolymers (Table 2.6). The addition of the hydrophobic homopolymer to the system water/n-octane/$C_8G_1$/1-octanol with $\phi_o = 0.5$, and $\gamma_1 = 0.043$, leaves the phase behaviour unchanged. The concentrations of the added homopolymer was between 0.7-1.8 wt% corresponding to $\delta_{film} = 0.09$-$0.22$ if all the polymer are present in the film. These values are exceeding the amounts of the homopolymers that are present in the diblock copolymers.

## 6.5 Diffusion measurements of bicontinuous microemulsions

The microstructures of the microemulsions have been studied with the NMR diffusometry technique. The aim was to obtain the self-diffusion coefficients of the components as a function of polymer concentration and relate them to the curvature of the monolayer film. A short general review of self-diffusion measurements in microemulsions will follow.

In oil swollen micelles (o/w), water diffusion is rapid, while that of surfactant and the solubilized oil is slow; the surfactants have a slightly faster diffusion coefficient than water due to the fact that the surfactant has a fraction of free surfactant, $P_{S,f}$ in the bulk solution whereas all the oil is solubilized in the micelles. The exchange for a surfactant in a micelle to bulk solution is fast on the NMR timescale (see section 4.3) In water swollen micelles, the diffusion of the oil is fast while those of water and surfactant is slow. In a bicontinuous system, the constituents of the monolayer film generally diffuse slowly, while the oil and water diffuse rapidly. In bicontinuous microemulsions, the water and

63

oil domains are assumed to have the same properties as the neat liquids, with the self-diffusion coefficient roughly the same as for neat liquids, $D_0$. When the ratio $D/D_0$ deviates from unity (neglecting solvation effects), this is due to obstruction effect by the monolayer film. In a balanced microemulsion the ratio $D/D_0 \approx 2/3$ (2/3 due to the fact that the neat liquid is free to diffuse in 2 dimensions). The geometrical obstruction factor depends on the water-to-oil ratio. It is common to perform an expansion around the balanced state, for water and oil.

$$D_w / D_{w,0} = 0.66 - \beta(\theta_o - 1/2) \tag{6.10}$$

$$D_o / D_{o,0} = 0.66 + \beta(\theta_o - 1/2) \tag{6.11}$$

Where $D_w$, $D_{w,0}$, $D_o$ and $D_{o,0}$ are the self-diffusion of the water, neat water, oil and neat oil. $\theta_o$ is the volume fraction of oil, and $\beta$ is the expansion coefficient. The surfactant self-diffusion coefficient is at its maximum for the balanced state, and the corresponding expansion is

$$D_S / D_{S,lat} = 0.66 - \beta'(\theta_o - 1/2)^2 \tag{6.12}$$

where $D_{S,lat}$ is the lateral diffusion of the film (2-dimensions) and $\beta'$ another expansion coefficient.

  The self-diffusion coefficients of water, $D_w$, and n-octane, $D_{oct}$, at 298 K were normalized with the corresponding quantities obtained from a polymer-free system[83] to make it possible to compare the polymer-free microemulsion with systems with polymers. The absolute values of $D$ for the surfactant and polymer will be given because the self-diffusion data that will be shown do not correspond to constant $\gamma_3$ (the amphiphilic amount increases with polymer concentration).

  The phase diagrams together with the self-diffusion NMR data are given in Figure 6.5. The self-diffusion of the polymer and surfactant are generally only slightly affected. The polymer diffusion is slower than the surfactant and with increasing amount of polymer the surfactant diffusion gets reduced more than the polymer self-diffusion (see Figure 6.5a). The water and oil self-diffusion are on the other hand affected significantly, depending on what type of polymer (and the balance between the block) that have been added. In Figure 6.5a a symmetric diblock copolymer $PEO_{43}PDDO_{41}$ have been added and the swelling behaviour is nearly symmetric (increase of middle phase at the expense of the bottom and top phase). The normalized self-diffusion behaviour of oil and water increases and has the same normalized self-diffusion coefficient at a concentration of $\delta_{film}$ corresponding to the X point. The interpretation of this
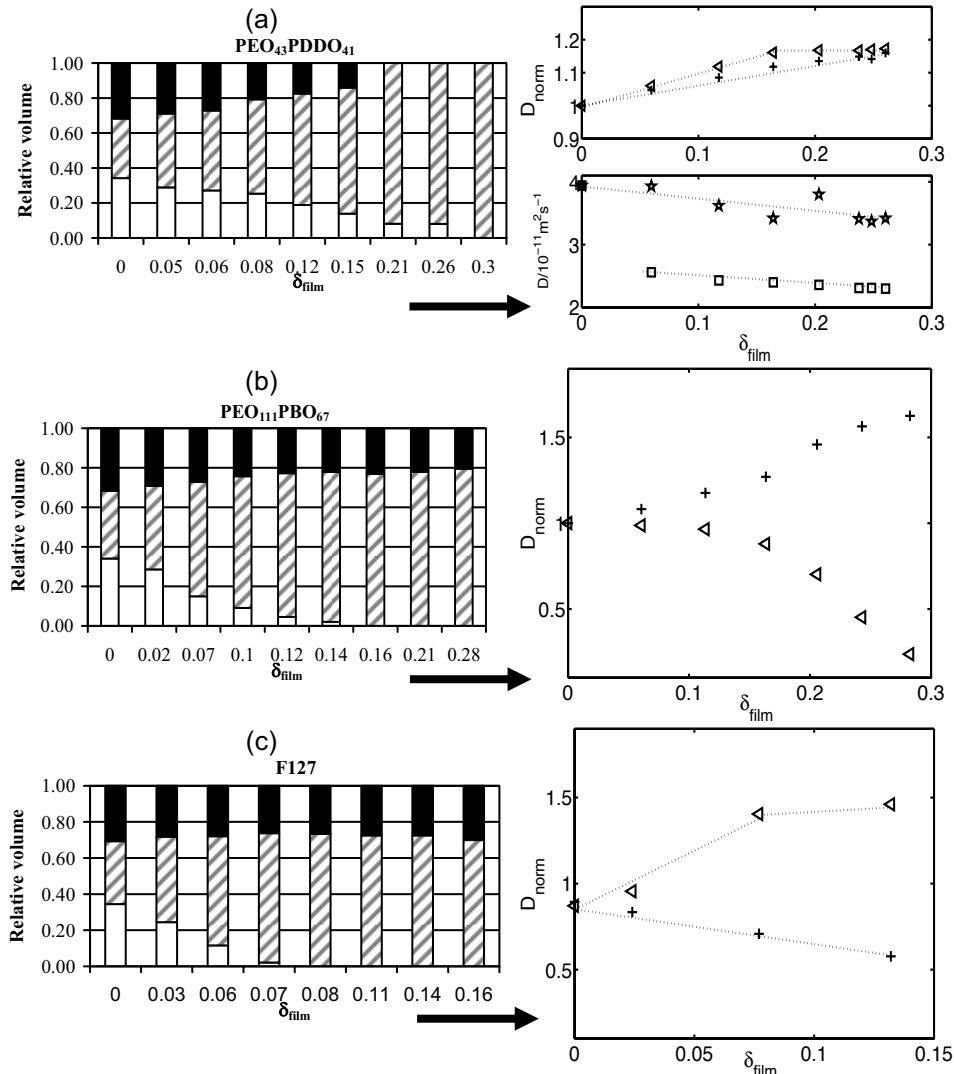
**Figure 6.5** Phase behavior of the system $D_2O$/n-octane/$C_8G_1$/n-octanol/diblock copolymer and self-diffusion measurement of the components in the systems at 298 K. $D_{norm}$ is the normalized water (or oil) self-diffusion with respect to the self-diffusion of water (or oil) in polymer free film.[83] For the self-diffusion studies deuterated n-octanol were used to simplify the spectrum. Please note that the phase studies are done with $D_2O$ and the polymers have been added to a given composition of amphiphilic amount $\gamma_1$ =0.047. The surfactants have not been replaced as in the phase diagrams given in Figure 6.4.

is that the water and oil mesh sizes have grown larger. Figure 6.5b shows the phase diagram with the diblock copolymer $PEO_{111}PBO_{67}$. The microemulsion phase expands here in volume by incorporating mostly water; the swelling is

highly antisymmetric. The normalized self-diffusion coefficient for water increases and for oil decreases. The self-diffusion behaviour can be explained by the fact that the microemulsion is curved towards the oil (see Figure 6.3d). Finally, in Figure 6.5c the phase behaviour of the microemulsion with F127 is given. Here the middle phase grows at the expense of the excess water phase, at $\delta_{film} = 0.08$ all excess water is taken up by the microemulsion. The oil excess phase remains almost constant and is unaffected by the addition of F127. At higher polymer concentration $L_\alpha$-phase is formed (not included in the figure). The self-diffusion for water increases and has a maximum value at $\delta_{film} = 0.08$ were all the excess water is taken up by the microemulsion. The normalized oil self-diffusion decreases linearly. Again we interpretate the results as the curvature of the film is towards the oil (see figure 6.3f).

# 7. Diffusion studies of a triblock copolymer

Molecular motion of a poly(ethylene oxide)poly(propylene oxide)poly(ethylene oxide) triblock copolymer was investigated in water with the aid of self-diffusion NMR. PGSTE experiments were used to study 1 wt % F127 in the temperature range from 288 to 313 K. The self-association of F127 has been studied by several other groups.[84-87] Our focus is not directly on the F127 system as such; we use it because it is a commonly used synthetic amphiphilic polymer with polydispersity both in molecular weight and composition. The polydispersity has consequences on the polymer self-assembly, which will be highlighted in the following discussions. In the literature there are reports of anomalous diffusion when Pluronic polymers self-assemble.[88-90] In these reports the mean squared displacement does not scale linearly with the diffusion time (see equation 4.3) and may show a power law dependence, $<z^2>\sim\Delta^\alpha$, instead of $<z^2>\sim\Delta$, where $\Delta$ is the diffusion time.[89] Other reports claim that the exchange time is slow on the NMR timescale between the self-assembled structure and monomer.[86]

Before going into the modulation of the PGSTE intensity decay (from NMR self-diffusion experiments), we review some of the different fitting and transformation approaches used to treat the PGSTE raw data.

## 7.1 Methods in treating self-diffusion data

There are several approaches to fit and transform complex self-diffusion data, $I$ versus $k$:

**Single exponent fit,** (equation 4.21) should always be considered first as it is the simplest most reliable fit.

**Biexponential fit**, for two diffusion coefficients. Fits in general most cases where a single exponent fails to fit the data. The biexponetial fit is often used in systems of polydisperse polymer. However care, should be taken when interpreting such diffusion coefficients (in most of the cases it is fast exchange on the NMR time scale).

$$I_n(k) = P_a \exp(-kD_a) + (1 - P_a)\exp(-kD_b) \qquad (7.1)$$

**Discrete (fit to sum of n exponentials)**. Fits the intensity decay curve using n exponentials. Could in principle be used for polydisperese polymer samples, when nothing else works and makes sense. The obtained results are n self-diffusion coefficients with n weighting factors. As the fitting parameters ($D_i$ and $P_i$) increase the uncertainty in its values increases.

$$I_n = \sum_i^n P_i \exp(-kD_i), \qquad \sum_i^n P_i = 1 \qquad (7.2)$$

**Stretched exponent.** Can be a useful way of analyzing complex polydisperse NMR self-diffusion data, when other fitting approaches fail. The data is best represented in a plot with $\log(I_n)$ versus $(\gamma\delta g)^2$. Bear in mind, using this approach $(\langle D^{-1}\rangle)^{-1} \neq \langle D\rangle$. This means that the calculated diffusion coefficient is not the true average diffusion coefficient.[91] The consequence of this is that the calculated diffusing coefficient will be more strongly weighted by the slowly diffusion species as the curvature (in a plot of $\log I_n$ versus $(\gamma\delta g)^2$) of the echo decay starts to increase.

$$I_n = \exp\left[ (-\gamma^2 \delta^2 g^2 \Delta D_{eff})^\beta \right] \qquad (0 < \beta \leq 1) \qquad (7.3)$$

$$\left\langle \frac{1}{D} \right\rangle = \frac{\Gamma(1/\beta)}{\beta D_{eff}} \qquad\qquad (7.4)$$

$\beta$ describes the width of the distribution of the self-diffusion coefficients, and $D_{\mathrm{eff}}$ is an effective self-diffusion coefficient. Both of these parameters are obtained from a least-square fitting.

**Fit to a log-normal distribution**. Here the result is described by a probability distribution function of self-diffusion coefficients $P(D)$ versus $\log(D)$ and the parameters obtained through least-square fitting are, $\sigma_D$ and $D_0$ where $\sigma_D$ is a measure of the width of the distribution and $D_0$ is the median self-diffusion coefficient. From the obtained parameters the average self-diffusion coefficient $\langle D\rangle$ can be calculated [92]. Using

$$P(D) = \frac{1}{D\sigma_D \sqrt{2\pi}} \exp\left( -\frac{\left[\ln(D) - \ln(D_0)\right]^2}{2\sigma_D^2} \right) \qquad (7.5)$$

$$\langle D \rangle = D_0 \exp(\sigma_D^2 / 2) \qquad\qquad (7.6)$$

**COmponent REsolved (CORE).**[93, 94] In the CORE approach a global fit to all significant data points in the raw PGSE (or PGSTE) NMR data set is performed. As a consequence the precision in the obtained parameters is improved, since all the available information in the spectrum is utilized effectively.

**Inverse Laplace Transformation (ILT)** is frequently used when the functional form of the distribution of self-diffusion coefficient is complex. If it is sufficient to fit the data with a log-normal distribution (equation 7.5) ILT should be avoided.[95] The ILT can produce artifacts, "ghost peaks", due to the fact that it is an ill-defined transform. It also broadens the peaks. The ILT routine requires

high quality data, and, the routine should always be checked against a sample with known distribution of self-diffusion coefficients.

$$I_n(k) = \int_0^\infty P(D)\exp(-kD)dD \tag{7.7}$$

A combination of the fitting approaches above and other transforms are naturally also possible. In paper VII single exponential and biexponential fits, lognormal distribution fits, CORE and ILT have been used to treat the self-diffusion data.

## 7.2 Interpreting and modeling self-diffusion data from F127

The aim of this section is to explain and model the intensity decay from NMR self-diffusion measurement (PGSTE), taking the physics of the self-associating polymer F127 into account. The background of the model is the following. Below the CMT (288 K), the PGSTE signal decays approximately linearly when the intensities are plotted on a logarithmic-linear scale (Figure 7.1a). At the CMT (302 ± 5 K), the signal decays are curved. Turning again to the signal decay at 288 K where the polymer is almost exclusively in the free form (no micelles exist), we see that the intensity decay shows a minor deviation from the single-exponential fit when plotted versus $k$ (see Figure 7.1a). The self-diffusion data at 288 K were fitted with a log-normal distribution (see equation 7.5). The obtained $P(D)$ (Figure 7.1b) is used to calculate the distribution in molecular weight, $P(M)$ (Figure 7.1c), using the scaling relations given by equation 7.8.

$$D = KM^{-\alpha} \tag{7.8}$$

where $M$ is the molecular weight, $K$ is a constant, and $\alpha$ is a scaling parameter. The value of the scaling parameter used was $\alpha = 0.55$ (taken from PEO at 298K [92]).

The basis of the model is the assumption that we have a multicomponent ideal mixture and that the phase separation model for micelle formation applies. [2, 3, 96] The model will be split up into different steps for clarity:

- $P(D)$ below CMT (288 K) is converted to $P(M)$ (equation 7.8 [92]).
- Polymer $i$ with molecular weight, $M_i$, is assigned a concentration of $C_i$, and a molar fraction $P_i$ in the polymer mixture (obtained from $P(M)$).
- We assume that the individual CMC values, $CMC_i$, for each polymer component increases logarithmically with the number of EO units (see Figure 7.1d).

- The global CMC (the effective CMC) is given by equation 7.9. The concentration of non-micellized polymer ($C_{i,free}$) is obtained from results for ideal mixing.[96]

$$\frac{1}{CMC} = \sum_i \left( \frac{P_i}{CMC_i} \right) \tag{7.9}$$

- We assume fast exchange on the NMR timescale between monomer and micelles.
- Finally, the NMR self-diffusion signal decay is synthesized by summing signal decays from each polymer component with the calculated fraction of free ($C_{i,free}/C_i$) and bound ($1-C_{i,free}/C_i$) polymer assuming reasonable values for free diffusion, $D_{free}$, and polymer that are aggregated, $D_{bound}$. The generated signal decay and the ILT are presented in Figure 7.1e and 7.1f, respectively. Clearly the model is capable of producing echo-decays that resemble the ones experimentally observed (cf. Figure 7.1a, 302 K).

Only a minute fraction of the polymer components have CMC values around the effective CMC, and thus have a diffusion coefficient between $D_{free}$ and $D_{bound}$, (remember, $D_{i,obs} = P_{i,free}D_{i,free} + (1-P_{i,free})D_{i,bound}$), while most of the polymers are almost completely micellized or free. The hydrophilic polymer components remain in solution and take little part in the association process, while the more hydrophobic polymers are to a large extent micellized.

The fact that we can write the observed echo decay signal in terms of two diffusion coefficients give us the possibility to further calculate important characteristic of the association process. One such characteristics is the ratio between the number of EO units and PO units for free, micellized and total as calculated from the deconvoluted spectra produced by CORE, see Figure 7.2a. The deconvoluted spectra have been further analyzed by integration of the peaks in the spectra. Prior to integration suitable corrections for $T_1$ and $T_2$ relaxation times (see equations 4.22 and 4.23) were done, see Table 7.1 for relaxation times. Figure 7.2b shows the ratio mEO/nPO for free, micellized and total versus temperature. Focusing on the ratio for the micellized F127, the ratio increases mildly as a function of temperature, indicating that at low temperature the more hydrophobic polymer components of F127 take part in the association, while the polymer components with larger ratios of EO to PO do not take part in the association. Turning to the ratio between EO to PO for the free polymer, the ratio also increases, but the increase is considerably more pronounced. At the
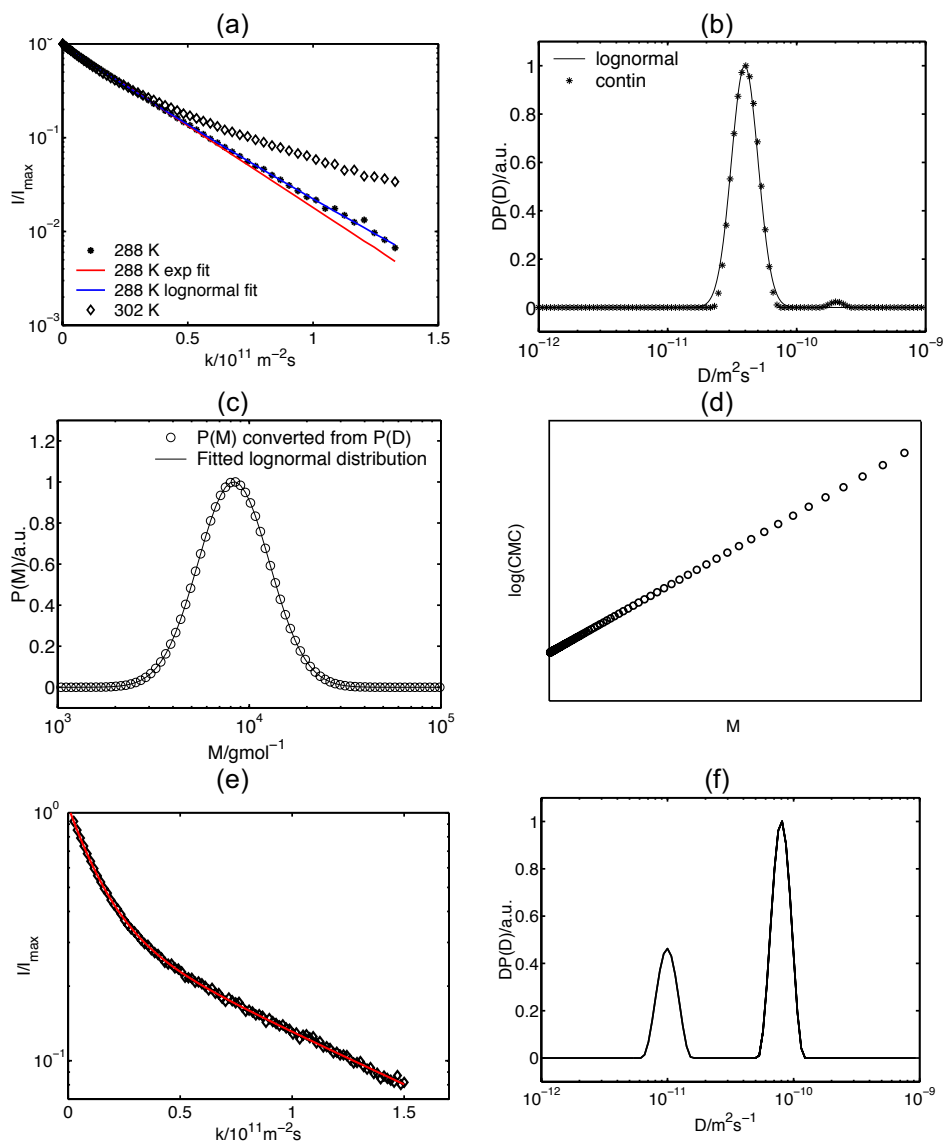
**Figure 7.1** (a) $I/I_{max}$ versus $k$ for 1 wt% F127 at 288 K and 302 K. In the graph are also predictions of an exponential fit, a log-normal distribution fit ($<D>$ = $4.31 \cdot 10^{-11} m^2 s^{-1}$ and $\sigma_D$ = 0.24) for the decay at 288 K. (b) $DP(D)$ versus $D$ obtained from the ILT approach (contin) and from the fit of a log-normal distribution. (c) $P(M)$ from the transformation of $P(D)$ versus $M$ ($M_0$ = 10000g/mol and $\sigma_M$ = 0.43). Also included is a fit to a lognormal $P(M)$. (d) Schematic illustration of logCMC versus $M$ (increasing number of EO units). (e) The generated signal attenuation, $I/I_{max}$ versus k. Included in the graph is also a ILT treatment (red colored line). Noise has been added to the data set. Values for $D_{free}$ and $D_{bound}$ are $1 \cdot 10^{-11}$ and $8 \cdot 10^{-11} m^2 s^{-1}$, respectively. (f) $DP(D)$ from the ILT performed on the generated signal attenuation versus $D$.

71

highest temperature investigated the remaining free polymer component is very rich in EO units.

Finally I pinpoint the main points:

- Many of the "anomalous" effects in the self-assembly of Pluronics are due to polydispersity and can be explained within the multi-component ideal mixing model.
- Always consider polydispersity when interpreting any data concerned with the self-assembly of polymer material, in particular in the context of exchange rates between aggregated and non-aggregated states.

**Table 7.1** Relaxation times, $T_1$ and $T_2$ for 1 wt% F127 as a function of temperature. Measurements made on a 200 MHz NMR spectrometer

| Temperature/K | EO (3.6ppm, Figure 3.5) | | CH$_3$(0.9 ppm, Figure 3.5) | |
|---|---|---|---|---|
| | $T_1$/s | $T_2$/s | $T_1$/s | $T_2$/s |
| 288 | 382 | 307 | 339 | 193 |
| 298 | 498 | 453 | 393 | 226 |
| 300 | 520 | 474 | 377 | 159 |
| 302 | 540 | 490 | 350 | 115 |
| 304 | 551 | 505 | 338 | 97 |
| 313 | 667 | 611 | 337 | 84 |
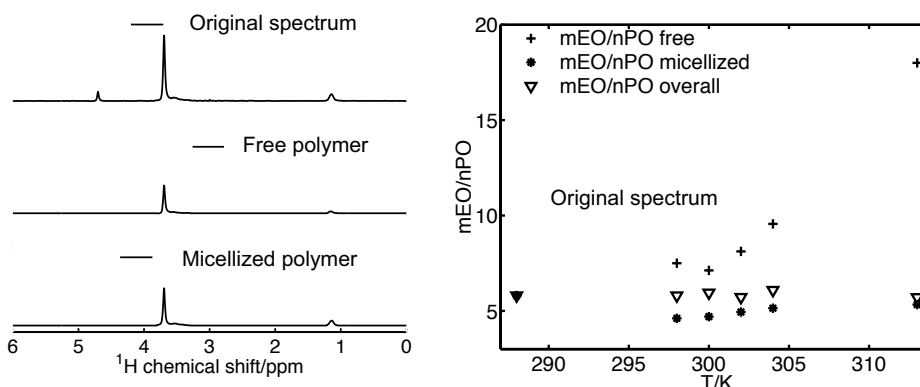


**Figure 7.2** (a) CORE approach applied to separate overlapping peaks for F127 at 1 wt% at 302K. (b) Ratio between the numbers of EO units (m) to PO units (n) versus $T$. The case of free micellized, and overall are shown.

# 8. Populärvetenskaplig sammanfattning

Vilka kemikalier finner man vardagligen i hemmet? Tvål schampoo, diskmedel, tvättmedel, färg, mediciner; listan kan göras väldigt lång. För alla dessa kemikalier finns det en gemensam nämnare, nämligen att de innehåller tensider (ytaktiva substanser) och polymerer. Den populärvetenskapliga sammanfattningen kommer att beskriva tensider och polymerer samt introducera begreppet diffusion. Kapitlet är indelat i två delar:

- *Del 1*: I del 1 definieras de viktiga begrepp inom området yt- och kolloid-kemi (verktygslådan), vilket är ett ämnes område inom kemi som behandlar tensider och polymerer på det mikroskopiska planet.
- *Del 2:* I del 2 kommer att fokusera på min egen forskning och dess resulat.

## Yt och kolloidkemi

En viktig fråga inom yt- och kolloid kemi är hur man blandar vatten och olja utan att de separerar i två faser (en vattenfas samt en oljefas). Tensider, även kallade ytaktiva substanser är molekyler som är "dualistiska" till sin natur; de består av två delar som är sammanlänkade. En del gillar vatten (hydrofil = vattenälskande) och den andre delen skyr vatten (hydrofob = vattenhatande) men tycker om olja och fett, se Figure 8.1. Den del som älskar vatten refererar man till som "huvudgrupp" medan den del som skyr vatten kallas "svans". Vatten och olja kan blandas då tensid tillsätts, genom att vattnet samt oljan fördelar sig på den sida av tensiden som de föredrar. Smuts är ofta någon form av olja eller fett som är ganska svårt att tvätta bort i vatten, men då tensid (t.ex. tvål) används försvinner smutsen genast. I vattenlösning aggregerar tensidmolekylerna på ett sådant sätt att de formar sfäriska klot kallade miceller, med den vattenälskande delen gränsande mot vattnet och då skyddas svansen på tensiden mot vattenkontakt. Dessa aggregat är som mikroskopiska oljedropar, vilka kan lösa in fett och olja. När micellen löser in olja eller fett kallas dropparna microemulsioner, vilka är stabila över tiden. Inom läkemedelsindustrin används mikroaggregat av tensider som behållare till den aktiva substansen (läkemedlet) vilket gör det möjligt att ha den aktiva substansen i vattenlösning. Den aktiva substansen i ett läkemedel är oftast totalt olösligt i vatten och behöver därför göras vattenlöslig.

Storleken (radien) på en micell (mikroemulsion) är mellan 2-100 nm. Namnet kolloid kommer av att det behandlar allt som är av en viss storleksordning 1 nm -10 μm.

Alla molekyler rör sig slumpmässig i vätskefas. Man kan mäta hur fort en partikel förflyttar sig, hur den diffunderar, ordet diffundera kommer av det Latinska namnet "diffundere" som betyder att utbreda. Kärnmagnetisk resonans, som på engelska förkortas NMR (Nuclear Magnetic Resonace), är en av de mest

använbara experimentella metoder som forskare inom den naturvetenskpliga disciplinen har att tillgå. Med hjälp av NMR-tekniken kan man mäta och bestämma molekylers struktur samt rörelse (dynamik). Vi har använt NMR för att mäta diffusionen hos molekyler i utspäddda vattenlösningar.

En <u>Polymer</u> är en molekyl som påminner om ett pärlhalsband, där varje pärla utgör en repeterande enhet kallad "<u>monomer</u>". En polymer kan ha olika monomerer sammanlänkande i olika ordningsföljder till exempel först några A-monomerer sedan några B-monomerer. De polymerer som studerats i denna avhandling består av två olika monomerer som vardera utgör ett block, $A_{50}$-$B_{30}$ (A-A-...-A-A-B-B-...-B-B), en <u>diblock polymer</u>. A monomeren och B monomerens kemiska egenskaper skiljer sig åt. A tycker om vatten och B tycker om olja, med andra ord liknar polymerena vi använt oss av stora tensidmolekyler.

## Forskning och resultat

I mitt arbete har jag främst studerat komplex mellan tensider samt cyclodextriner. Cyklodextrin är uppbyggd av glukosmolekyler ("socker" molekyler) som är sammanbundna på ett sådant sätt att cyclodextrin får en konisk struktur. Hålrummet i den koniska strukturen har andra kemiska och fysikaliska egenskaper än utsidan. Hålrummet kan innesluta molekyler och bilda vad man kallar ett <u>inneslutningskomplex</u>, där cyklodextrin kan liknas vid ett vandrarhem och den ineslutna molekylen är gästen. Hålrummet kan innesluta molekyler som inte är lösliga i vatten, till exempel den aktiva substansen hos ett läkemedel. Cyklodextriner används frekvent inom läkemedelsindustrin och färgindustrin. Som modell för att studera denna gäst-vandrarhem växelverkan används tensider. Den hydrofoba delen på tensiden växelverkar med hålrummet i cyklodextrinen. Hur stark denna växelverkan är mellan gästen (tensiden) och vandrarhemet (cyklodextrinen) har studerats av oss genom att mäta diffusionen i vatten av både vandrarhemmet och gästen med metoden kärnmagnetisk resonans. Man jämför diffusionen mellan gästen och vandrarhemmet. Vandrarhemmets diffusion är betydligt långsammare än gästens, och då ett komplex bildas mellan gästen och vandrarhemmet blir gästens diffusion nästan lika långsam som vandrarhemmets. Diffusionsdatan har modellerats och använts för att beräkna jämviktskonstanten samt stökiometrin.

I ett annat projekt studerade jag hur man kan göra mikroemulsioner mer effektivare; det vill säga lösa in så mycket olja och vatten som möjligt med minsta tillsats av tensid. Som modellsystem för att undersöka hur man kan göra tensid systemen mer effektiva användes en speciell typ av mikroemulsioner som kallas <u>bikontinuerliga mikroemulsioner</u>. Här kan man likna mikroemulsionen med en vanlig tvättsvamp (se Figure 8.1a). Svamp materialet i sig är tensiden medan några av hålrummen är fyllda med vatten och andra med olja. Vattnet har aldrig kontakt med oljan; svamp materialet (tensiden) är som en film som separerar vatten och olja. En del av tensiden ersattes med diblock polymer ($A_{50}$-

B$_{30}$). Resultatet visade att polymeren satte sig i filmen och svampen svällde kraftigt vid låga tillsatser av polymer. Polymeren verkade som en stor tensid molekyl och ett effektivare system uppnådes.
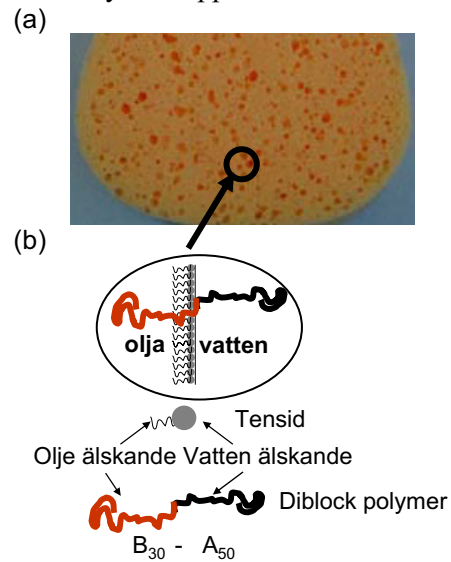


**Figur 8.1** (a) Tvättsvamp kan ungefär liknas vid en bikontinuerlig mikroemulsion, (b) mikrioskopisk inblick, filmen (tvättsvampen) avgränsar oljan från vattnet genom en tunn film bestående av tensid och polymer.

# Acknowledgement

# References

1.  Southall, N. T.; Dill, K. A.; Haymet, D. J., *J. Phys. Chem. B* **2002,** 106, 521-533.
2.  Fennell, D. E.; Wennerström, H., *The Colloidal Domain where Physics, Chemistry, Biology and Technology Meet*. 2nd ed.; Wiley-VCH: New York: Chichester, 1999.
3.  Holmberg, K.; Jönsson, B.; Kronberg, B.; Lindman, B., *Surfactants and Polymers in Aqueous Solution*. 2nd ed.; John Wiley & Sons Ltd: Chichester, 2003.
4.  Zana, R., *J. Colloid Interface Sci.* 78, 330-337.
5.  Mukerjee, P.; Mysels, K. J., *Critical Micelle Concentrations of Aqueous Systems*. National Bureau of Standards: Wasington, DC, 1971.
6.  Fennell, D. E.; Wightman, P. J., *Colloid Interf. Sci.* **1981,** 86, 515-524.
7.  Menger, F. M.; Littau, C. A., *J. Am. Chem. Soc.* **1990,** 113, 1451-1452.
8.  Menger, F. M.; Littau, C. A., *J. Am. Chem. Soc.* **1993,** 115, 10083-10090.
9.  Alami, E.; Beinert, P.; Zana, R., *Langmuir* **1993,** 9, 1465-1467.
10. Alami, E.; Levy, H.; Zana, R., *Langmuir* **1993,** 9, 940-944.
11. Danino, D.; Talmon, Y.; Zana, R., *Langmuir* **1995,** 11, 1448-1456.
12. Frindi, B.; Michels, B.; Levy, H.; Zana, R., *Langmuir* **1994,** 10, 1140-1145.
13. Zana, R.; Benrraou, M.; Rueff, R., *Langmuir* **1991,** 7, 1072-1075.
14. Menger, F. M.; Wrenn, S., *J. Phys. Chem.* **1974,** 78, 1387-1390.
15. Yiv, S.; Kale, K. M.; J., L.; Zana, R., *J. Phys. Chem.* **1976,** 80, 2651-2655.
16. Yiv, S.; Zana, R., *J. Colloid Interface Sci.* **1980,** 77, 449-455.
17. Zana, R.; Yiv, S.; Kale, K. M., *J. Colloid Interface Sci.* **1980,** 77, 456-465.
18. Whiddon, C.; Reimer, J.; Söderman, O., *Langmuir* **2004,** 20, 2172-2176.
19. Alexandridis, P.; Hatton, A. T., *Colloids Surf. A* **1995,** 96, 1-46.
20. Alexandridis, P.; Holzwarth, J. F.; Hatton, A. T., *Macromolecules* **1994,** 27, 2414-2425.
21. Fusco, S.; Borzacchello, A.; Netti, P. A., *J. Bioactive Compatible Polymers* **2006,** 21, 149-164.
22. Wanka, G.; Ulbricht, W., *Macromolecules* **1994,** 27, 4145-4159.
23. Karlström, G., *J. Phys. Chem.* **1985,** 89, 4962-4964.
24. Öberg, E. Syntes ock karaterisering av di-block copolymerer. Master thesis, Tekniska Högskolan, Linköpings Universitet, Linköping, 2007.
25. Allgaier, J.; Willbold, S.; Chang, T., *Macromolecules* **2007,** 40, 518-525.

26. Hedges, R. A., *Chem. Rev.* **1998,** 98, 2035-2044.
27. Szejtli, J., *Chem. Rev.* **1998,** 98, 1743-1753.
28. Saenger, W.; Jacob, J.; Gessler, K.; Steiner, T.; Hoffmann, D.; Sanbe, H.; Koizumi, K.; Smith, S. M.; Takaha, T., *Chem. Rev.* **1998,** 98, 1787-1802.
29. Conners, K. A., *Chem. Rev.* **1997,** 97, 1325-1358.
30. Briggner, L.; Wadsö, I., *J. Chem. Thermodynamics* **1990,** 22, 1067-1074.
31. Sabadini, E.; Cosgrove, T.; do Egídio, F. C., *Carbohydr. Res.* **2006,** 341, 270-274.
32. Bonini, M.; Rossi, S.; Karlsson, G.; Almgren, M.; Lo Nostro, P.; Baglioni, P., *Langmuir* **2006,** 22, 1478-1484.
33. Wimmer, R.; Aachmann, L. F.; Larsen, L. K.; Peterson, S. B., *Carbohydr. Res.* **2002,** 337, 841-849.
34. Guerrero-Martínez, A.; Gonzaléz-Gaitano, G.; Vinas, M. H.; Tardajos, G., *J. Phys. Chem. B* **2006,** 110, 13819-13828.
35. Callaghan, P. T., *Principles of Nuclear Magnetic Resonance Microscopy*. Oxford University Press Inc.: New York, 1995.
36. Levitt, M. H., *Spin Dynamics Basic of Nuclear Magnetic Resonance*. John Wiley & Sons, LTD: Chichester, 2006.
37. Abragam, A., *The Principles of Nuclear Magnetic Resonance*. Oxford University Press: Oxford, 1978.
38. Harris, R. K., *Nuclear Magnetic Resonance Spectroscopy*. Logman Scientific & Technical: Harlow, 1986.
39. Atkins, P. T.; de Paula, J., *Physical Chemistry*. 7th ed.; Oxford University Press: Oxford, 2002.
40. Bloembergen, N.; Purcell, E. M.; Pound, R. V., *Nature* **1947,** 160, 475.
41. Gwendolyn, N.; Hoult, D. I., *Concepts Magn. Reson.* **1990,** 2, 131-149.
42. Hahn, E. L., *Phys. Rev.* **1950,** 80, 580-594.
43. Purcell, E. M.; Carr, H. Y., *Phys. Rev.* **1954**, 630-638.
44. Meiboom, S.; Gill, D., *Rev. Sci. Instr.* **1958,** 29, 688-691.
45. Reif, F., *Fundamentals of Statistical and Thermal Physics*. McGraw Hill: New York, 1965.
46. Kimmich, R., *NMR Tomography Diffusometry Relaxometry*. Springer-Verlagen: Berlin, 1997.
47. Price, W. S., *Concepts Magn. Reson.* **1997,** 9, 299-336.
48. Nydén, M. NMR diffusion Studies of Microheterogeneous Systems surfactant solutions Polymers solutions and Gels. Doctoral thesis, Lund University, Lund, 1998.
49. Malmborg, C.; Topgaard, D.; Söderman, O., *J. Magn. Reson.* **2004,** 169, 85-91.
50. Stejskal, E. O.; Tanner, E., *J. Chem. Phys.* **1965,** 42, 288-292.
51. Tanner, J. E., *J. Chem. Phys.* **1970,** 52, 2523-2526.

52. Johnsson, J. C. S., *Prog. Magn. Reson.* **1999,** 34, 203-256.
53. Lévay, B., *Acta. Chim. Acad. Sci. Hung.* **1972,** 74, 143-150.
54. Rymdén, R.; Carlfors, J.; Stilbs, P., *J. Incl. Phenom.* **1983,** 1, 159-167.
55. Schneider, H. J.; Hacket, F.; Rüdiger, V., *Chem. Rev.* **1998,** 98, 1755-1785.
56. Cameron, K. S.; Fielding, L., *J. Org. Chem.* **2001,** 66, 6891-6895.
57. Cameron, K. S.; Fielding, L., *Magn. Reson. Chem.* **2002,** 40, S106-S109.
58. Lévay, B., *J. Phys. Chem.* **1972,** 77, 2118-2121.
59. Söderman, O.; Stilbs, P.; Price, W. S., *Concept Magn. Reson.* **2004,** 23A(2), 121-135.
60. Deranleau, D. A., *J. Am. Chem. Soc.* **1969,** 91, 4044-4049.
61. De Lisi, R.; Lazzara, G.; Miliotio, S.; Muratore, N., *J. Phys. Chem. B* **2003,** 107, 13150-13157.
62. De Lisi, R.; Miliotio, S.; Muratore, N., *J. Chem. Phys. B* **2002,** 106, 8944-8953.
63. Garcia-Rio, L.; Leis, J. R.; Mejuto, J. C.; Navarro-Vazquez, A.; Perez-Juste, J.; Rodriguez-Dafonte, P., *Langmuir* **2004,** 20, 606-613.
64. Satake, I.; Yoshida, S.; Hayakawa, K.; Maeda, T.; Kusumoto, Y., *Bull. Chem. Soc. Jpn.* **1986,** 59, 3991-3993.
65. Liljequist, P.; Kronberg, B., *J. Colloid Interface Sci.* **2000,** 222, 159-164.
66. Tanford, C., *The Hydrophobic Effect: Formation of Micelles and Biological Membranes*. John Wiley & Sons, Inc.: New York, 1973.
67. Liveri, T. V.; Cavallaro, G.; Giammona, G.; Pitarresi, G.; Puglisi, G.; Ventura, C., *Thermochimica Acta* **1992,** 199, 125-132.
68. Guerrero-Martínez, A.; Palafax, M. A.; Tardajos, G., *Chem. Phys. Lett.* **2006,** 432, 486-490.
69. Lyon, A. P.; Banton, N. J.; Macartney, D. H., *Can. J. Chem.* **1998,** 76, 843-850.
70. Rekharsky, V. M.; Inoue, Y., *Chem. Rev.* **1998,** 98, 1875-1917.
71. Helfrich, W., *Z Natureforsch C* **1973,** 28, 693-703.
72. Sottmann, T.; Kluge, K.; Strey, R.; Reimer, J.; Söderman, O., *Langmuir* **2002,** 18, 3058-3067.
73. Kabalnov, A.; Olsson, U.; Wennerström, H., *Langmuir* **1994,** 10, 2159-2169.
74. Kabalnov, A.; Olsson, U.; Thuresson, K.; Wennerström, H., *Langmuir* **1994,** 10, 4509-4513.
75. Jakobs, B.; Sottmann, T.; Strey, R., *Langmuir* **1999,** 15, 6707-6711.
76. Jakobs, B.; Sottmann, T.; Strey, R., *Tenside Surf. Det.* **2000,** 37(6), 357-364.
77. Kumar, A.; Uddin, H. M.; Kunieda, H.; Furukawa, H.; Harashima, A., *J. Disp. Sci. Tech.* **2001,** 22(2&3), 245-253.

78.     Endo, H.; Allgaier, J.; Gompper, G.; Jakobs, B.; Monkenbusch, M.; Richter, D.; Sottmann, T.; Strey, R., *Phys. Rev. Lett.* **2000,** 85, 102-105.

79.     Endo, H.; Mihailescu, M.; Monkenbusch, M.; Allgaier, J.; Gompper, G.; Richter, D.; Jakobs, B.; Sottmann, T.; Strey, R.; Grillo, I., *J. Chem. Phys.* **2001,** 115, 580-600.

80.     Gompper, G.; Richter, D.; Strey, R., *J. Phys. Condens. Matter* **2001,** 13, 9055-9074.

81.     Frank, C.; Sottmann, T.; Stubenrauch, C.; Allgaier, J.; Strey, R., *Langmuir* **2005,** 21, 9058-9067.

82.     Byelov, D.; Frielinghaus, H.; Holderer, O.; Allgaier, J.; Richter, D., *Langmuir* **2004,** 20, 10433-10443.

83.     Reimer, J.; Söderman, O.; Sottmann, T.; Kluge, K.; Strey, R., *Langmuir* **2003,** 19, 10692-10702.

84.     da Silva, R. C.; Olofsson, G.; Schillén, K.; Loh, W., *J. Chem. Phys. B* **2002,** 106, 1239-1246.

85.     Jörgen, J.; Schillén, K.; Olofsson, G.; da Silva, R. C.; Loh, W., *J. Chem. Phys. B* **2004,** 108, 82-92.

86.     Malmsten, M.; Lindman, B., *Macromolecules* **1992,** 25, 5440-5446.

87.     Yu, G.; Dalton, S.; Wang, Q.; Attwood, D.; Price, C.; Booth, C., *J. Chem. Soc. Faraday Trans.* **1992,** 88, 2537-2544.

88.     Walderhaug, H., *J. Phys. Chem. B* **1999,** 103, 3352-3357.

89.     Walderhaug, H.; Nyström, B., *J. Phys. Chem. B* **1997**, 1524-1528.

90.     Walderhaug, H.; Nyström, B., *Trends Phys. Chem.* **1997,** 6, 89-106.

91.     Nydén, M.; Söderman, O., *Macromolecules* **1998,** 31, 4990-5002.

92.     Håkansson, B.; Nydén, M.; Söderman, O., *Colloid Polym. Sci.* **2000,** 278, 399-405.

93.     Stilbs, P.; Paulsen, K., *Rev. Sci. Instrum.* **1996,** 67, 4380-4386.

94.     Stilbs, P.; Paulsen, K.; Griffiths, P. C., *J. Phys. Chem. B* **1996,** 100, 8180-8189.

95.     Griffiths, P. C.; Cheung, A. Y. F.; Davies, J. A.; Tipples, C. N.; Winnington, A. L., *Magn. Reson. Chem.* **2002,** 40, 40-50.

96.     Holland, P. M.; Rubingh, D. N., *J. Phys. Chem.* **1983,** 87, 1984-1990.